



UNIVERSITY OF
LINCOLN

**THERMORESPONSIVE MOLECULAR
INTERFACE FOR ON-DEMAND RELEASE
OF SURFACE-IMMOBILISED PROTEINS**

Angela Saccardo

Doctor Of Philosophy

College of Science – School of Life Sciences

June 2020

I declare that this thesis has been composed solely by myself and that it has not been submitted, in whole or in part, in any previous application for a degree. Except where stated otherwise by reference or acknowledgement, the work presented is entirely my own.

Signature: 

Name: Angela Saccardo

Date: 16/06/2020

ABSTRACT

In the last decades, biomedicine opened its doors to stimuli-responsive biomaterials, with applications ranging from tissue engineering to drug delivery systems. Among them, polymers are by far the most investigated, thanks to their biocompatibility and their vast range of properties, tunable to match their end-use.

Protein-based thermoresponsive materials are increasingly being studied, especially for drug delivery applications, where dedicated chemistries for on-demand capture and release of biomolecules at the solid-liquid interface are essential. This is an important requirement for the synthesis of switchable surfaces used in analytical devices and for the assembly of novel smart materials with complex architectures and functions.

Here the design, synthesis and characterisation of novel peptide tags for reversible protein capture and thermoresponsive release from a solid surface are reported. The peptide sequences were inspired by the self-assembling protein machinery dedicated to vesicle fusion in eukaryotes, known as the SNARE proteins.

The three proteins involved, named SNAP25, syntaxin and VAMP, all present a highly preserved strand (SNARE motif) that allows them to assemble in a tight coiled-coil structure upon interaction, called SNARE

complex. This four α -helix bundle has remarkable chemical and thermal stability, withstanding temperatures up to 80°C and changes of pH.

The structural features of the native ternary protein complex were engineered to yield a binary self-assembling polypeptide system. The first element of the binary system is a universal protein substrate immobilised on a solid surface. This protein mimics the neuronal SNAP25, which is involved in the docking and fusion of synaptic vesicles to the synaptic membrane. The second element is a protein fusion of syntaxin and VAMP, acting as a polypeptide tag; it includes SNARE motifs from both syntaxin and VAMP, capable of self-assembly in a coiled-coil structure when coupled with SNAP25, even when immobilised on a surface. This interaction is strong but fully-reversible; therefore, this polypeptide tag can be recombinantly fused to a protein of interest to allow spontaneous assembly and stimuli-sensitive release from the surface upon heating at a predetermined temperature.

Two VAMP-syntaxin protein fusions were produced, with different VAMP lengths: in the first, VAMP's SNARE motif spans for 54 amino acids, matching syntaxin's length. In the second, VAMP has been reduced to 25 amino acids, truncated before the residue involved in the ionic layer, which helps stabilise the coiled-coil structure of the SNARE complex. The protein fusion with the shortened VAMP has been designed to weaken the SNARE complex thermal stability and test its disassembly temperature.

The recombinant proteins described above were characterised with pulldown assays and circular dichroism spectroscopy, testing their ability to form a stable SNARE complex. Two VAMP-syntaxin thermoresponsive tags are described: results show that the first one, with the 54-amino acid VAMP, presents remarkable thermal stability with T_m of the order of 80°C. The second tag, with the truncated VAMP, disassembles at a substantially lower temperature of about 45°C. The latter is a promising candidate for remote-controlled localised delivery of therapeutic proteins: the physiologically tolerable local increase of temperature in the 40-45°C range, also known as hyperthermia, can be achieved using magnetic fields, infra-red light or focused ultrasound. Notably, these two novel polypeptides provide an example for the engineering of future functional proteins with predictable folding and response to external stimuli.

ACKNOWLEDGEMENTS

First and foremost, I am very grateful to Dr Enrico Ferrari, my mentor, for his constant support and guidance during the running of this project. His passion and enthusiasm towards research were vital in inspiring me to think outside the box and to pursue a career in research. To him and Dr Mikhail Soloviev a big thanks for all the exciting conversations in front of a coffee during the time spent at the Diamond Light Source Synchrotron.

Thanks to the University of Lincoln, the School of Life Sciences and all its members for the friendly environment I found inside and outside the lab. During this PhD, I had the chance to participate in a Horizon-2020 program: heartfelt thanks to Dr Nicholson, his wife and all the people I met at Temple University and in Philadelphia for their insights and encouragement.

I am extremely grateful for the overwhelming support I received from family and friends throughout this PhD. A special mention goes to my crazy lab mates Gareth, Mel, Dan and all the others: these years in Lincoln would have been way more boring without you! Thanks for the advice and the funny gatherings in the lab and out. Grazie mille! Thanks also to all my Lincoln friends, who became my extended family, in particular to Vale and Fra, for our dinners together and for all the special moments I will treasure forever.

Un grande grazie alla mia famiglia, che più di tutte mi ha supportato in questo percorso lontano da casa. Dovunque mi abbia portato e mi porterà questa vita, il vostro amore è sempre stato e sarà un porto sicuro da cui partire e a cui ritornare. Grazie di cuore!

TABLE OF CONTENTS

ABSTRACT	I
ACKNOWLEDGEMENTS	IV
TABLE OF CONTENTS	V
ABBREVIATIONS	VII
1. INTRODUCTION	- 1 -
1.1 Biomaterials for pharmaceutical applications	- 1 -
1.1.1 Stimuli-responsive materials	- 5 -
1.1.2 Thermoresponsive materials.....	- 7 -
1.1.3 Protein-based thermoresponsive materials	- 9 -
1.2 SNARE proteins	- 11 -
1.2.1 Structure	- 13 -
1.2.2 SNARE complex formation	- 18 -
1.2.3 SNARE complex properties.....	- 19 -
1.3 Biochemical & biophysical characterisation of the SNARE complex -	22 -
1.3.1 SDS-PAGE and GST-pulldown assay.....	- 22 -
1.3.2 Circular Dichroism spectroscopy	- 24 -
1.4 Engineering of recombinant SNAREs	- 27 -
1.5 Aim of the project.....	- 29 -
1.5.1 Modulation of the SNARE complex's thermal stability	- 30 -
1.5.2 Engineering of binary SNARE complexes.....	- 32 -
1.5.3 Thermo-release of surface-immobilised proteins.....	- 34 -
2. MATERIALS AND METHODS	- 35 -
2.1 Protein design	- 35 -
2.1.1 Design of SNARE fusions.....	- 38 -
2.2 Cloning	- 39 -
2.2.1 Subcloning of synthetic genes.....	- 40 -

2.2.2 Propagation of unmethylated plasmid DNA.....	- 40 -
2.2.3 Double digestion of origin and destination plasmids	- 41 -
2.2.4 Purification of a double digested DNA insert	- 44 -
2.2.5 Synthesis of a DNA insert by annealing of ssDNA oligos.....	- 45 -
2.2.6 Ligation	- 46 -
2.2.7 Verification of the cloning	- 48 -
2.3 Protein expression and purification.....	- 50 -
2.3.1 Transformation of competent cells	- 50 -
2.3.2 Low-T expression and purification of GST fusion proteins	- 51 -
2.3.3 Protein elution	- 54 -
2.3.4 Fluorescent labelling	- 55 -
2.3.5 Fast Protein Liquid Chromatography.....	- 56 -
2.4 Protein characterisation	- 57 -
2.4.1 Protein concentration determination	- 58 -
2.4.2 Synchrotron Radiation Circular Dichroism	- 58 -
2.4.3 Pull-down and controlled release.....	- 59 -
3. RESULTS	- 62 -
3.1 Modulation of SNARE complex thermal stability.....	- 62 -
3.2 Engineering of binary SNARE complexes.....	- 67 -
3.3 Thermoresponsive protein release.....	- 75 -
4. DISCUSSION	- 84 -
5. REFERENCES.....	- 98 -
6. APPENDIX	- 116 -
A. Protein sequences	- 116 -
B. DNA sequencing data	- 118 -
C. Protein purification	- 125 -
D. Protein fusion attempts.....	- 136 -
E. Published outputs from the project (printed copies only).....	- 137 -

ABBREVIATIONS

BCA: BiCinchoninic Acid

BSA: Bovine Serum Albumin

Cy5: Cyanine 5

DTT: DiThioThreitol

EDTA: EthyleneDiamineTetraAcetic acid

ELPs: Elastin-Like Polymers

FPLC: Fast Protein Liquid Chromatography

GNPs: Gold NanoParticles

GSH: Glutathione (reduced)

GST: Glutathione S-Transferase

HEPES: 4-(2-Hydroxyethyl)-1-piperazineethanesulfonic acid

HH: SNAP25' Helix 1 and Helix 2 linked together

IPTG: Isopropyl β -D-1-thiogalactopyranoside

LB: Luria-Bertani medium

NIR: Near-Infrared

NSF: N-ethylmaleimide-Sensitive Factor

OD: Optical Density

PAGE: PolyAcrylamide Gel Electrophoresis

PDB: Protein Data Bank

PEG: PolyEthylene Glycol

SNAP25: Synaptosomal-Associated Protein 25

SNAREs: Soluble N-ethylmaleimide-sensitive factor Attachment protein
Receptors

SDS: Sodium Dodecyl Sulfate

SOB: Super Optimal Broth

SRCD: Synchrotron Radiation Circular Dichroism

T_m: melting temperature

T_t: transition temperature

TBE: Tris-Borate-EDTA

TCEP: Tris 2-CarboxyEthyl Phosphine

VAMP: Vesicle-Associated Membrane Protein, Synaptobrevin

VS: VAMP-syntaxin fusion protein

1. INTRODUCTION

1.1 Biomaterials for pharmaceutical applications

Biomaterials are materials applied in biomedicine that have been engineered to safely interact with organisms, regulating therapeutic and diagnostic procedures (1,2). They can be of both organic and inorganic origin: ceramics, metals and polymers are the three main classes of biomaterials that are currently employed in medicine. Many of them can replace tissues, mimicking their biological, mechanical and chemical properties (1). Their compatibility with living systems makes them suitable to be used in implants, medical devices, as well as being used for pharmaceutical applications, for example, drug delivery. Bioactive glasses are commonly used as bone substitutes (3); stainless steel has been routinely utilised for dental implants, as well as bone replacements (once coated with calcium phosphate or other organic substances). Biomaterials require different properties (biodegradability, strength, durability, elasticity) that, especially for synthetic polymers, can be tuned to match the end-use. Some examples of polymer biomaterials are colloids, hydrogels and biofilms (4,5).

Polymers have an undoubted advantage in being flexible, making them the most utilised material in biomedical applications, from orthopaedics to drug delivery systems. They are relatively easy to produce, with a broad range of chemical and physical properties. Polymers can be synthetic or organic macromolecules, both entailing units covalently linked together. Most of their features can be tuned (molecular weight, composition, surface charges) to fit the desired scope. External stimuli can also be applied to trigger changes in some polymers, which is extensively being studied for biomedical applications, mainly to use them as drug delivery systems (6,7).

Proteins were used as drugs for decades. One of the earliest examples is insulin, discovered at the University of Toronto in 1921 (8); Macleod and Banting won the Physiology Nobel Prize in 1923 for their breakthrough. Monoclonal antibodies are another excellent example of proteins used in a medical context (9); using “phage display”, Winter directed the evolution of antibodies, which led to the development of new pharmaceuticals, notably against autoimmune diseases (as rheumatoid arthritis). He began his work in the late '80s and received the Chemistry Nobel Prize thirty years later, in 2018, for his contribution to engineer therapeutic proteins.

Proteins have been increasingly studied for their pharmaceutical applications since the introduction of recombinant DNA technology.

This new know-how has the potential to turn many proteins into a medicinal drug, even if proteins are usually less stable than other pharmaceutical compounds and tend to biodegrade quickly in the bloodstream. Their compatibility with living organisms is a strength: a native (or slightly modified) protein can be highly specific without causing any harm or adverse reaction in an organism.

Cancer therapy extensively uses protein nanoscale carriers and drugs, including multi-specific antibodies (mostly monoclonal antibodies) and fusion proteins; moreover, numerous immunotoxins against lymphoma are currently in clinical trials ⁽¹⁰⁾. The development of new cytotoxic drugs capable of reaching a specific target is crucial to increase drug concentrations in tumoural tissues and avoid dangerous side effects. Further modifications of cytotoxic proteins can lead to self-assembly and self-activation. Proteins can be associated with conventional drugs as a targeting agent (e.g. antibodies), or act as drug themselves. Olaratumab (monoclonal antibody) against sarcomas of the soft tissues, PEGylated Interferon against melanomas, Etanercept (trade name of a complex fusion protein) against lymphomas are only a few examples of protein drugs already employed for cancer therapy (see Figure 1.1).

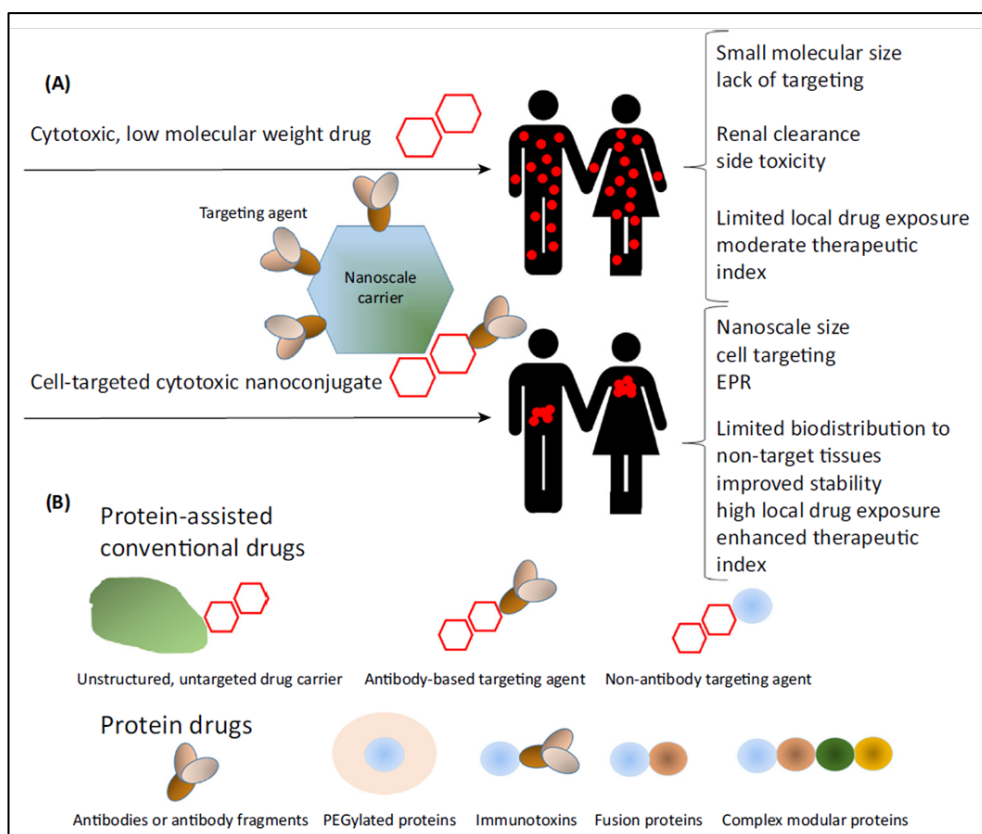


Figure 1.1 Simplified scheme of anti-cancer drugs and their features. A) The standard chemotherapy approach is the use of chemicals (in red) that present cytotoxicity to both tumour and healthy cells. Their small molecular size (<5 nm, permitting renal clearance) and absence of target-specificity result in a distribution in the whole body. Linking such chemicals to nanoscale carriers and/or functionalising them with targeting agents can reduce their renal clearance and increase the drug concentration locally. B) Various roles of proteins for cancer therapy formulations. Abbreviations: EPR = Enhanced Permeability and Retention; PEGylation = linkage to polyethylene glycol. Image from Serna et al. ⁽¹⁰⁾.

Despite an increase in the use of proteins in pharmaceutical science, the development of protein-based biomaterials remains less explored.

1.1.1 Stimuli-responsive materials

Scientists are developing both synthetic and modified biological materials that can sharply and reversibly change their conformation or phase in response to a stimulus. Stimuli can be either endogenous (changes in pH, enzyme concentration or redox gradients) or exogenous (magnetic field, ultrasound intensity, light or electric pulses, variations in temperature) ⁽¹¹⁾. In biomedicine, these ‘smart’-polymers give life to, among others, biomimetic actuators, immobilised biocatalysts, drug delivery systems, cell culture surfaces, diagnostic and thermoresponsive surfaces ^(6,12).

Polymers behaving like linear chains in solution can be triggered to fold and unfold or assist other proteins in avoiding possible aggregation ^(13,14). Polymers can also form gels through a network of cross-linked monomers: changes in their structure (like shrinking and stretching) can modify their pores’ size, releasing or retaining useful molecules.

Bioactive molecules such as nucleic acids, small organic molecules, and peptides were combined with stimuli-responsive materials ⁽¹²⁾. They range from the micro- to the nano-scale, with infinite possibilities of combinations between stimuli, carrier and carried polymers ⁽¹⁵⁾ (see Figure 1.2).

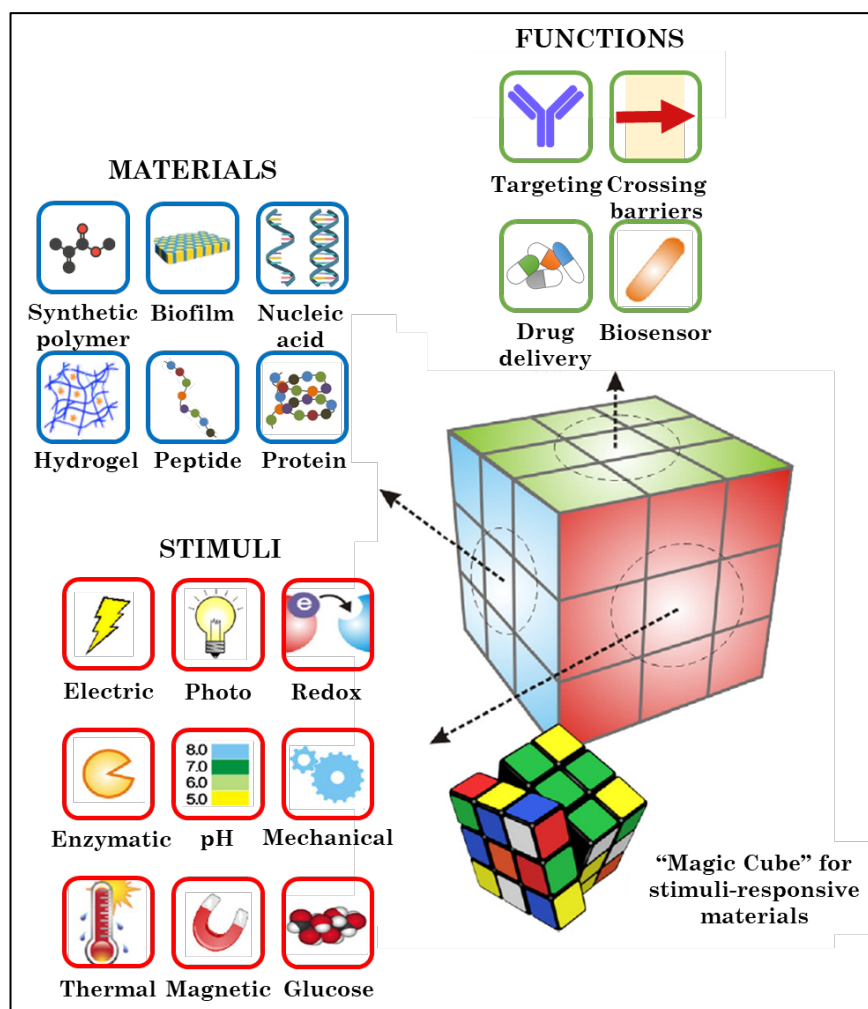


Figure 1.2 Schematic of “Magic Cube” for stimuli-responsive materials. Combination of a variety of triggering mechanisms and carrier formulations for the delivery of a broad spectrum of functional proteins. Figure partially adapted from Lu et al. (15).

Some thermoresponsive systems are capable of self-regulating their release rate thanks to a feedback mechanism. They can act directly inside the body and change their structure without any external triggering system (11,14,16). One excellent example are self-regulated insulin release systems (17,18,19); they make use of glucose-sensitive materials in the form of matrices and gels, releasing insulin in response to a change in glucose concentration.

'Smart' polymers face many challenges before their clinical approval, mainly due to their potential cytotoxicity. Drug delivery systems carrying peptides and nucleic acids, which primarily act within the cells, encounter the most difficulties (12).

1.1.2 Thermoresponsive materials

Amongst the stimuli-responsive materials, thermoresponsive polymers can serve numerous purposes (20). They are of particular interest in biomedicine to trigger novel drug delivery systems, as local changes of temperatures are technologically achievable using a wide range of methods. Once the smart polymers are inside the body, the temperature can be modulated either internally or externally (14), expanding their applicability in the field. The use of magnetic fields (21,16) and near-infrared lasers (22,23) is widespread in the biomedical field to activate thermoresponsive delivery systems. Focused ultrasounds is another external tool to induce changes in thermoresponsive polymers, where this stimulus triggers the rapid release of a drug and increases the temperature to facilitate diffusion (16,24).

Moreover, some cancers generate a slight increase in body temperature (1-2°C) (25), while fever is a common reaction to inflammation. This temperature rise could help the activation of smart polymers *in loco*; however, these changes are not controllable, while temperature as an external stimulus can be modulated and employed locally (15,26,27).

In order to deliver their payload in response to an increase in the temperature, thermoresponsive materials used in drug delivery need to change their structure rapidly. Their non-linear relationship with their triggering stimulus is of fundamental importance for their drug-release task, as they necessarily need to work as a binary switch with a controlled threshold (5,28,29).

Hydrogels are found amongst the thermoresponsive materials and were extensively studied in the last few decades (30). They are simple polymer solutions at room temperature, acquiring a gel-form in physiological conditions, without any external-induced temperature modulation. Their high water content allows for swelling once injected into the body, releasing the moieties shielded between their cross-linked molecules (31,32).

One of the main obstacles in the design of protein-based materials is how to increase their half-life. As an example, studies showed that the addition of polyethylene glycol (PEG) drastically improves smart polymers' half-life

during circulation in the body, increasing the effectiveness of their deliverable payload ^(33,34,35). Small bioactive molecules such as PEGs improve aqueous solubility, extend plasma half-life and reduce renal clearance; they help to perform active intracellular delivery, and they show potential for targeted delivery. PEGylation (the addition of PEG on a polymer) was also performed on thermoresponsive drug delivery systems, showing increased stability and half-life ⁽³⁶⁾.

1.1.3 Protein-based thermoresponsive materials

Biomaterials include different substances with a variety of properties, each suitable for a specific function. Among them, protein-based materials are by far the most adaptable to different purposes. Excellent examples of such materials are present in nature: spider webs are known for their remarkable strength, comparable to steel, and their extension properties ⁽³⁷⁾. The human body has numerous polymers with unique characteristics, from collagen's mechanical strength to elastin's flexibility ⁽³⁸⁾.

Elastin is an insoluble protein, highly cross-linked, responsible for the structural integrity and elasticity of tissues and organs, from lungs to blood vessels. It is one of the critical components of the extracellular matrix and elastic fibres. Elastin's properties gained the attention of many

researchers: elastin, in fact, is capable of self-assembly and rearranging its structure depending on the temperature; these properties are shared with tropoelastin, its precursor protein. Above the so-called Transition Temperature (T_t), elastin and tropoelastin rearrange in a more ordered phase; this reversible event is called “inverse phase transition” (39,40). Elastin’s properties were ideal for the development of new protein-based materials, that were called elastin-like polymers (ELPs): ELPs are artificial derivatives of tropoelastin’s hydrophobic domains.

The first ELPs were synthesised by Urry and his research group (40), where they extensively studied their properties in solution as well as their biomedical applications. Elastin-like polymers are soluble in solution; when heated to the transition temperature, they aggregate, becoming insoluble. This process is reversible, with a loss of water by the hydrophobic domains that can be reabsorbed once the temperature decreases below the critical threshold. ELPs are therefore considered a thermosensitive polymer: its conformational change directly depends on the temperature.

Elastin-like polymers represent an excellent example of versatile thermoresponsive polymer; applications in biomedicine vary from tissue engineering (41), surface biofunctionalisations (42) to drug delivery systems (43,44,45). Some ELPs were developed to be soluble at body temperature and rapidly aggregate with a moderate increase of temperature (to 40-42°C).

The exploit of ELPs' thermoresponsiveness to mild hyperthermia permitted targeting of solid tumours and increased drug uptake *in loco* (43,46). Elastin-like polymers were often associated with chemotherapeutics as doxorubicin, with promising results also in association with nanoparticles (47,48).

Protein-based materials are increasingly being studied for their biocompatibility and tunable properties (49). In the last decade, numerous studies were conducted on protein-based thermoresponsive materials, often coupled with metal nanoparticles as a starting template, creating a vast range of versatile nanostructures (15,28,50,51).

1.2 SNARE proteins

The eukaryotic cell contains numerous organelles, each one with a dedicated function. These different compartments are maintained in equilibrium by rigid mechanisms. Homeostasis conducts this regulatory work on the material exchanged among the organelles, and what goes in and out of the cell. Vesicular transport is one of the selective exchange methods used by eukaryotes. Secretory vesicles are formed on the surface of an organelle, and they consequentially fuse with their target membrane (of another organelle). Coat proteins regulate the formation of the vesicle

from an organelle or a cell surface. At the same time, the fusion on the target membrane is controlled by a family of proteins, known as SNAREs (Soluble N-ethylmaleimide-sensitive factor Attachment protein REceptors) (^{52,53,54}). They are distributed both on the vesicle and the acceptor membrane: the fusion is possible thanks to their interaction (⁵⁴).

The SNAREs were initially identified in yeast when studying its secretory pathway (⁵⁵), then proved to be present in all eukaryotic cells (^{56,57}). The evolutionary conservation of the SNARE complexes among eukaryotes is indicated by the high similarity between yeast, endosomal and neuronal SNARE complexes (^{58,59,60}). SNAREs can interact with their corresponding SNARE partners bringing membranes close together; therefore, SNAREs are to be considered “the engine of the membrane fusion” (⁶¹) (Figure 1.3).

Three proteins participate in the formation of the SNARE complex: a Vesicle-Associated Membrane Protein (shortened as VAMP), syntaxin, and SNAP25, a 25kDa protein (⁵⁵). Rothman and colleagues classified these proteins into two groups, vesicle (v-SNAREs) or target SNAREs (t-SNAREs), based on their localisation (^{55,58}). VAMP is a v-SNAREs, as it is located on the vesicle’s membrane; SNAP25 and syntaxin are t-SNAREs, as they are part of the target membrane (see Figure 1.3).

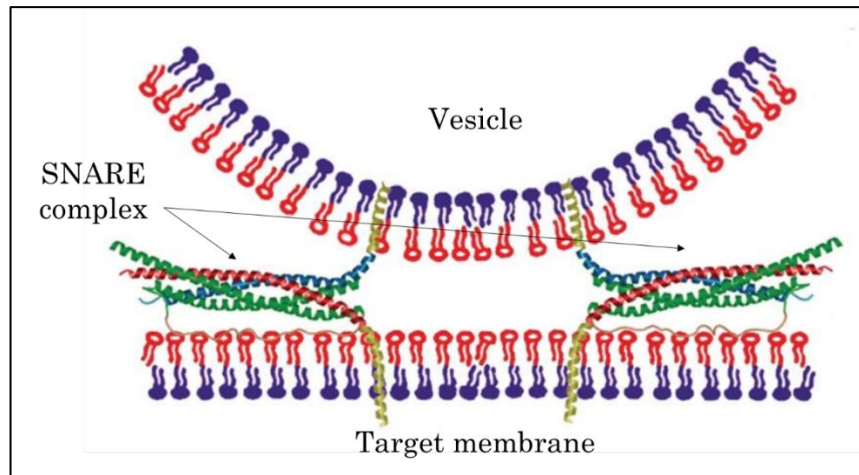


Figure 1.3 Model of two SNARE complexes during vesicle docking. The proteins that form the SNARE complex are represented in different colours: VAMP in blue, syntaxin in red, both with a yellow transmembrane domain; in green, SNAP25. Their interaction brings membranes close together, leading to membrane fusion. Figure adapted from Brunger et al. (62).

SNAREs guide membrane fusion in most of the endo- and exocytotic pathways, including the release of neurotransmitters: these proteins are responsible for the docking of synaptic vesicles with the presynaptic membrane in neuronal cells (61).

1.2.1 Structure

All SNARE proteins are characterised by the presence of a SNARE motif: this is a ~60 amino acid strand organised in heptad repeats, allowing the formation of a coiled-coil structure arrangement with other SNARE motifs (63,64). In a SNARE motif, hydrophobic amino acids are overrepresented in

positions 1 and 4 (residues “A” and “D” in Figure 1.4). As a consequence of this pattern, the hydrophobic amino acids on different α -helices face each other within the core of the coiled-coil structure and the α -helices “zip” together from the N- to the C- terminal via the formation of hydrophobic layers. A central ionic layer helps with the overall stability of the core structure. The SNARE motif is highly conserved among the SNARE superfamily.

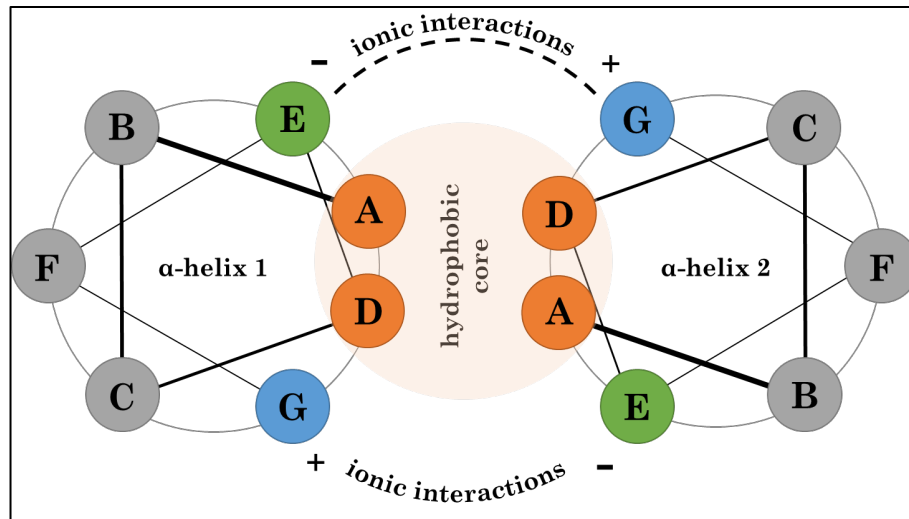


Figure 1.4 A downward cross-sectional view of the α -helical heptad repeats for a heterodimer forming a coiled-coil structure. Coiled-coil structures are made of aligned motifs with multiple heptad repeats (seven residues); in SNARE proteins, such strands are called SNARE motifs and are responsible for the formation of the SNARE complex. The scheme shows two α -helices with their axes orthogonal to the paper plane, and highlights the interactions between their heptad repeats: the seven residues are labelled with letters from “A” to “G”. Hydrophobic residues “A” and “D”, in orange, are involved in the formation of the hydrophobic core; charged residues “E” and “G” stabilise the overall structure forming salt bridges (positively charged = blue, negatively charged = green). Residues “B”, “C” and “F” are usually charged or polar. The SNARE complex is a tetrameric α -helix bundle, and the four α -helices behave as the heterodimer showed here, with the formation of the hydrophobic core thanks to hydrophobic residues of all four helices. SNAREs are characterised by a central ionic layer: the heptad repeats involved in its formation do not have hydrophobic residues in position “A” and “D”, but rather a glutamine or arginine residue, depending on the protein involved.

Syntaxin consists of three main domains: an N-terminal domain (here called NTD), a SNARE motif and a C-terminal transmembrane domain (TM) (see Figure 1.5 A). The transmembrane domain provides anchorage to the surface of the presynaptic plasma membrane, while the NTD is responsible for switching between an open and closed conformation ⁽⁶⁵⁾. The conformational change of the N-terminal domain allows or prevents the interaction with other SNARE domains and has a regulatory function.

VAMP has a short N-terminal region, the SNARE motif and a C-terminal transmembrane domain (TM) (Figure 1.5 A).

SNAP25 has two SNARE motifs, located at the N- and C-terminal of the protein, which may work as independent domains (see Figure 1.5 A). It has no transmembrane region, as it is linked to the post-synaptic membrane through lipid anchors. Four cysteine residues present on the strand between the two SNARE motifs of SNAP25 covalently bind four palmitic acid residues on the surface of the membrane through S-palmitoylation.

Syntaxin and VAMP contain one SNARE motif, while SNAP25 contains two (Figure 1.5 A). All the isolated SNARE motifs are largely unstructured ^(66,67,68,69); upon interaction, they fold tightly together, forming the SNARE complex (Figure 1.5 B).

VAMP and syntaxin present transmembrane regions as part of the synaptic vesicle and presynaptic membrane, respectively (Figure 1.5 C).

Since the transmembrane and other accessory domains are not required for the assembly of the SNARE complex, in a significant proportion of the literature studying SNARE complex's structure, the experiments were carried out with truncated recombinant SNAREs (62). These recombinant proteins can form a vast range of α -helical bundles structures, with different compositions and configurations (67,70).

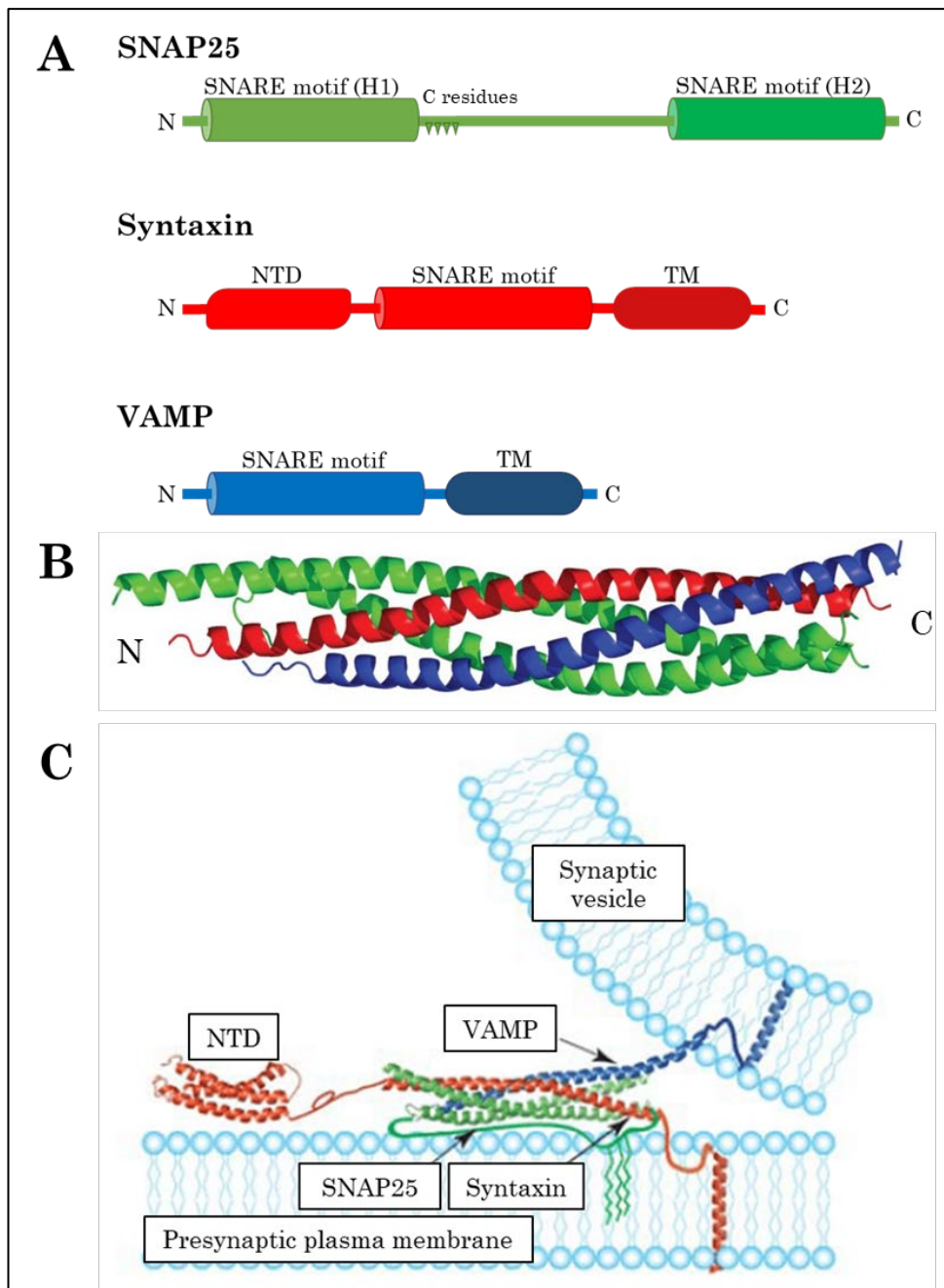


Figure 1.5 The neuronal SNARE complex. (A) Primary structure diagram for SNAP-25 (green), syntaxin (red), and VAMP (blue). SNARE motifs of each protein are represented by cylinders. Syntaxin and VAMP have a transmembrane domain (TM) at their C-terminal; syntaxin has an additional domain on its N-terminal (NTD). The two helices of SNAP25 are named H1 and H2. (B). X-ray crystal structure of the core of the *Rattus norvegicus* neuronal SNARE complex, formed by the SNARE motifs only (PDB ID 1SFC). The alignment is parallel, so all the α -helices are oriented N- to C- terminal. (C) The SNARE complex during neuronal vesicle docking. The proteins that form the SNARE complex are represented in different colours as in (A). Figure adapted from Brunger et al. (62).

1.2.2 SNARE complex formation

As mentioned above, all the SNAREs have one or two SNARE motif domains, which are very conserved among eukaryotes. The SNARE motif is the domain required to form the SNARE complex (see Figure 1.5 B); the four motifs together form an elongated four α -helix bundles with a parallel coiled-coil structure ⁽⁵⁹⁾. The SNARE complex formation starts from the N-terminal and proceeds towards the C-terminal direction ⁽⁷¹⁾.

The interactions between side chains of the four α -helices form the core of the bundles: 16 layers, mainly hydrophobic, with a central ionic layer involving three glutamine (Q) and one arginine (R) residues provided by the four α -helices (Figure 1.6). Other than the t- and v-SNARE classification, these proteins can be categorised based on the amino acid at the ionic layer, resulting in the R- and Q-SNAREs nomenclature ⁽⁷²⁾.

The ionic layer, also known as '0' layer, is protected from solvent thanks to the adjacent hydrophobic layers. It is highly conserved, although it can assume alternate conformations, as it has a role in the NSF-mediated disassembly of the SNARE complex (NSF stands for N-ethylmaleimide-sensitive factor) ⁽⁷³⁾.

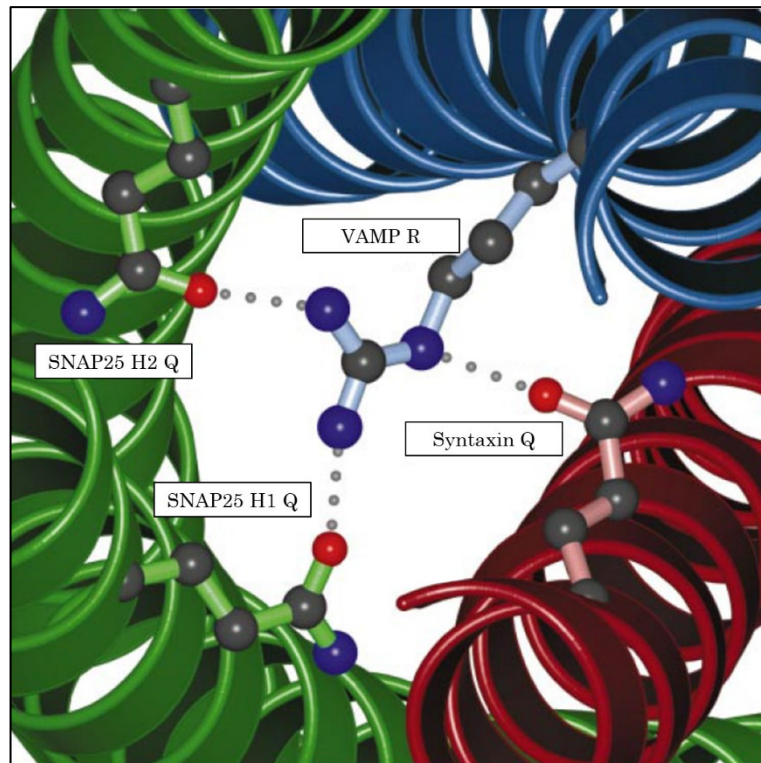


Figure 1.6 Ionic layer of the synaptic fusion complex. The side chains involved in the 'O' layer of the SNARE complex are labelled with their respective protein and amino acid; they are displayed as balls and sticks. Backbones of the proteins are shown as ribbons. Figure adapted from Sutton et al. (59).

1.2.3 SNARE complex properties

The SNARE complex shows remarkable thermal and chemical stability. The interaction between SNARE proteins is not covalent; however, it is unusually stable and essentially irreversible. In fact, disassembly of the SNARE complex in physiological conditions happens enzymatically (NSF-mediated) rather than being spontaneous. *In vitro*, the SNARE complex can withstand the denaturing conditions of Sodium Dodecyl Sulfate (SDS)

(⁷⁴), even though this property is not present in all eukaryotes (⁷⁰). Alternatively, the forced disassembly can occur upon heating over 90°C. Also, the SNARE complex exhibits resistance to cleavage by neurotoxins, whereas individual SNARE proteins are susceptible to them (⁷⁴).

The SNARE complex formation occurs thanks to the interaction between SNAP25, syntaxin and VAMP. Although largely unstructured when in solution, they acquire a strong α -helical conformation when together. The strength of the SNARE complex is needed to bind the two membranes together and form the fusion core; membranes are typically negatively charged, and therefore would not fuse spontaneously due to electrostatic repulsion. The amount of energy required to fuel the membrane fusion is provided by the assembly of the SNARE complex, which then allows the vesicle to release its content inside the target membrane. Studies on the formation of the SNARE complex showed a hierarchical interaction between the three proteins. SNAP25 and syntaxin's closeness on the plasma membrane surface leads to the formation of a binary complex between the two proteins (^{68,75,76}). Even when incubated together, there is a two-step assembly: the formation of a heterodimer of SNAP25-syntaxin happens first, then VAMP joins the other two proteins to form the ternary SNARE complex (see Figure 1.7). The formation of the SNAP-25-syntaxin binary complex significantly improves VAMP's binding affinity more than the single proteins alone (^{74,75}).

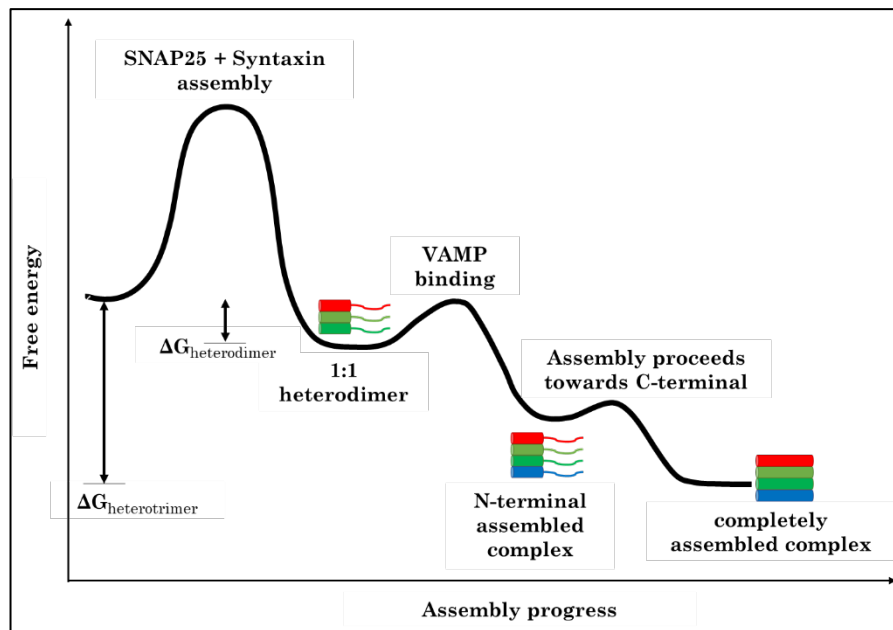


Figure 1.7 Simplified energy profile of the formation of the neuronal SNARE complex. The diagram shows that SNAP25 and syntaxin, both present on the plasma membrane, partially assemble into a heterodimer. The activation energy required for this step is lower ($\Delta G_{\text{heterodimer}}$), possibly due to other factors *in vivo*. The SNAP25-syntaxin heterodimer has a high affinity for VAMP; the proteins initially assemble at their N-terminal, proceeding towards C-terminal. The total energy released by the formation of the entire complex is indicated with $\Delta G_{\text{heterotrimer}}$. Figure reworked from Wiederhold et al. (75).

As seen in Figure 1.7, the formation of the four α -helix bundles releases energy, which is used to guide membrane fusion (61). The ternary complex has substantial stability compared to the heterodimer formed by SNAP25 and syntaxin.

Numerous researches were conducted on SNAREs, ranging from the investigation of complex formation (60,64) to detail studies on membrane fusion (77,78,79). The SNARE motifs play a vital role in the formation of the complex, and SNAREs were often engineered (through truncation, single amino acid modification) to study their behaviour (68,69,74,80).

1.3 Biochemical and biophysical characterisation of the SNARE complex

Several methods have been applied to characterise SNAREs and their interactions. This section reports examples from the literature of the most common biochemical characterisation method, Sodium Dodecyl Sulfate PolyAcrylamide Gel Electrophoresis (SDS-PAGE), and the most common biophysical tool, Circular Dichroism. Examples where protein-protein interaction was analysed by pulldown assays are also reported.

1.3.1 SDS-PAGE and GST-pulldown assay

Sodium dodecyl sulfate polyacrylamide gel electrophoresis, abbreviated as SDS-PAGE, is a well-known method to separate proteins based on their molecular weight. Samples, buffer and the gel contain sodium dodecyl sulfate; SDS is an anionic detergent that coats proteins with a uniform negative charge, masking the intrinsic protein charges. A reducing agent is also present within the loading buffer, usually β -mercapto ethanol or dithiothreitol (DTT), which, along with SDS, helps to disrupt the tertiary structure of proteins by breaking disulphide bonds. SDS coats proteins with a uniform negative charge; therefore, they run as linear molecules on the gel, with electrophoretic mobility depending only on their molecular

weight. The electric field attracts the SDS-coated proteins (negatively charged) towards the positive pole; larger proteins move slower than the small ones, caused by larger friction due to the viscosity of the gel. Protein standards, containing protein of known size, are run along with the protein samples to help identify their molecular weight.

SDS-PAGE is used for the characterisation of SNARE proteins not only to assess their size but also to study the formation of the complex. Previous studies showed that the SNARE complex could withstand the denaturing conditions of the SDS-PAGE gel ^(60,74,81). By heating samples containing the SNARE complex, Hayashi et al. were able to analyse the single components and their stoichiometry; moreover, they demonstrated that the SNARE complex did not disassemble upon freezing and thawing, and it was stable even when exposed to temperatures up to 60°C for 5 minutes ⁽⁷⁴⁾. SDS-PAGE has also been used as a readout to better understand the interactions and hierarchy of the SNARE complex formation, for example, through pulldown assays.

Pulldown assays are generally used to characterise protein binding interactions. The protein of interest is expressed (or later modified) as a glutathione S-transferase (GST) fusion protein to be paired with glutathione (GSH) Sepharose beads. This technique can be used for both purifying a protein from a lysate and for studying its interactions with other proteins when incubated together.

GST-pulldown assays are useful to analyse protein-protein interactions between the SNARE proteins and are routinely used to study the formation of the SNARE complex and the proteins involved in it (60, 82, 83).

As mentioned above, pulldowns can be analysed with SDS-PAGE; other methods such as fluorescence, can be utilised to assess protein-protein interaction when the protein carries a fluorescent probe (84).

1.3.2 Circular Dichroism spectroscopy

Circular dichroism spectroscopy is a technique in which the circular dichroism (CD) of molecules is measured over a specific range of wavelengths. CD spectroscopy can assess the changes in the secondary structure or conformation of macromolecules, particularly of proteins that have a secondary structure sensitive to its environment, temperature or pH (85, 86, 87). For thermo-sensitive proteins, it is possible to understand their conformational changes with the increase of the temperature (88).

Circular dichroism was widely used as a rational way to analyse SNAREs (60, 68, 69, 75), since their SNARE domains are unstructured when taken individually, acquiring an α -helical conformation only when placed together. When measured by CD spectroscopy, each one of the three main protein conformations generates a different type of curve in the spectrum.

A marked double minimum at 208 and 222 nm indicate α -helical structure, while a single minimum below 200 nm or around 217 nm reflects random-coil and β -sheet, respectively (Figure 1.8).

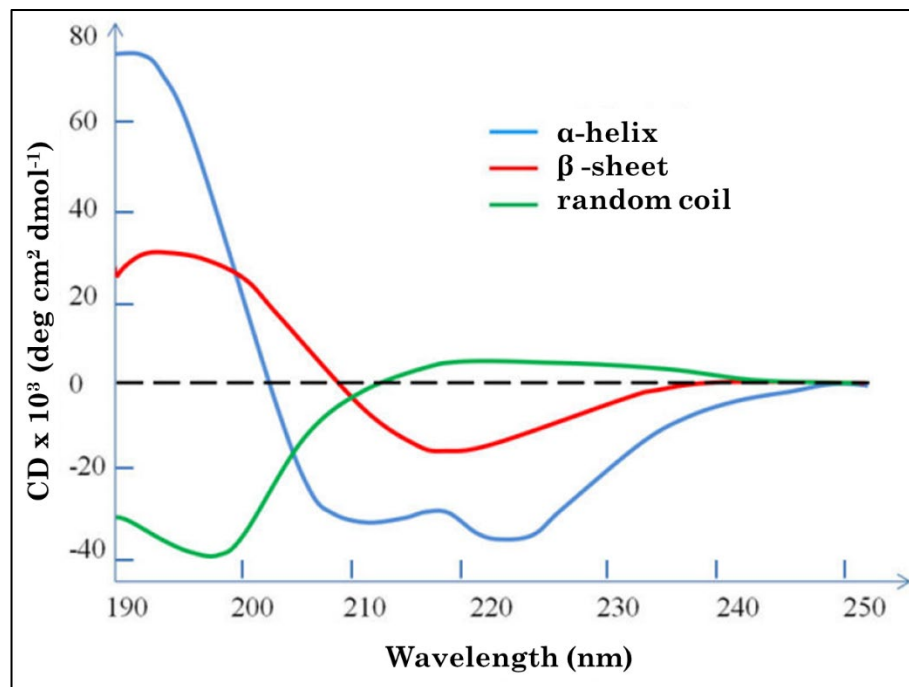


Figure 1.8 Typical far-UV SRCD spectra of proteins' secondary structures. Differences between CD spectra of α -helix, β -sheet and random coil's secondary structures. In blue, two minima peaks at 208 and 222 nm characterise α -helical structures; in red, a single minimum at 217 represents β -sheets, while in green the random coil conformation shows a minimum peak below 200nm. Figure from Wei et al. (89).

SNAREs follow the typical circular dichroism α -helix pattern, with a double minimum at 208 and 222 nm, due to the interactions between SNAP25, syntaxin and VAMP's SNARE motifs, the strands responsible for the formation of the four α -helix bundles. Figure 1.9 below shows that the α -helical component of the SNARE complex reduces when diluting syntaxin's concentration. SNARE motifs are unstructured when separated, acquiring

an α -helical conformation when in solution together with the formation of the four α -helix bundles (⁹⁰).

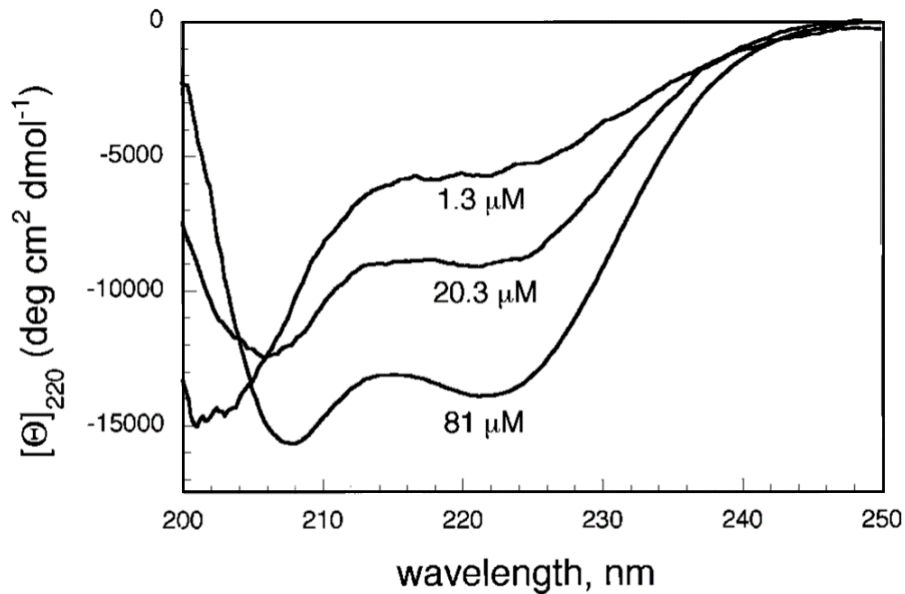


Figure 1.9 Far-UV SRCD spectra of SNARE complexes with different syntaxin concentration. SNAP25, syntaxin and VAMP were mixed together to allow the formation of the SNARE complex. SNAP25 and VAMP were maintained at the same concentration (81 μ M), while the quantity of syntaxin was reduced (to 20.3 and 1.3 μ M). The spectra show a progressive decrease in α -helicity upon dilution of syntaxin SNARE motif. CD spectra were recorded at three different protein concentrations (40 mM sodium phosphate buffer). The minima peaks correspond to 208 and 222 nm, characteristic features of the α -helical secondary structure. Figure from Margittai et al. (⁹⁰).

SNAP25, syntaxin and VAMP spontaneously assemble into a strong ternary complex, with a melting temperature (T_m) around 90°C. Circular dichroism spectroscopy is, therefore, a valid tool to analyse SNAREs' secondary structure and its conformational changes concerning temperature variations (^{59,60,91}). Melting curves can be obtained analysing the CD signal at 222nm at different set temperatures, allowing the analysis of SNARE's behaviour upon heating to high temperatures.

1.4 Engineering of recombinant SNAREs

SNAREs have been engineered for decades to study and understand their structural features. Most of them focused on the investigation of complex formation (^{60,64}), with detailed studies on their role in membrane fusion (^{77,78,79}) and binding regions (⁹²).

SNAREs were often engineered, for example, through truncation and single amino acid modification, to study their ability to form the SNARE complex (^{68,69,74,80}). The SNARE motifs play a vital role in the formation of the four α -helix bundles, a structure with remarkable strength and thermal stability despite being non-covalently bound. SNAREs' sequences were manipulated to test its ability to retain such properties. Evidence showed that the formation of the complex is still possible with one truncated helix; however, the strength of the complex is reduced (^{60,69,93}).

There are numerous studies on SNAREs as a bioconjugation system: Darios et al. used SNAP25, syntaxin and VAMP as versatile tags for a modular medicinal toxin, botulinum neurotoxin A. The research group linked two of the three SNARE proteins with the toxin's domains that are inactive when taken individually: once reassembled driven by SNARE complex formation, the toxin became active and inhibited the release of neurotransmitters by targeted neuronal cells (⁸⁴). SNARE tagging can,

therefore, be employed to target specific cells. Analogously, Ferrari et al. demonstrated that SNAREs could be exploited as protein tags for the irreversible combination of different protein domains ⁽⁹⁴⁾.

SNAREs can also be used to develop new immobilisations systems: Ferrari et al. demonstrated that it is possible to immobilise SNARE proteins on gold nanoparticles ⁽⁸¹⁾. They engineered the three SNARE proteins into two fusions, linking together VAMP and SNAP25, subsequently proving the ability of this SNARE fusion to bind its partner, syntaxin. A second set of SNARE fusions, with VAMP linked to syntaxin and SNAP25 acting as intended partner, was developed; thanks to a GST-fusion tag, they were both immobilised on different gold nanoparticles (GNPs). The SNARE fusion protein immobilised on the GNPs was capable of capturing the second component in solution, with no changes on their ability to form the SNARE complex. This study proves the possibility to engineer the ternary SNARE complex into a binary one, with the preservation of the ability to form the complex even when immobilised on a surface.

1.5 Aim of the project

The aim is to develop a binary protein complex, immobilised on a surface, able to assemble spontaneously and disassemble in response to a change of temperature.

This work is built on previous evidence that SNAREs can be used for immobilisation on surfaces^(81,82) (see Section 1.4), and its α -helices can be manipulated to modify its stability⁽⁹³⁾. Shortening of a SNARE domain was attempted before⁽⁹³⁾; however, it has never been exploited for thermoresponsive materials.

The project's three main aims:

- (i) modulation of the SNARE complex's melting temperature by shortening of SNARE domains;
- (ii) re-arrangement of SNARE domains, including the shortened ones, to engineer a thermoresponsive binary SNARE complex;
- (iii) immobilisation and temperature-mediated release of the binary SNARE complex from a surface.

1.5.1 Modulation of the SNARE complex's thermal stability

The SNARE proteins assemble in a parallel coiled-coil secondary structure with significant stability. The research focuses on *Rattus norvegicus* neuronal SNAREs, extensively studied in past literature (72,95,96). The design of new recombinant SNAREs focuses on the preservation of the SNARE motif, eliminating the transmembrane domains from the designed sequences.

Numerous studies indicate that the SNARE complex can form even when one of the helices involved is truncated (60,68,80,94), yet it weakens its chemical stability. The ionic layer has a crucial role in the maintenance of the core complex stability so it is omitted in the design of the shortened α -helix. Among the three proteins contributing to the SNARE complex, SNAP25 and syntaxin initially bind on the plasma membrane's surface. VAMP is the last one to associate for the formation of the complex (68) and is hence chosen to be manipulated. Two versions of VAMP are designed: a 54- and a 25-amino acid long protein, the latter truncated on the C-terminus (see Figure 1.10). Previous studies showed that mutations at the N- and C-terminal side of SNARE proteins had different effects on the formation of the complex. Mutations at the N-terminal reduced the assembly of the complex, while C-terminal ones displayed no collateral effects (71).

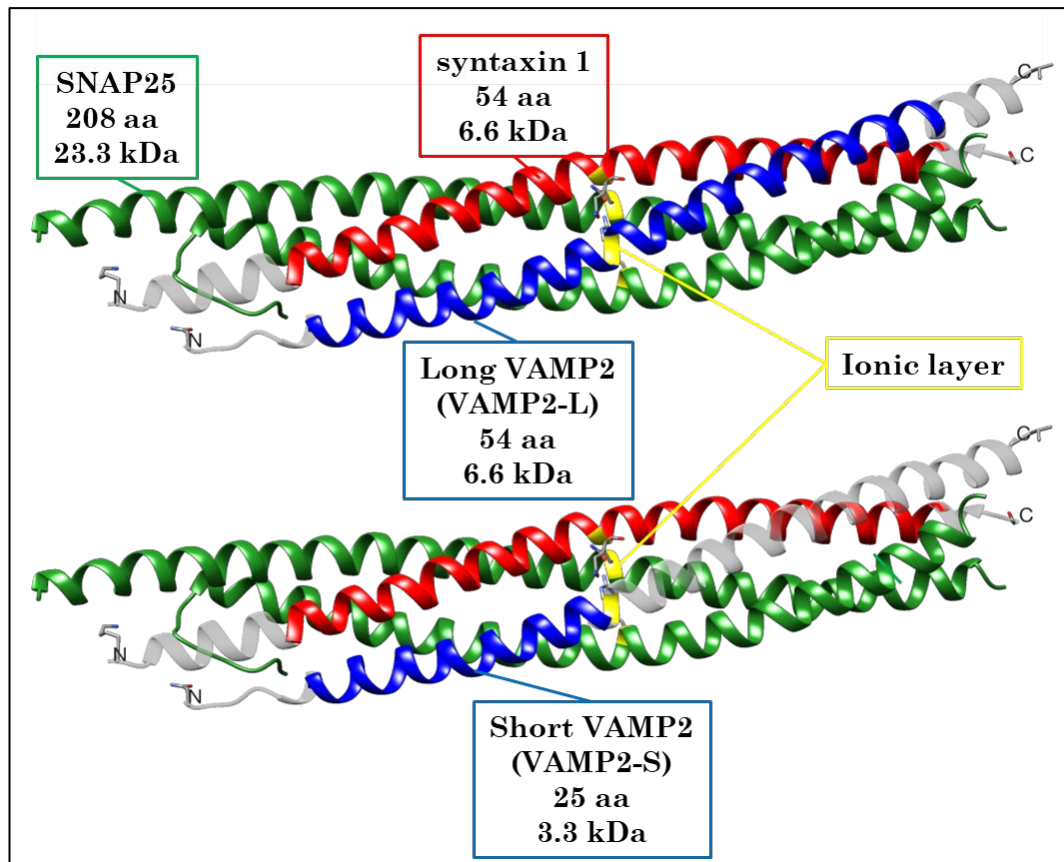


Figure 1.10 Truncation of the SNARE complex. The SNARE complex structure (PDB ID: 1SFC) is here represented with colour-coded sequences, highlighting the SNARE domains preserved in this project's design. The SNARE complex has parallel alignment and, in this representation, the N-terminals of each polypeptide are all on the left. The N- and C-terminals of the SNARE domain polypeptides were chosen to span from the first coil (N-terminal) of the VAMP2 to the last coil (C-terminal) of Syntaxin 1, while preserving the same overall polypeptide length. This represents the 'core' SNARE complex, which presents typical features of a coiled-coil structure. SNARE motifs of SNAP25, syntaxin 1 and VAMP2 are colour-coded, in green, red and blue respectively. Molecular weight and amino acid length are included in the description box. A second VAMP2, which differs in length and was named VAMP2-S (Short), spans for 25 amino acids, as its sequence was truncated before the ionic layer (highlighted in yellow). The shortened version of VAMP2 was designed to weaken the complex's thermal stability. On the top, the structure of the SNARE complex, with the three 54 amino acids long proteins highlighted in different colours. On the bottom, the newly designed version of the SNARE complex with the shortened version of VAMP2, truncated before the ionic layer (highlighted in yellow).

1.5.2 Engineering of binary SNARE complexes

The SNARE proteins assemble in a supramolecular structure formed by four α -helices, with three proteins contributing to the formation of the bundle. However, this ternary system is not entirely suitable for biotechnological applications (^{81,84,94}).

The design of a binary SNARE complex would be favourable, as one element of the complex could be immobilised, whereas the second could be captured and released. The possibility to link together different SNARE fragments to form a recombinant protein allows the design of a variety of different combinations. Studies on the interactions between different SNARE proteins were examined; previous research showed that the binding affinity between VAMP and syntaxin is the weakest among the SNARE proteins (⁸⁰). Therefore, the new SNARE fusion protein consists of syntaxin and VAMP linked together, whereas the second protein is a derivative of SNAP25 (Figure 1.11).

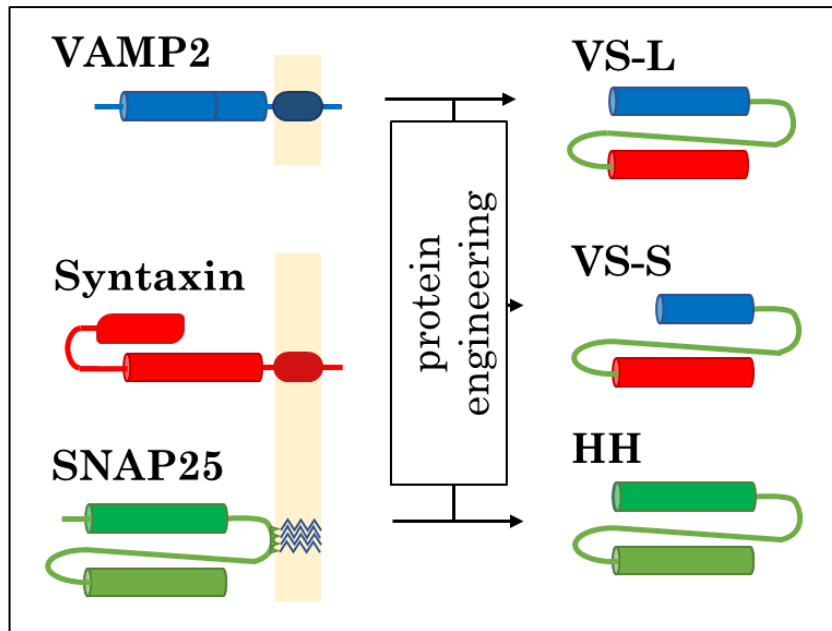


Figure 1.11 From ternary to binary: engineering of the SNARE complex. The three SNARE proteins are rearranged into SNARE fusions. Syntaxin and VAMP's SNARE motifs, represented as cylinders, are fused together into two separate SNARE fusions (VS), differing on the VAMP's length (L-Long and S-Short). The linker between the two motifs is the naturally occurring linker found between the two α -helices of SNAP25. HH is an analogue of SNAP25: its two SNARE motifs, represented as cylinders, are preserved along with the linker between the two of them. In all the fusion proteins, the four cysteine residues present in the linker, responsible of securing the protein to the membrane, are mutated to Alanine to avoid the formation of disulphide bonds. HH and VS partner to form the SNARE complex.

1.5.3 Thermo-release of surface-immobilised proteins

SNARE proteins have never been developed as thermoresponsive materials. The binary SNARE complex above addresses this as its properties are suitable for self-assembly and temperature-triggered disassembly. A SNAP25 derivative is immobilised on a solid-liquid interface by the addition of a GST domain⁽⁹⁷⁾ (see Figure 1.12).

The ability of the immobilised SNAP25 to capture and release the VAMP-syntaxin fusion in response to temperature increase is reported here and represents the first evidence of a new thermoresponsive released system based on engineered SNARE proteins.

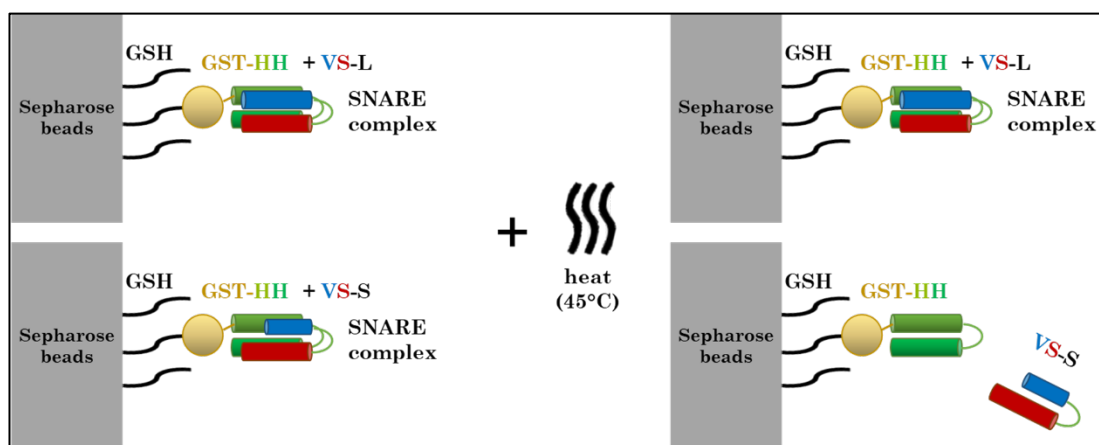


Figure 1.12 Schematic representation of the immobilisation and release of a binary SNARE complex from a surface. HH is expressed as a GST-fused protein and immobilised onto GSH Sepharose beads thanks to the high affinity between GSH and GST. GST-HH is capable to bind both kinds of VS (Long and Short), forming the SNARE complex. Upon mild heating (45°C), the shortened version can be disassembled from GST-HH, while the longer VS, more stable, is still attached to the beads.

2. MATERIALS AND METHODS

2.1 Protein design

All the SNARE mimics used throughout this work were from *Rattus norvegicus*. The design focused on the neuronal SNARE motifs, omitting transmembrane and other accessory domains, with the exception of the linker in between the two SNARE domains of SNAP25 (see Table 2.1).

Construct	Components	Original name	UniProtKB	Amino acids
SNAP25	\	Rat SNAP25B	P60881	1-206
Syntaxin 1	\	Rat Syntaxin 1A	P32851	149-202
VAMP2-L	\	Rat VAMP2	P63045	31-84
VAMP2-S	\	Rat VAMP2	P63045	31-55
Syntaxin 3	\	Rat Syntaxin 3	Q08849	200-253
HH	H1	Rat SNAP25B	P60881	28-81
	l	Rat SNAP25B	P60881	82-148
	H2	Rat SNAP25B	P60881	149-202

Table 2.1 SNARE protein constructs. Single and fusion proteins list, their UniProtKB access numbers and relative amino acidic sequence. All the mentioned proteins are neuronal SNAREs from *Rattus norvegicus*. The HH construct is an alternative to SNAP25, formed by H1, H2 and l. H1 and H2 are the two α -helix sequences of SNAP25, while l is the unstructured linker located between them. The amino acid sequence of all proteins can be found in the Appendix (Table A.1).

VAMP2 was designed in two forms, one long (L) and one short (S) to manipulate the SNARE complex's thermal stability. VAMP2-L is 54 amino acids long and spans the entire SNARE motif. In VAMP2-S, however, the C-terminal was truncated before the ionic layer, resulting in a total length of 25 amino acids (see Table 2.2). The removal of the ionic layer was intended to avoid possible interference with the assembly of experimental conditions other than temperatures, such as change of pH and subsequent change of the overall charge. Also, improved assembly upon removal of the ionic layer of a shortened SNARE (syntaxin), in comparison to a shortened domain inclusive of the ionic layer, was reported before ⁽⁹⁴⁾. The shortened VAMP2 was designed to study the impact of shortening on the formation and thermal stability of the SNARE complex. A cysteine residue was added at the C-terminal of both VAMP2-L and VAMP2-S to facilitate site-directed chemical cross-linking modifications, for example, fluorescent labelling (see below).

PROTEIN	SEQUENCE												
	5	10	15	20	25	30	35	40	45	50	54		
VAMP2-L	RLQQTQAQVDEVVVDIMRVNV	DKVLE	RDQKLSE	LDDRADALQAGASQFET	SAAKL							54 aa	
VAMP2-S	RLQQTQAQVDEVVVDIMRVNV	DKVLE										25 aa	

Table 2.2 Sequences of VAMP2. Two different VAMP2 were designed, one spanning the entire SNARE motif (54 amino acids), the other truncated just before the ionic layer (25 amino acids). The sequences are represented from N- to C- terminal; the residue taking part in the ionic layer is highlighted in yellow.

Syntaxin 1 was also 54 amino acids long, which spans the entire SNARE motif and matches the length of VAMP2-L. Syntaxin 3 with same amino acid length was used in some experiment and constructs, due to its better expression rate in bacteria and engineering potential, compared to the most common partner of the neuronal SNARE complex syntaxin 1 (84).

SNAP25's expression plasmid was kindly provided by the MRC Laboratory of Molecular Biology (Cambridge, UK). The plasmid encoded the full-length protein but all the four cysteine residues in between the SNARE domains, which are involved in post-translational modifications in eukaryotes, were mutated into Alanine to avoid the unwanted formation of disulphide bonds. An alternative version of SNAP25 named HH was designed to have its SNARE motifs matching the amino acid length of VAMP2-L and the syntaxins (54 amino acids). The C-terminal and N-terminal SNARE domains of SNAP25 were truncated to 54 amino acids and fused using the same linker of SNAP25 above (the linker is named l in Table 2.1), with all the four cysteine residues mutated into Alanine. The fusion protein was named HH to underline the presence of the two SNAP25 α -helical (H) domains (see Table 2.1).

2.1.1 Design of SNARE fusions

Besides individual SNARE proteins, several hybrid fusion proteins, including SNARE domains from different SNAREs were designed; the purpose was to make a binary version of the naturally ternary SNARE complex. Sequences from Table 2.1 were combined, as indicated in Table 2.3, but many SNARE fusions were either poorly expressed or difficult to elute due to low solubility (data not shown). The full synthesis and characterisation of binary complexes were carried over only for the most promising SNARE fusions (number 9, 10, and 11 in Table 2.3).



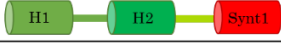
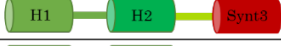
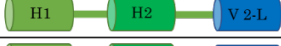
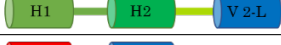





Nr	Final name	SNARE fusions	Intended partner
1	N/A	Synt1-l-H1-l-H2 	VAMP2-L or VAMP2-S
2	N/A	H1-l-H2-l-Synt1 	VAMP2-L or VAMP2-S
3	N/A	H1-l-H2-k-Synt1 	VAMP2-L or VAMP2-S
4	N/A	H1-l-H2-k-Synt3 	VAMP2-L or VAMP2-S
5	N/A	H1-l-H2-l-VAMP2-L 	Syntaxin 1 or 3
6	N/A	H1-l-H2-k-VAMP2-L 	Syntaxin 1 or 3
7	N/A	Synt1-l-VAMP2-L 	HH
8	N/A	Synt1-l-VAMP2-S 	HH
9	VS-L	VAMP2-L-l-Synt3 	HH
10	VS-S	VAMP2-S-l-Synt3 	HH
11	VS-L2	VAMP2-L-k-Synt3 	HH

Table 2.3 List of SNARE fusion designed and attempted. Eleven different SNARE fusion proteins were designed and expressed. SNARE motifs are represented as cylinders, while linkers as horizontal lines. The colour code helps distinguish the different motifs: red from syntaxins, green for SNAP25 (light for the first helix, dark for the second one), blue for VAMP2. The truncated VAMP2 is in light blue; the SNAP25 linker is in green, while the alternative one is represented in yellow. The protein fusions highlighted in grey were carried over and are described in detail in the following sections.

The new SNARE fusions were named VS-L (-L for Long) and VS-S (-S for short), concerning the length of the VAMP2 (54 or 25 amino acids long). The shortened version was designed to weaken the thermal stability of the overall complex. They were cloned, synthesised and characterised along with individual SNAREs as described in the following sections. An alternative version of VS-L, carrying the linker k and named VS-L2, was designed to exclude any interference of the linkers in the ability to form the SNARE complex. This artificial linker is a sequence of 48 glycine and serine residues, slightly smaller than the SNAP25 linker (67 amino acids long). Glycine and serine were chosen to give flexibility to the linker without carrying any charged residue.

2.2 Cloning

The amino acid sequences of target proteins were reverse translated⁽⁹⁸⁾ to DNA using a codon table for optimal expression in *E. coli*. A leading (TCTAGATGATCA) and an ending sequence (GGATCCTAGGAGCTC), respectively carrying the restriction sites of *Bcl*I and *Sac*I, were added so that the DNA could be cut and inserted into a pGEX-KG GST gene fusion system (Addgene) via double enzymatic digestion, isolation of the fragment and consequent ligation. Synthetic DNA was purchased as synthetic genes cloned in pBSK II SK(-) vectors (Dundee Cell Products) encoding individual

SNARE domains or linkers designed as described in the previous section, except for VAMP2-S polypeptide, that was obtained by annealing of two ssDNA oligos with complementary sequence (IDT DNA Technologies).

2.2.1 Subcloning of synthetic genes

Purchased cloning vectors containing the DNA of interest were subcloned in expression vector pGEX-KG (Addgene). The constructs for SNARE fusions and HH, requiring more than one DNA sequence, were cloned iteratively, using a convenient modular approach developed for this project (see Section 2.2.3).

2.2.2 Propagation of unmethylated plasmid DNA

As *Bcl*I digestion is sensitive to DNA methylation, plasmids were propagated in methyltransferase-deficient *E. coli* competent cells (C2925I, New England BioLabs). 1 μ l of the vector was incubated for 30' in ice with 30 μ l of C2925I competent cells, followed by heat shock (42°C for 2' then in ice for 4') for DNA uptake. 300 μ l of super optimal broth (SOB) medium pre-warmed at 37°C were used to grow the bacteria for 1 h at room

temperature under agitation (1000 rpm). After incubation, 10 µl and 100 µl of the culture were spread onto two Luria-Bertani (LB) agar plates containing 100 µg/ml ampicillin to select only the transformed cells. The plates were incubated over-night at 37°C until colonies were big enough to be well visible. One colony was selected to grow in a 20ml sterile tube with 5 ml of 2xTY (16 g/L tryptone, 10 g/L yeast extract, 5.0 g/L NaCl) medium containing 50 µg/ml ampicillin. The mini-culture was grown overnight at 37°C to bring the population at saturation. Once grown, 2 ml of the culture were pipetted into 2ml Eppendorf tubes to harvest bacteria by centrifugation using a benchtop centrifuge at 3000 g. QIAprep Spin Miniprep Kit (QIAGEN) was used to extract the plasmids from each pellet, following the procedure indicated by the supplier. Once the column dried, the DNA was eluted with 50 µl of milli-Q water in a 1.5 ml Eppendorf tube. 2 µl of purified plasmid DNA were used to measure DNA concentration and purity using a Nanodrop spectrophotometer (Thermo Fisher Scientific).

2.2.3 Double digestion of origin and destination plasmids

Un-methylated pBSK vector containing the insert of interest and pGEX-KG expression plasmid (Addgene) were double digested for subsequent oriented annealing and ligation. The destination vector was digested at the

multiple cloning site using *Bam*HI and *Sac*I, while *Bcl*II and *Sac*I were used for the origin vector, as these pairs result in matching sticky ends (Figure 2.1). Specifically, *Bam*HI and *Bcl*II digestions both produce a GATC overhang, but upon annealing and ligation of a *Bcl*II end onto the *Bam*HI end from the destination vector, the original *Bam*HI restriction site 5'-GGATCC-3' will become 5'-GGATCA-3' and the vector will be protected from further *Bam*HI digestion at this location. All the inserts used in this work have been provided with an adaptor at the 3' end which carries a *Bam*HI site just before the stop codon and the *Sac*I restriction site. Therefore, the subcloning will produce a plasmid that can be still digested using the *Bam*HI/*Sac*I pair and serve as the destination vector of another *Bcl*II/*Bam*HI insert that will be expressed at the C-terminal of the product of the first sequence.

This modular approach was designed to iteratively clone different combinations of SNARE domains, starting from a limited number of building blocks (BB). For example, three iterations of the cloning using three different BBs designed with same adaptors would result in the tandem 5'-BB1-BB2-BB3-3'. The sequence at the adaptors at both ends and in between the BBs conveniently encodes for the amino acids glycine and serine, providing an uncharged, small and yet flexible linker between domains.

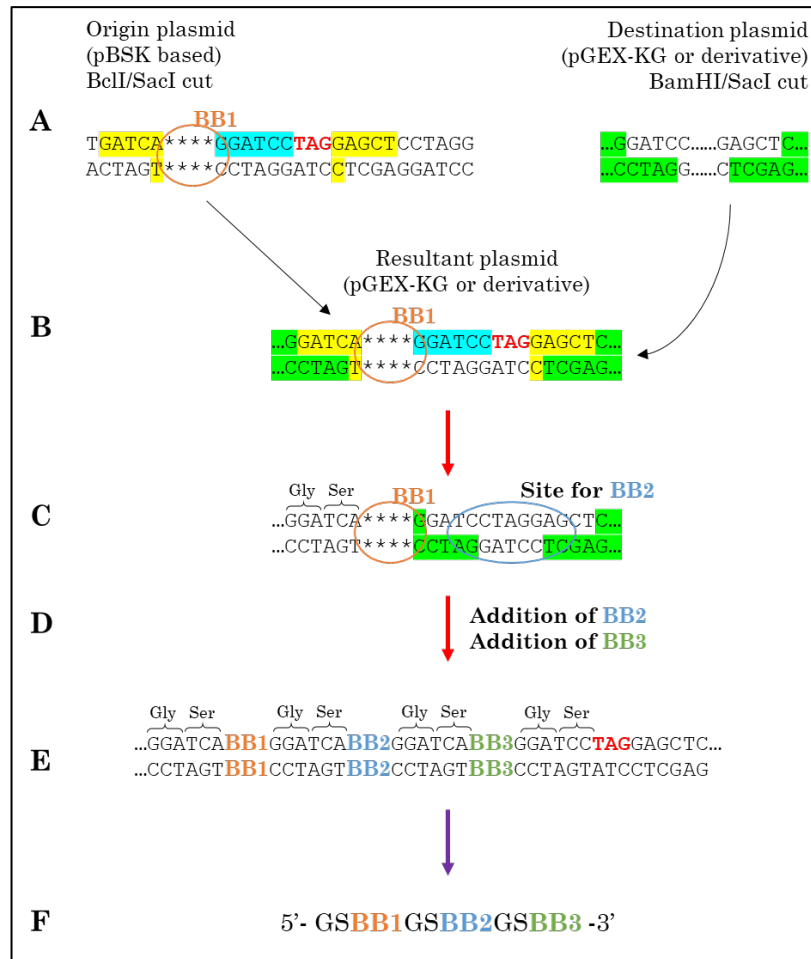


Figure 2.1 Outline of the modular cloning strategy. (A) Enzymatic digestion generates sticky ends in both origin and destination plasmid (highlighted in yellow and green, respectively); the stars (*) represent Building Block 1 (BB1), the first DNA segment of interest. (B) The result of the ligation: BB1 was inserted in the pGEX-KG plasmid. A new *Bam*HI site (turquoise), followed by a red stop codon, allows a “reset” of the resultant plasmid. (C) The same plasmid becomes a new destination plasmid that can host an insert with the same design (highlighted in green the sticky ends generated by the new *Bam*HI/*Sac*I cut). (D) Thanks to this cloning strategy, BB 2 and 3 can be added to the plasmid. (E) GGATCA bases between Building Blocks codify for a Glycine and Serine residues. (F) The Building Blocks will be expressed as one protein, separated by GS residues.

Double digestions were performed as follows. All the enzymes used were provided by New England BioLabs. 6 µl of the destination vector pGEX-KG were mixed with 7 µl of milli-Q water, 1.5 µl of 10x CutSmart Buffer and

0.25 µl of both *Bam*HI_HF and *Sac*I. 35 µl of un-methylated pBSK vector containing the insert were mixed with 4 µl of 10x CutSmart Buffer and 0.5 µl of both *Bcl*II and *Sac*I. The reactions were incubated at 37°C for 1 h; *Bcl*II/*Sac*I double digestions were incubated for one extra hour at 50°C, as it is *Bcl*II's optimum incubation temperature. All the reactions were then incubated for 10' at 65°C to inactivate the enzymes and limit non-specific digestion products that may occur with extended incubations. pGEX-KG was stored for subsequent use in ligation reactions, whereas the DNA insert of interest was purified from the digested origin vector using the procedure described below.

2.2.4 Purification of a double digested DNA insert

To ensure a high yield of the purified insert for easy extraction from an agarose gel, the volume of the insert digestion above was set to 40 µl. First, 5 µl of the digestion mixed with 1 µl of 6X DNA loading buffer was loaded in 1% Agarose gel containing 1X SYBR safe (Thermo Fisher Scientific), along with a sample of the corresponding uncut plasmid and 1Kb DNA ladder, to check for successful enzymatic digestion. The gel ran in tris-borate-EDTA (TBE) buffer for 30' at 100 V. Once the presence of the fragment was confirmed, the remaining 35 µl of the digestion were mixed with 7 µl of 6X loading buffer and loaded on the same gel along with a 100

bp DNA ladder under the same conditions as the last run. To isolate the DNA fragment, the gel was excised with a scalpel in a dark room on a UV transilluminator, and the part was placed in a 2 ml Eppendorf tube. The fragment was purified with a QIAquick Gel Extraction Kit following the procedure indicated by the supplier. The DNA insert was eluted in 50 µl of milli-Q water and stored at -20°C for further insertion into the relevant destination vectors.

2.2.5 Synthesis of a DNA insert by annealing of ssDNA oligos

As agarose gel purification of short DNA inserts and their subclonings present challenges, the small insert required to encode VAMP2-S was obtained from DNA oligos instead of using synthetic genes and the subcloning procedure described so far. The amino acid sequences of VAMP2-S was reverse translated to DNA as the genes described above. Also, a reverse complement was obtained, naming the two sequences Oligo1 and Oligo2, respectively. A leading (GATCA) and ending (GGATCCTAGGAGCT) sequences were added to Oligo1. Only a leading sequence (CCTAGGATCC) and a simple nucleotide T at the end were added to Oligo2. These were required for the cloning; moreover, they facilitated the insertion of another fragment following the modular

approach (see Section 2.2.3). The synthetic oligos service was provided by IDT DNA Technologies as standard desalted oligos shipped dried in tubes (0.05 micromoles). A 100 μ M working stock solution of the oligos was prepared by mixing Oligo1 and Oligo2, along with 200 mM NaCl and milli-Q water. The mixture was incubated at 95°C in a heat block for 10' and left to cool down at room temperature for 2 h.

As the design and the resulting sticky ends of the annealed oligos are fully compatible with the modular cloning strategy described above, the DNA insert was used in subsequent ligation in the same way as any other building block obtained from synthetic genes.

2.2.6 Ligation

The ligation reactions between DNA fragments presenting oriented sticky ends were assembled using 16 μ l of purified or annealed DNA insert, 2 μ l of 10x T4 DNA Ligase buffer, 2 μ l of digested pGEX-KG (or pGEX-KG containing previously subcloned building blocks) and 1 μ l of T4 Ligase (New England Biolabs), in a total volume of 20 μ l. The reaction took place at 37°C for 2 h. After this, the ligase was inactivated at 65°C for 20'.

1 μ l of the ligation reactions was used to transform 30 μ l of competent cells. C2925I methyltransferase-deficient competent cells were utilised whenever additional cloning steps were required; alternatively, XL1 blue

competent cells (Agilent) were used when plasmids did not require any subsequent restriction using methylation-sensitive *BclI*. The cells and ligation product mixture were incubated for 30' in ice, followed by a heat shock (42°C for 2' then in ice for 4'). 300 µl of SOB medium pre-warmed at 37°C were added to grow bacteria for 1 h at room temperature in agitation (1000 rpm). To select only cells with ligation products, 10 µl and 100 µl of the sample were spread on LB agar plates containing 100 µg/ml ampicillin. The two different concentrations were used due to the unknown transformation efficiency after ligation.

The plates were incubated over-night at 37°C until colonies were big enough to be visible. Three or four colonies were collected, and each was grown in a 20 ml sterile tube with 5 ml of 2xTY containing 50 µg/ml ampicillin. The mini-cultures were grown overnight at 37°C, and 2 ml of saturated cultures were pipetted into 2 ml Eppendorf tubes to harvest bacteria by centrifugation on a benchtop centrifuge at 3000 g. QIAprep Spin Miniprep Kit (QIAGEN) was used to extract the plasmid, using the procedure indicated by the supplier. Once the column dried, the DNA was eluted with 50 µl of milli-Q water in a 1.5 ml Eppendorf tube. 2 µl of purified plasmid DNA was used to measure DNA concentration and purity using a Nanodrop spectrophotometer (Thermo Fisher Scientific).

2.2.7 Verification of the cloning

Samples of three to four purified plasmids per ligation were screened for the presence of the target DNA using double digestion. A 15 µl reaction was made up of 6µl of plasmid DNA, 7 µl of milli-Q water, 1.5 µl of 10x CutSmart Buffer and 0.25 µl of two selected enzymes between *SacI*, *NarI*, *AvrII* and *EcoRV*. The exact pair was selected depending on the target sequence, so one restriction site was within the expected insert and the other elsewhere in the expression vector. The double digestion reaction was incubated at 37°C for 1 h, then 10' at 65°C to inactivate the enzymes. To check the digestion pattern, 5 µl of the reaction were mixed with 1 µl of 6X DNA loading buffer and loaded on 1% Agarose gel containing 1X SYBR safe (Thermo Fisher Scientific), along with a sample of undigested plasmid and 1 Kb DNA ladder. The gel ran for 1h at 100 V.

An example of such verification is shown in Figure 2.2, where the plasmid coding for VAMP2-L+linker is compared to the VAMP2-L alone. The digestion of these two plasmids with *AvrII* and *EcoRV* produces different fragments, visible on the gel. From their size, it is possible to assess which clones have been successfully ligated.

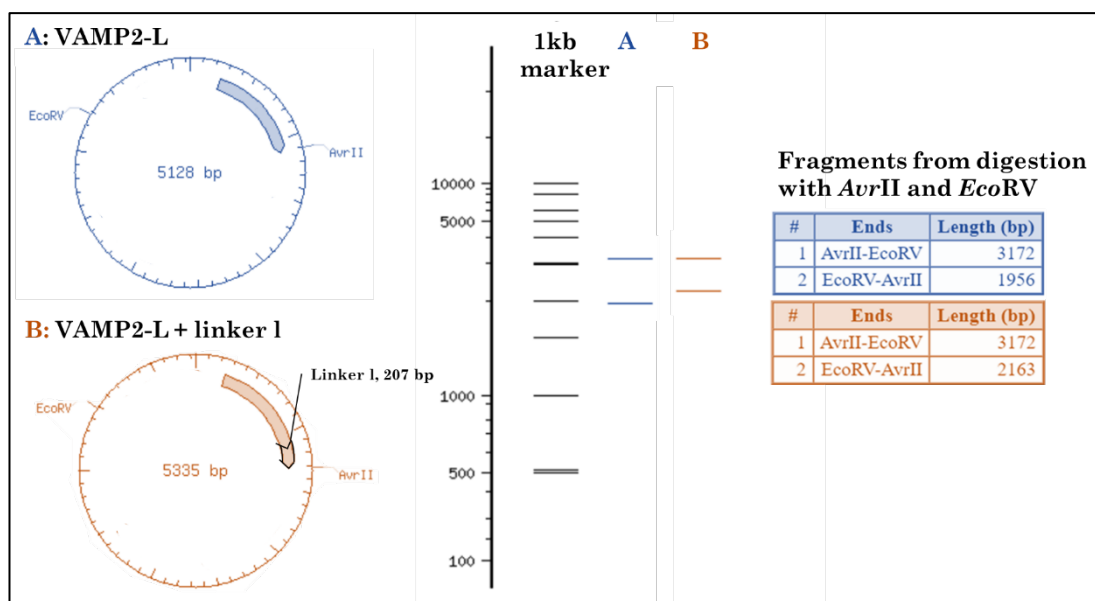


Figure 2.2 Example of successful insertion verification. On the left, the plasmid map of pGEX-KG_VAMP2-L and pGEX-KG_VAMP2-L+linker I. The arrows represent the inserts of interest; on the bottom one, the addition of linker I has been marked in black. The enzymes chosen for this specific digestion were *AvrII* and *EcoRV*, with sites indicated on the map; the sequence recognised by *AvrII* (CCTAGG) can be found near the end of both inserts, as it is part of the ending sequence added during the first step of the cloning process (GGATCCTAGGAGCTC, see Section 2.2). In the central part of the image, the view of fragments originated from the restriction run on a 0.7% agarose gel, along with a 1kb DNA ladder. A stands for VAMP2-L while B indicates VAMP2-L+linker I. The insertion of the linker adds 207 bp to the *EcoRV-AvrII* fragment; therefore, the difference between the two plasmids is easily identifiable on the gel run. On the right, the restriction fragments obtained *in silico*, following the colour scheme: blue for VAMP2-L and orange for VAMP2-L+linker I. Images reworked from results obtained with NEBCutter2.0 (New England Biolabs).

The selected plasmids, whose digestion pattern suggested the presence of an insert, were delivered to Source Bioscience (Rochdale) and sequenced using the standard primer pGEX5 to confirm the sequence of the insert and conclusively select the successful clones (see Section B of the Appendix for DNA sequencing data).

2.3 Protein expression and purification

All the recombinant proteins were expressed in BL21-gold (DE3) pLysS cells, which is a strain of *E. coli* suitable for low-temperature expression induced by isopropyl β -d-1-thiogalactopyranoside (IPTG).

2.3.1 Transformation of competent cells

30 μ l of BL21-gold (DE3) pLysS cells (Agilent) were incubated for 30' in ice with 1 μ l of the expression vector containing the desired insert. The procedure used was similar to the one described for cloning. However, in addition to ampicillin used to select the plasmid containing the DNA insert, 100 μ g/ml chloramphenicol were also added to the LB plates and media, as the induction-control plasmid pLysS carried by this strain expresses a chloramphenicol resistance gene. Moreover, the volumes of the bacterial culture spread onto the plates were smaller compared to the transformations described for cloning, specifically 5 μ l and 50 μ l, due to the extremely high transformation efficiency and fast growth rate of these *E. coli* competent cells.

2.3.2 Low-temperature expression and purification of GST fusion proteins

Selected individual colonies from the transformation plates were placed in 50 ml falcon tubes with 5 ml of 2xTY (16 g/L tryptone, 10 g/L yeast extract, 5.0 g/L NaCl) medium containing 50 µg/ml of ampicillin and 50 µg/ml of chloramphenicol. Falcon tubes were incubated overnight at 37°C; the resulting saturated cultures were poured into 500 ml of 2xTY medium within 2-litre flasks, containing 50 µg/ml of both ampicillin and chloramphenicol. The large volume of the flasks ensured adequate aeration during the 2 h 30' incubation at 37°C in a shaker incubator (Innova S44i, Eppendorf). The incubation was stopped when the optical density (OD) at 600 nm was between 0.5 and 0.7. This OD value corresponds to the optimal exponential phase of bacterial growth, as they have not yet reached the stationary phase, leaving them space to grow further without compromising their vitality.

Protein expression was induced by adding 0.1 mM IPTG (Melford), and the flasks were incubated overnight at 18°C in agitation. The bacterial cultures containing the overexpressed protein were poured into 500 ml polycarbonate bottles and were spun at 3000 g for 20' in a Beckman J25 centrifuge equipped with a JLA-10.500 rotor to pellet the bacteria and remove the growth media. Pelleted bacteria were kept in ice, suspended in

10 ml of 20 mM HEPES (4-(2-hydroxyethyl)-1-piperazine-ethane-sulfonic acid, ThermoFisher Scientific), 500 mM NaCl and 1 mM EDTA (ethylenediaminetetraacetic acid, Sigma-Aldrich). Once transferred into 50 ml falcon tubes, 300 μ l of complete protease inhibitor cocktail (Roche, from a 50X stock) were added, along with 10 μ l of 1 mM DTT (dithiothreitol, Sigma-Aldrich). Cell walls were disrupted by temperature shock using fast-freezing in liquid nitrogen for 10', followed by thawing in the water at room temperature for 30'. 12 μ l of 1M MgCl₂ stock were added along with 400 μ l of 1 mg/ml deoxyribonuclease I from bovine pancreas (Sigma-Aldrich) to reduce the viscosity of the lysate due to nucleic acids. The mixtures were left to rotate at room temperature for 10'. 1.5 ml of 0.1% v/v triton (TX-100) was added to achieve a final concentration of 2% and incubated for 20' at 4°C to disrupt cell membranes.

Affinity purification was carried out using Glutathione Sepharose 4B resin (GE Healthcare). As all the proteins of interest were expressed as a C-terminal fusion to a GST affinity tag from pGEX-KG derived expression plasmids, the glutathione (GSH)/GST interaction allowed their easy separation from other proteins in the bacterial lysate. 1 ml of GSH Sepharose beads was washed twice by centrifugation for 1' at 1500 g within a 15 ml falcon tube and using a 20 mM HEPES, 100 mM NaCl, 0.1% v/v TX-100 and 1 mM EDTA Low Salt buffer. The lysate was pelleted at 10000 g for 20' at 4°C using a J25 centrifuge (Beckman) equipped with JA-25.50 rotor. The pellet containing insoluble fraction was discharged, while the

soluble protein-rich supernatant was poured onto the GSH Sepharose beads and incubated in constant and slow rotation for 1 h 30' at 4°C.

The unbound fraction (flow-through) was removed by centrifugation using the same conditions used when washing the beads. The beads were washed twice using a 20 mM HEPES, 1 M NaCl, 1 mM EDTA and 0.1% v/v TX-100 buffer with the same centrifuge settings. 15 µl of 1 mM DTT were added at each washing step to prevent the formation of unwanted disulphide bonds. Two extra washes were carried out in the same way with Low Salt buffer (see above), which was also used for final resuspension to a volume of 7 ml. Additional 15 µl of 1 mM DTT and 8ml of glycerol were added to the beads and mixed well before storage at -20°C. 1 µl of supernatant, 1 µl of flow-through and 2 µl of washed beads were mixed with 10 µl of 1X loading buffer. Samples were heated at 100°C for 5' and then loaded on an SDS PAGE gel (12% pre-cast polyacrylamide gel, Expedeon) along with a protein marker (Precision Plus, BioRad). The gel was run at 170 V for 1 h with 1X SDS RunBlue running buffer (Expedeon) and stained using InstantBlue (Expedeon) to verify protein expression and purity.

2.3.3 Protein elution

Proteins were eluted from affinity GSH Sepharose beads using thrombin cleavage site (amino acid sequence LVPRGS) encoded in pGEX-KG and located between the GST tag gene and the multiple cloning site. The beads with the GST protein captured were washed twice with storage buffer (20 mM HEPES, 100 mM NaCl, pH=7.4), the volume of the suspension was brought to 2 ml, and the beads were transferred in a 2 ml Eppendorf tube. 100 μ l of thrombin (Sigma-Aldrich) were added to the beads; the mixture was incubated for 1 h at room temperature under mild agitation.

After incubation, the beads were loaded on a spin column with a filter cup (Thermo Fisher Scientific) and centrifuged at 3000 g on a benchtop centrifuge to separate GSH Sepharose beads from the eluate. 30 μ l of Protease Inhibitor Cocktail (Roche) were added to the eluate to stop thrombin cleavage. The beads were then resuspended in 1.5 ml of storage buffer. 2 μ l of the beads before and after cleavage and 1 μ l of the eluate were prepared for SDS-PAGE by mixing with 10 μ l of loading buffer. Samples were heated at 100°C for 5' and load on the gel after cooling. The gel was run at 170 V for 1 h with 1X SDS RunBlue running buffer. InstantBlue stained gel was used to evaluate the efficacy of elution by thrombin cleavage.

Proteins for which the GST tag was retained (GST-HH and control GST), were eluted using excess glutathione in solution instead of proteolysis. The GSH Sepharose beads with the GST-protein immobilised on them were washed twice with storage buffer, and then incubated for 30' at 4°C in 5 ml of GSH elution buffer (15 mM Glutathione H, 20 mM HEPES and 250 mM NaCl, pH=8.5).

After incubation, the beads were spun, and the eluate was saved. 1 ml of extra GSH elution buffer was added again to the beads and incubated for 15' at 4°C to increase the yield of elution. The beads were spun again, and the second eluate was saved. 5 ml of storage buffer were used to resuspend the beads. 2 µl of first and second eluate and the resuspended GSH Sepharose beads were loaded onto an SDS-PAGE mixed with 10 µl of loading buffer. Samples were heated to 100°C for 5' before loading. The gel was run at 170 V for 1 h with 1X SDS RunBlue running buffer and stained with InstantBlue to verify the elution.

2.3.4 Fluorescent labelling

Eluted proteins requiring incorporation of a fluorescent probe were labelled after elution using Cy5-maleimide (GE Healthcare), which reacts with free thiols at cysteine residues. A Vivaspin column (GE Healthcare) with a

molecular weight cut off of 3 kDa (VAMP2-S) or 10 kDa (all other proteins) was used to reduce the volume of the eluate down to ~600 µl.

The proteins (>50 µM concentration) were incubated with 4 µl of 0.5 M tris 2-carboxyethyl phosphine (TCEP), a reducing agent, for 2 h at room temperature. 10 µl of maleimide-activated Cy5 (10 mg/ml in DMSO) were added and initially incubated for 30' at room temperature. Incubation was prolonged at 4°C overnight to increase the yield of the reaction. Excess fluorophore was removed following subsequent purification by size exclusion chromatography (see below). SDS-PAGE of fluorescently-labelled proteins was analysed using Odyssey (LI-COR Imaging System). The gel was observed at the 700 nm channel, as Cy5 absorbance peak is at 649 nm.

2.3.4 Fast Protein Liquid Chromatography

A Vivaspin column (GE Healthcare) with a molecular weight cut off of 10 kDa (3 kDa in the case of VAMP2-S) was used to reduce the volume of the eluate down to ~600 µl. The concentrated protein was separated by size exclusion chromatography using an ÄKTA Pure chromatography system (GE Healthcare) equipped with Superdex 75 10/300 GL column (alternatively, a Superdex 200 10/300 GL column).

The elution in storage buffer (20 mM HEPES, 100 mM NaCl) was collected in 1ml fractions, and those showing high absorbance at 280 nm were loaded onto an SDS-PAGE gel to confirm molecular weight. 9 μ l of the samples were mixed with 3 μ l of 4X loading buffer, heated to 100°C for 5', and loaded with a protein marker (Precision Plus, BioRad). The gel was then run at 170 V for 1 h with 1X SDS RunBlue running buffer and stained using InstantBlue.

The fractions where the protein of interest was confirmed by molecular weight and the concentration was visibly high were combined, aliquoted and stored at -80°C.

2.4 Protein characterisation

The SNARE proteins and SNARE constructs characterisation is described below; it started with the determination of their concentration, followed by tests on their SNARE complex's formation capabilities and thermal stability. In addition, their capture-and-release abilities were examined.

2.4.1 Protein concentration determination

Protein determination was obtained by bicinchoninic acid (BCA) assay (Pierce, Thermo Fisher Scientific) and performed in triplicate for each protein against a standard curve obtained from Bovine Serum Albumin (BSA) standards (ThermoFisher). The assay was performed using the microplate procedure documented by the supplier, and absorbance of standards and unknown samples were read using an Infinite 200 Pro plate reader (TECAN).

2.4.2 Synchrotron Radiation Circular Dichroism

Synchrotron Radiation Circular Dichroism (SRCD) was used to assess the formation of the SNARE complex once the SNARE proteins were mixed. All the Circular Dichroism measurements were performed at the B23 beamline for SRCD at Diamond Light Source (UK) ⁽⁸⁵⁾. Each test contained 2 μ M protein solutions diluted in 5mM HEPES (pH 7.3) and 25 mM NaCl. Far-UV SRCD spectra, in the range of 180-260 nm, were recorded using a cylindrical cuvette with 0.2 mm optical path (Starna) in constant rotation.

Temperature scans were obtained using a custom Peltier device embedded into the cuvette holder at the B23 beamline. The temperature span chosen for the thermal unfolding assay was 25-95°C. The SRCD spectra were recorded at increasing temperatures with an interval of 2.5°C. The temperature was increased at the rate of 1°C per minute, followed by a 2 minutes equilibration before collecting the spectrum.

The thermal unfolding curves were plotted by selecting the data points at 222 nm over the range of temperatures scanned (⁹⁹). All SRCD spectra were processed using the software CDApps (¹⁰⁰).

2.4.3 Pull-down and controlled release

Pull-down assays were performed to study protein-protein interactions (¹⁰¹). A traditional pull-down experiment was used to assess the ability of GSH Sepharose beads modified with GST-HH to capture VS-L and VS-S, forming the SNARE complex. A modified pull-down assay with washing steps at different temperatures was also developed to evaluate the responsive release of engineered SNAREs in a range of temperatures.

GSH Sepharose beads were incubated with 5 μ M of either GST-HH or GST (acting as a negative control) for 1 hour at constant agitation. Further 1-hour incubation with 7.5 μ M of VS was followed by thorough washing with 20 mM HEPES pH7.3 and 100 mM NaCl. SDS-PAGE electrophoresis of beads after washing was carried out using 12% RunBlue SDS pre-cast protein gels (Expedeon), stained using InstantBlue (Expedeon) and imaged using ChemiDoc imaging system (Biorad). SDS-PAGE of beads could only provide a qualitative estimation of the protein amount retained.

To easily detect the signal of the amount of protein immobilised on the GSH Sepharose beads after pull-down and monitor their controlled release at different temperatures, a 5 μ M excess of either VS-L-Cy5 or VS-S-Cy5 were incubated with Sepharose-GST-HH beads, as for the pull-down mentioned above. After 1 h of incubation, the excess of VS was removed through two washes with a 20 mM HEPES pH7.3 and 100 mM NaCl (pH storage buffer followed by 1' centrifugations at 7000 g. Nine fractions of the Sepharose-GST-HH/VS complexes were incubated for 20 minutes at a set temperature (from 20°C to 80°) in a heat block. A set of Eppendorf tubes containing 2 ml of 20 mM HEPES and 100 mM NaCl buffer were incubated along with the samples. After a 30" centrifugation at 7000 g, the quick removal of the supernatant (which contained the unbound protein) was followed by a wash with the above-mentioned heated buffer at the same incubation temperature. The samples were then re-spun at 7000 g for 1'. The supernatant was removed again and the Sepharose-GST-HH/VS

complexes were resuspended in storage buffer at 20°C. The residual Cy5 fluorescence in the fractions was measured with Infinite 200 Pro plate reader (TECAN), excitation and emission wavelength of 640 and 680 nm, respectively. This number represents the proportion of VS still bound to the surface at each tested temperature.

Furthermore, the ability to capture and release VS has been tested with repeated cycles of heating and cooling at 20°C. The heating temperature varied according to the VS used: the Sepharose-GST-HH/VS-L-Cy5 system was heated up to 90°C, while VS-S-Cy5 reached a maximum temperature of 50°C. The repeats were carried out on five different sets of solutions, from 0 up to 4 cycles.

3. RESULTS

3.1 Modulation of SNARE complex thermal stability

The native SNARE complex shows self-assembling properties combined with exceptional thermal stability, with a melting temperature around 85°C (67). This property derives from the highly stable coiled-coil structure formed by the four α -helices of the three SNARE proteins. The initial aim was to verify whether shortening of VAMP2's SNARE domain would result in a decreased melting temperature of the SNARE complex so that a new set of engineered SNAREs could be technologically used to modulate the dissociation temperature of protein complexes.

Two versions of VAMP2 were designed: a long (VAMP2-L) and a short one (VAMP2-S). SNAP25, syntaxin 1, VAMP2-L and VAMP2-S (see Supplementary Table A.1 for their sequences) were expressed and purified as described in Section 2.3; affinity purification, elution and FPLC chromatography results of all the proteins are shown in Section C of the Appendix.

To assess the ability of the recombinant SNAREs to form the expected α -helical coiled-coil, the proteins were tested using Synchrotron Radiation Circular Dichroism (SRCD). When individually tested, the SNARE proteins were unstructured as expected, whereas the α -helical structure formed when all the three SNAREs were combined, showing a prominent peak at 222 nm in the SRCD spectrum (Figure 3.1).

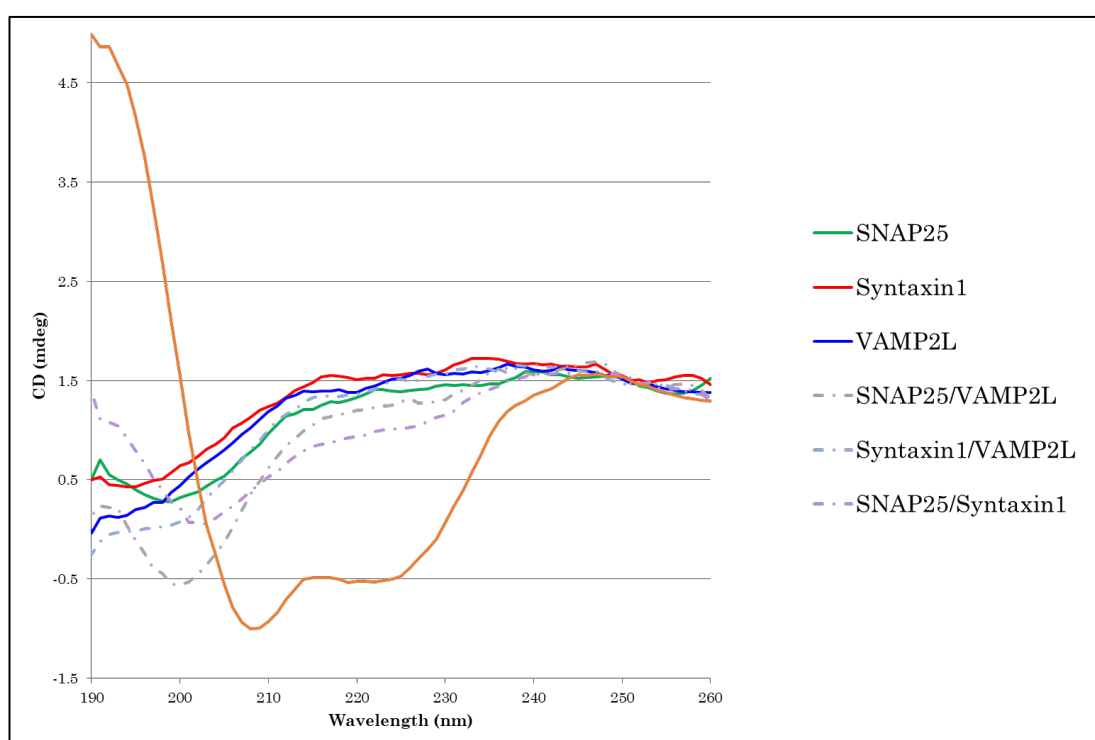


Figure 3.1 Far-UV SRCD spectra of SNARE proteins. SNAP25, syntaxin 1 and VAMP2-L were tested individually, in pairs and ternary complexes. Each protein was 2 μ M, pH=7.3, at room temperature (20°C). The SNARE complex formed with VAMP2 Long is shown in orange and displays the typical α -helix spectrum. The data shown represents the average of three different measurements (n=3).

To rule out possible interactions between pairs of SNARE proteins, SNAP25, syntaxin 1 and VAMP2-L were tested alone and also in pairs. When SNAP25 was assessed in combination with syntaxin 1 there was some proportion of α -helical structure, suggesting some interaction between these components as previously reported (75). When assembled, SNAP25, syntaxin, 1, and VAMP2-L produced an SRCD spectrum with a clear α -helix pattern, with a double minimum at 208 and 222 nm.

Previous evidence showed that shortening of one of the components of the SNARE complex does not prevent complex formation (94). However, it was not clear if this modification would affect the complex's melting temperature and, therefore, its stability. SNARE complexes formed by SNAP25, syntaxin 1 and VAMP2-S or VAMP2-L were first compared using SRCD to analyse their secondary structure at the equivalent concentrations. Figure 3.2 shows that both complexes present the α -helix pattern, with a double minimum at 208 and 222 nm. The CD signal of the VAMP2-S complex is less well defined than the complex formed with VAMP2-L, most likely as the shortened VAMP domain leads to a shorter α -helical coiled-coil in the overall complex.

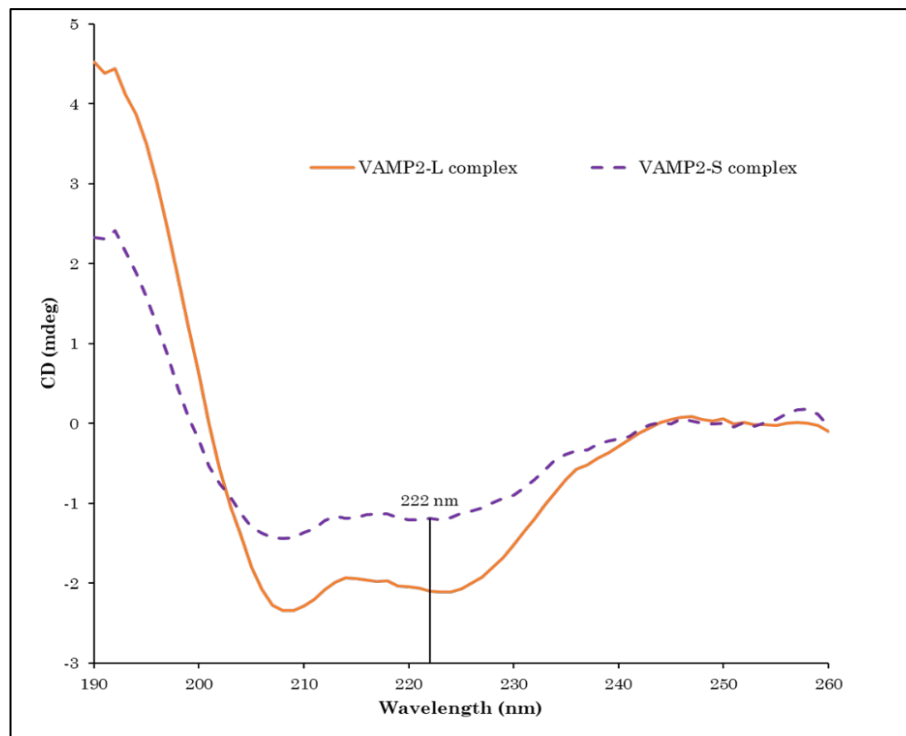


Figure 3.2 Far-UV SRCD spectra of VAMP2-L and VAMP2-S complexes. Both SNARE complexes, formed by SNAP25, syntaxin, and VAMP2 (S or L), were tested under the same conditions (2 μ M, pH=7.3, 20°C). The peak highlighted at 222 nm corresponds to one of the characteristic features of the α -helical secondary structure, and was later used to show the disassembly of the complex. The data shown represents the average of three different measurements (n=3).

SRCD can be used to show changes in the secondary structure of proteins in response to their environment, temperature or pH. A melting temperature assay was designed to estimate the thermal stability of SNARE complexes with different VAMP2 lengths. Far-UV SRCD spectra were recorded while the complexes were gradually heated from 20°C to 95°C degrees. After plotting the CD signal at 222 nm versus the temperature, the melting temperature (T_m) of the complexes was calculated as the temperature at which 50% of the maximum intensity at 222 nm (% unfolding) was lost (Figure 3.3). The results show that the

melting temperature dropped significantly from 79.6°C to 42.5°C as a consequence of shortening of one helix, suggesting that this is a sufficient protein modification that can be used to modulate the SNARE complex's thermal stability.

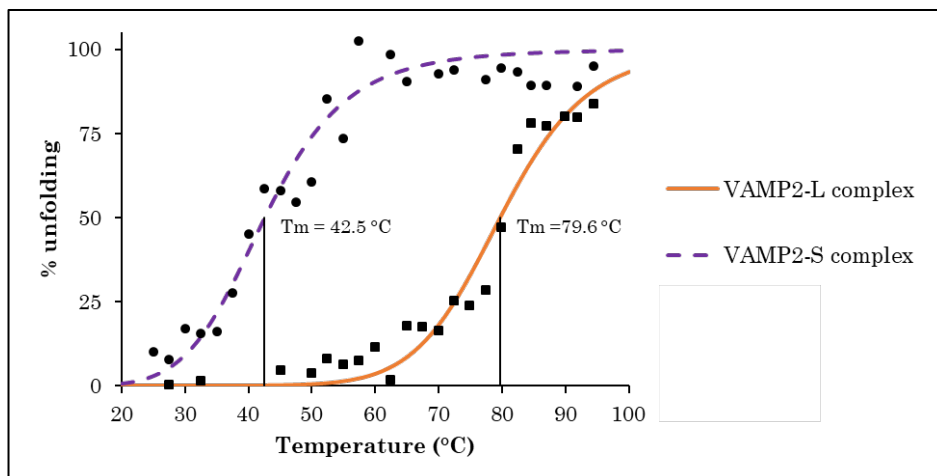


Figure 3.3 CD temperature scan of VAMP2-L and VAMP2-S SNARE complex. The SNARE complex unfolding is expressed here as the percentage of change of CD signal at 222 nm (over a value of 100 extrapolated at an infinite temperature and corresponding to a fully denatured protein). The melting temperature (T_m) is derived by fitting the data to a sigmoid and represents the temperature value at which 50% unfolding is achieved. Each data point represents the average of three measurements at the given temperature.

3.2 Engineering of binary SNARE complexes

Having established that the SNARE complex's thermal stability can be modulated by shortening of a SNARE domain, we speculated that the ability of a shortened SNARE complex to dissociate at relatively low temperature could be harnessed to engineer a thermoresponsive interface for the release of proteins. The system being binary, rather than ternary, would facilitate the immobilisation of one component on a surface, for the consequent release of the second moiety. The released molecule could be used as a thermoresponsive tag for the fusion of target proteins, for which reversible immobilisation on surfaces is required.

Previous attempts at making binary SNARE complex for protein immobilisation on surfaces exist ⁽⁸⁴⁾. However, no systematic design or temperature sensitivity has been reported.

The design of the binary complex was examined to establish an optimal combination of SNARE domains and identify a suitable unstructured linker to connect the structured domain in their native parallel coiled-coil conformation. The naturally occurring linker that connects the first and second SNARE domain of native SNAP25 was chosen to link also other SNARE domains, such as the SNARE motifs of syntaxin or VAMP. To avoid possible formation of unwanted intermolecular disulphide bridges that would complicate the interpretation of assembly and disassembly data, all

the cysteine residues were converted to alanine. When producing fusions of two of the three SNARE proteins together via this linker, many of those SNARE fusions (see Table 2.3) were either poorly expressed or difficult to elute due to low solubility (see Section D of the Appendix).

Many of the attempts made involved the use of syntaxin 1. As previously reported (⁸⁴), this protein has lower expression in bacteria compared to syntaxin 3 (see Table 2.1), which was chosen to replace syntaxin 1: their ability to form the SNARE complex were compared performing SRCD, along with SNAP25 and VAMP2-L (See Figure 3.4). The use of syntaxin 3 showed no differences in the formation of the complex, and it was therefore selected as one of the final components of the SNARE fusions.

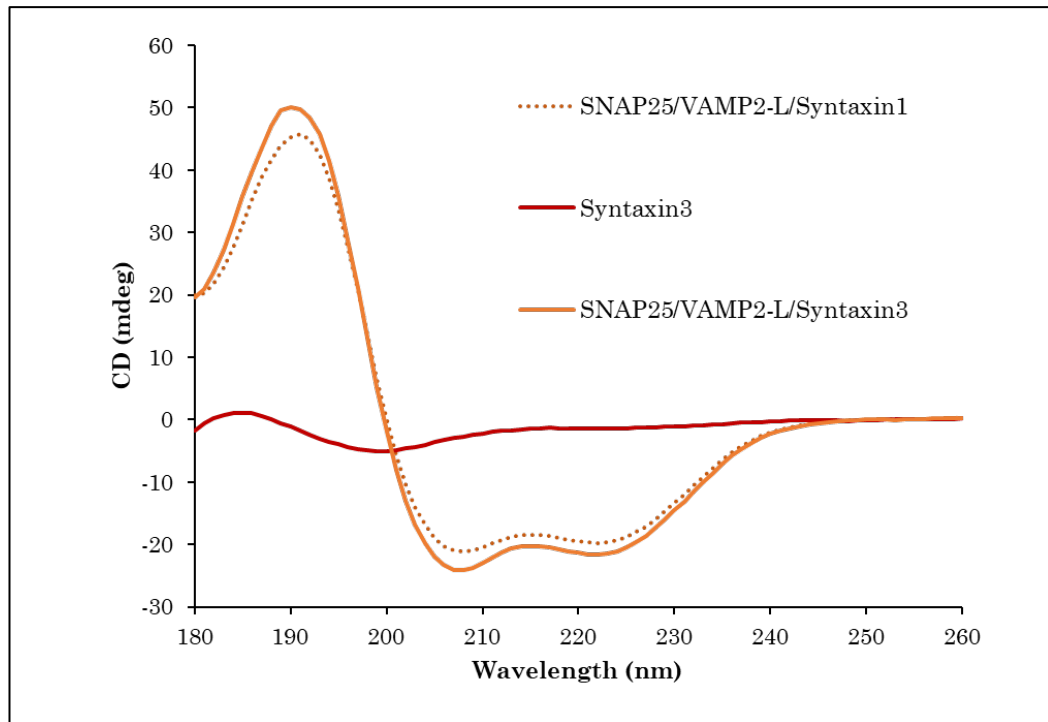


Figure 3.4 Far-UV SRCD spectra of SNARE complexes with different syntaxins.

The SNARE complexes made of SNAP25, VAMP2-L and either syntaxin 1 or syntaxin 3 were tested under the same conditions: 20 μ M, pH=7.3, 20°C. Both complexes show the typical α -helical secondary structure, regardless of the type of syntaxin involved in the complex. In red, the spectrum of the Syntaxin 3 alone is shown. The data shown represents the average of three different measurements (n=3).

The SNARE fusions' final design took into consideration the previous attempts and resulted in the fusion of VAMP2 at the N-terminal and syntaxin3 at the C-terminal, separated by the mimic of the SNAP25 linker (see Section 2.1.1). Two proteins were obtained, and they were named VS-L and VS-S, depending on the length of the VAMP2 domain, which had equivalent lengths to those tested above.

Another SNARE fusion named HH was developed as an alternative to SNAP25. HH was designed to match the SNARE motif length of VAMP2-L and syntaxin (54 amino acids). The C-terminal and N-terminal SNARE domains of SNAP25 were truncated and fused using the naturally occurring linker between helices of SNAP25 (see Table 2.1). HH was the intended partner for the VS SNARE fusions in the formation of the SNARE complex. The purification results of HH, VS-L and VS-S can be seen in Appendix Figure C.6, C.7 and C.8 respectively.

Tests to assess VS-L and VS-S ability to form a SNARE complex with HH were performed using SRCD (see Figure 3.5). Both VS fusion proteins were able to form a SNARE complex with HH, as evidenced by the spectra suggesting the prominent presence of α -helices, whereas individual HH, VS-L and VS-S spectra were compatible with an unstructured conformation.

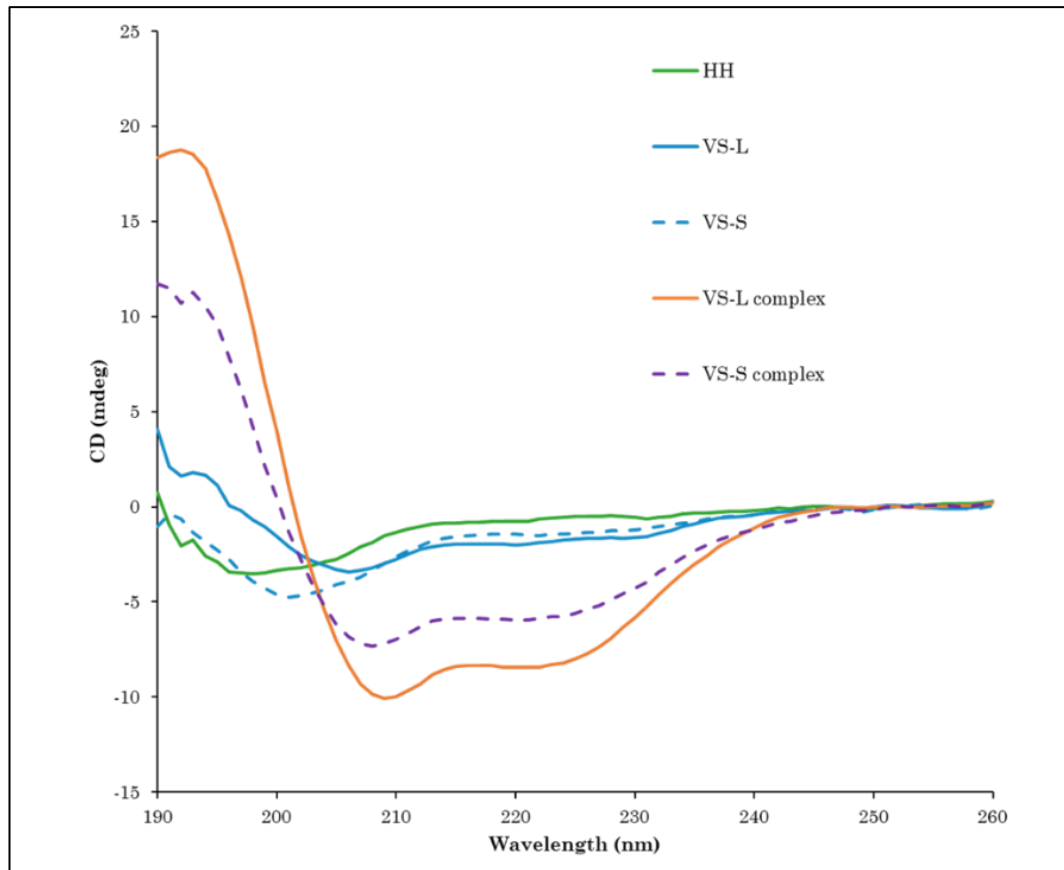


Figure 3.5 Far-UV SRCD spectra of VS-L and VS-S complexes and their single components. HH, VS-L and VS-S were tested under the same conditions: 8 μ M, pH=7.3, 20°C. They are unstructured when tested individually in solution; when assembled, they form a clear α -helical secondary structure, with minima peaks at 208 and 222 nm. The data shown represents the average of three different measurements (n=3).

These results were in line with those obtained with the ternary equivalents of the SNARE complexes, with both the ternary and binary complexes containing VAMP2-S showing less α -helical component than those containing VAMP2-L.

A melting temperature assay was performed with VS-L and VS-S complexes (see Section 2.4.2) using SRCD, similarly to those made using ternary complexes (Figure 3.6). The T_m of the full-length and shortened fusion complexes show a remarkable difference, 79.9° and 43.3°C respectively. The melting temperature drop is consistent with the results obtained for the ternary complexes' melting curves. This result suggests that the disassembly properties depends on the length of the SNARE domains, rather than on their specific arrangement in the form of a ternary or binary complex.

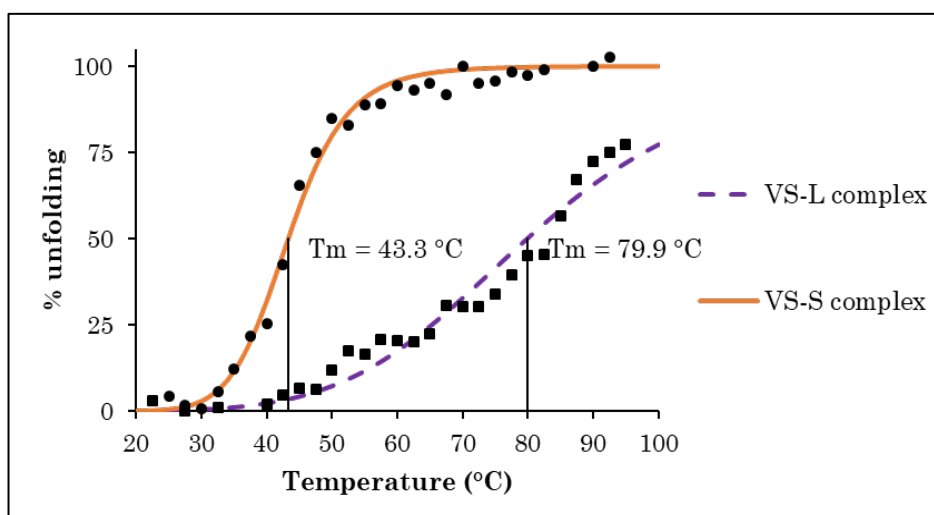


Figure 3.6 CD temperature scan of VS-L and VS-S SNARE complex. The SNARE complex unfolding is here expressed as the percentage of increase of CD signal at 222 nm (over a value of 100 extrapolated at an infinite temperature). The melting temperature (T_m) is derived by fitting the data to a sigmoid and represents the temperature value at which 50% unfolding is achieved. Each data point represents the average of three measurements at the given temperature.

An alternative linker was designed to rule out any effect of the unstructured strand in the formation of the SNARE complex. This artificial linker, named k, is a sequence of glycine and serine residues. It was used in the design of an alternative VS-L, called VS-L2 (see Table 2.3): SRCD spectra of the two SNARE fusions combined with HH were collected and compared to test the formation of the SNARE complex (see Figure 3.7).

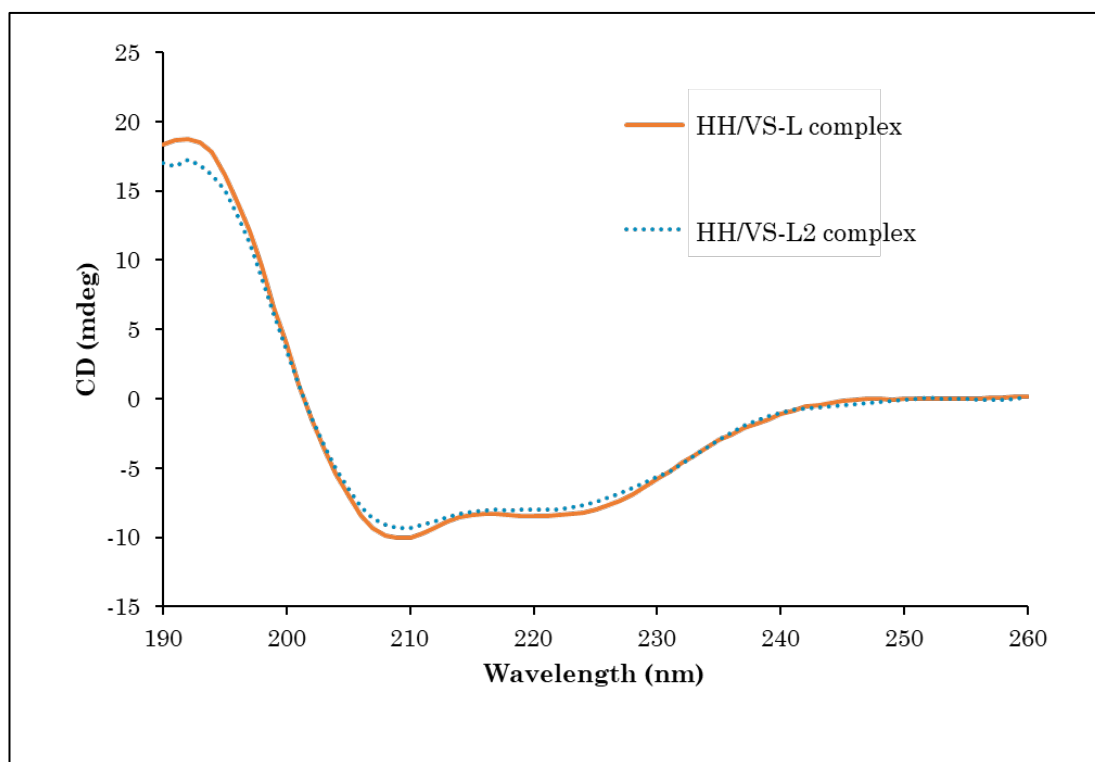


Figure 3.7 Far-UV SRCD spectra of VS-L and VS-L2 complexes. The two HH/VS complexes were tested under the same conditions: 8 μ M, pH=7.3, 20°C. HH and VS with different linkers (VS-L and VS-L²) do not show substantial differences in their ability to form the SNARE complex. The data shown represents the average of three different measurements (n=3).

Besides, an SRCD melting temperature assay was performed on HH/VS-L2 to test its thermal stability (see Section 2.4.2). The temperature scans

of both VS-L and VS-L2 complexed to HH were used to obtain their melting temperatures (see Figure 3.8). The T_m measured for HH/VS-L2 was 79.1°C, which is less than 1°C below the T_m of HH/VS-L (79.6°C, see also Figure 3.3).

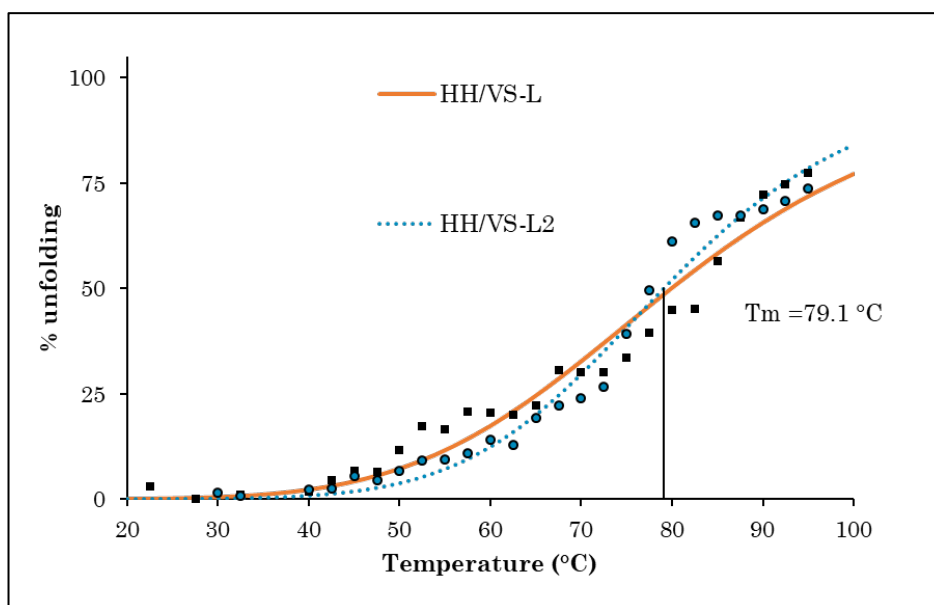


Figure 3.8 CD temperature scan of VS-L and VS-L2 SNARE complexes. As for previous temperature scans, the unfolding of the SNARE complex was measured as an expression of increase of CD signal at 222 nm (in percentage, over a value of 100 extrapolated at an infinite temperature). The temperature value at which 50% unfolding is achieved represents the melting temperature (T_m), derived by fitting the data to a sigmoid; each data point represents the average of three measurements at the given temperature.

The results of Figures 3.7 and 3.8 together show that the alternative linker k does not affect the assembly nor the thermal stability properties of the binary SNARE complex formed by VS with HH, suggesting that the self-assembly and melting properties of artificial binary SNARE complex can be entirely modulated by only shortening of VAMP2.

3.3 Thermoresponsive protein release

As a proof of concept for thermoresponsive release of proteins from a solid surface, HH was immobilised on GSH Sepharose beads to assess the release of VS-L and VS-S at different temperatures. GSH Sepharose beads with cross-linked glutathione (GSH) were used to easily immobilise HH via recombinant Glutathione S-Transferase (GST) tag fused at the N-terminal of HH (see Figure 3.9 A).

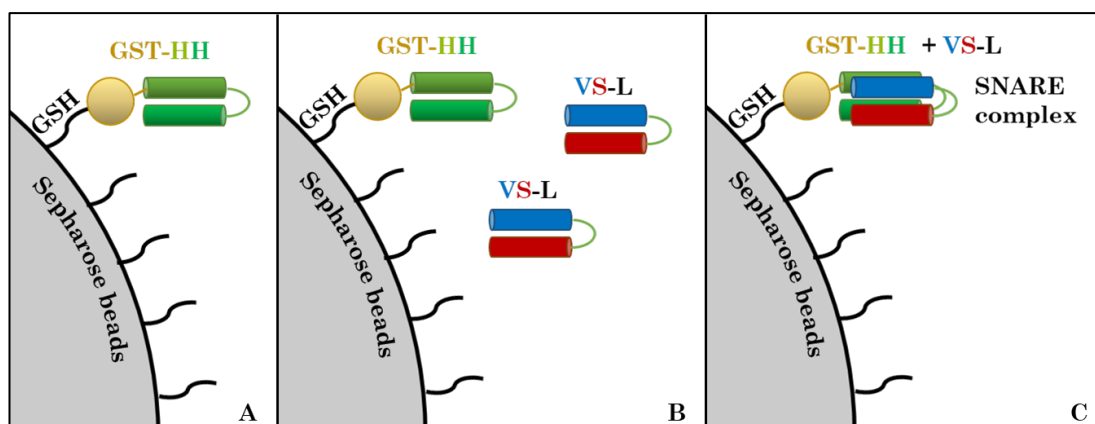


Figure 3.9 CD Immobilisation of GST-HH on Sepharose beads and SNARE complex formation with VS-L. (A) GST-HH binds to the GSH Sepharose beads. (B) VS-L (alternatively VS-S, here not represented) is added in solution. (C) After 1 hour, VS-L is bound to the GST-HH, forming the SNARE complex.

GSH Sepharose beads are routinely used in pull-down assays to confirm known protein-protein interactions⁽¹⁰²⁾ and here the pull-down assay was adapted to include an assessment of the interaction at different temperatures. Once incubated with VS-L or VS-S (Figure 3.9 B), the ability

of the Sepharose-GST-HH beads to capture VS-L and VS-S, thus forming the SNARE complex, was tested (Figure 3.9 C).

After extensive washing, the GSH Sepharose beads were loaded on an SDS-PAGE gel to visualise the bound proteins (Figure 3.10). The presence of VS-L and VS-S bands on lanes containing GST-HH proved that there is binding between HH and both VSs. A negative control where GST without HH fusion was incubated with VS was used to prove that the binding is actually specific between HH and VSs. The lack of any VS band in the control confirms that no interaction occurs between GST and both VSs.

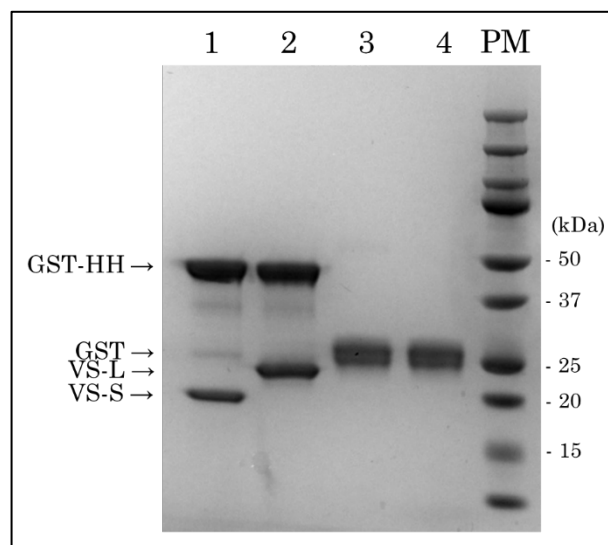


Figure 3.10 SDS-PAGE gel of the pull-down of VS-L and VS-S by functionalised Sepharose beads. Lane 1 and 2 show Sepharose-GST-HH incubated with excess VS-S (1) and VS-L (2). As shown by the arrows on the left, the band on both lanes corresponds to GST-HH (45.3 kDa), and the other bands correspond to the molecular weight of VS-L (21.3 kDa, lane 2) and VS-S (17.2kDa, lane 1) respectively. Lane 3 and 4 are negative controls where Sepharose-GST with no HH was incubated with an excess of VS-S (3) and VS-L (4). In these lanes there is only one band indicated by the arrow on the left, corresponding to GST's mass (28.6 kDa), whereas no pull-down of VS was observed. PM = protein marker with relative masses of the standards.

These results are consistent with the results observed for binary SNAREs in solution obtained using SRCD (Figure 3.5). It is essential to point out that, whereas it is possible to determine the secondary structure of protein immobilised on surfaces using SRCD (^{99,103,104}), this technique would not be applicable in this exact design. The structure of the GST tag has several alpha-helices which would contribute to the CD peaks at 208 and 222 nm, regardless of the assembly status of the SNARE domains, so the interpretation of the results would not be as straightforward as it was for the SNAREs in solution.

Since the amount of proteins used in these experiments is small (2-10 μM), VS-L and VS-S were fluorescently labelled with maleimide-activated Cy5 to make it easier to detect their capture and release from HH (Figure 3.11).

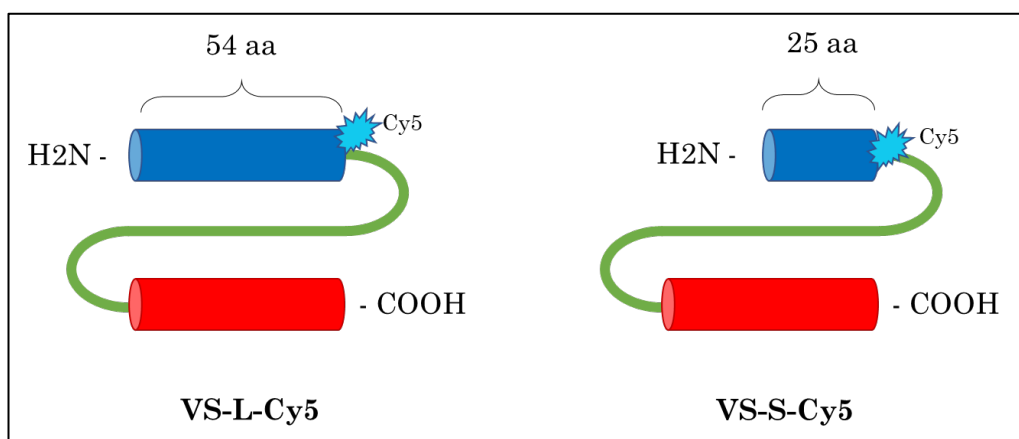


Figure 3.11 Schematic representation of the VS-L-Cy5 and VS-S-Cy5 constructs. Cylinders represent SNARE domains: VAMP2 in blue, syntaxin 3 in red; the green line represents the naturally occurring linker between the two α -helices of SNAP25, used here to combine VAMP2 and syntaxin3 in a single polypeptide. At the C terminal of VAMP2 (both long and short), the presence of a cysteine allows the modification via chemical cross-linking with a Cy5-maleimide fluorophore molecule.

VAMP2-L and VAMP2-S, and consequently VS-L and VS-S, carry a cysteine residue to facilitate site-specific chemical cross-linking of the fluorophore to the thiol group of such amino acid. Neither native VAMP nor syntaxin carry a cysteine residue in the proximity of the SNARE motif, so the amino acid was introduced at the end of VAMP2's sequence. VS is a SNARE fusion arranged as VAMP2-linker-syntaxin3; therefore, the cysteine is positioned at one-third of the overall sequence (See Figure 3.11).

After purification by size exclusion chromatography, the fluorescently-labelled proteins were run on an SDS-PAGE gel and analysed using Odyssey (LI-COR Imaging System). The gel was imaged at both 600 and 700 nm channels: Cy5 absorbance peak is at 649 nm and its emission is visible at 700 nm. The 600 nm channel was used to highlight some of the bands of the protein marker (Figure 3.12).

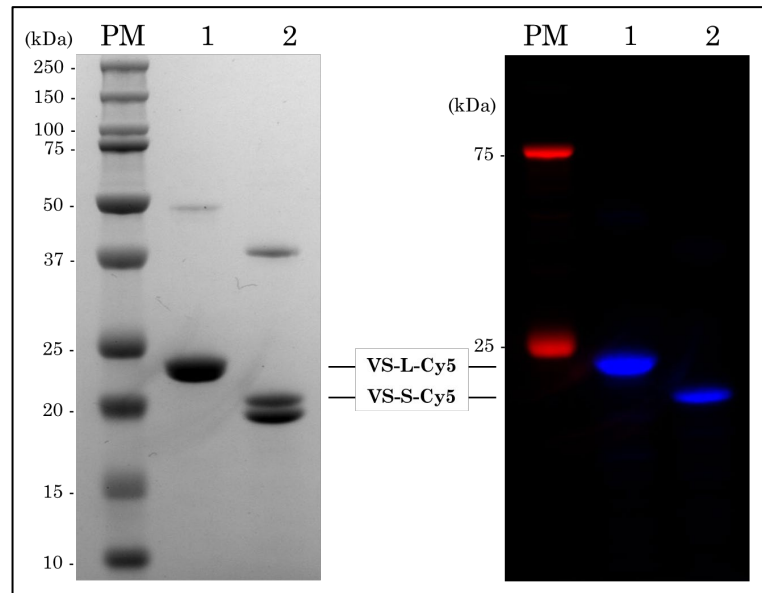


Figure 3.12 SDS-PAGE gel of VS-L and VS-S labelled with maleimide-activated Cy5. On the left, the Coomassie-stained gel shows the bands corresponding to VS-L-Cy5 and VS-S-Cy5, indicated by the labels. The presence of a double band is due to the different migration of the labelled proteins, behaving as a slightly higher molecular weight protein (clearly visible in lane 2). The conjugation efficiency can be therefore estimated as around ~50%. The high molecular weight bands (between 37 and 50 kDa) are likely VS-L and VS-S dimers formed by disulphide bonds between unreacted thiols on the cysteine residues. PM stands for protein marker (Precision Plus, BioRad), with relative masses on the left side of the gel. On the right, the same gel imaged with Odyssey Imaging System (LI-COR Biosciences) to highlight the fluorescent properties of the two constructs. 600 nm and 700 nm channel in red and blue, respectively.

To assess temperature response of SNARE complexes immobilised on GSH Sepharose beads, a large volume of complexes were assembled; fractions of the fully-formed Sepharose beads-GST-HH and VS complexes were incubated at different temperatures. GST-HH was tested at a concentration of 3 μM , adding 5 μM of each labelled VS to saturate the system. Once the excess of unbound protein was removed, the residual Cy5 fluorescence intensity was measured, representing the quantity of VS

retained at any set temperature. At the highest temperature (80°C), neither VS-L-Cy5 nor VS-S-Cy5 were bound to the resin. While 60% of VS-L-Cy5 was still bound to the surface at 50°C, the amount of VS-S-Cy5 at the same temperature was negligible, as most of VS-S-Cy5 was abruptly released below that temperature (Figure 3.13).

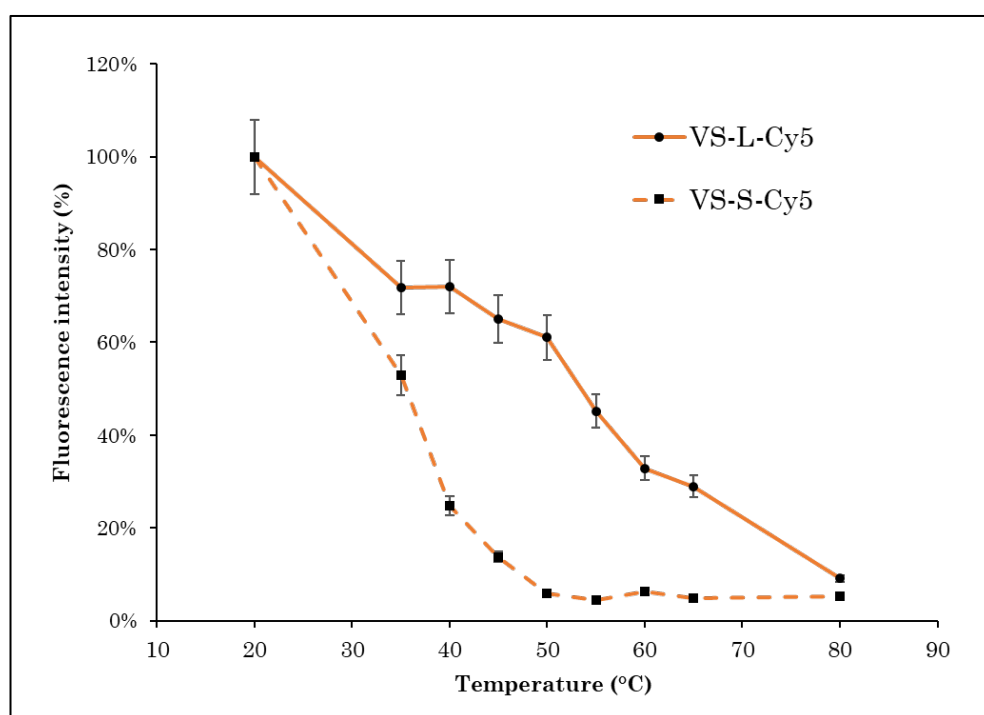


Figure 3.13 VS-L-Cy5 and VS-S-Cy5 residual fluorescence intensity. The data in this plot represent the residual fluorescence measured on Sepharose-GST-HH bound to VS-L-Cy5 and VS-S-Cy5 after incubation at different temperatures. Data points and error bars represent, respectively, the average of three measurements and standard deviation. GST-HH was 3 μ M, while both VS were used in excess, 5 μ M each.

The different response to the temperature of the two surface-immobilised complexes is consistent with what observed for SNAREs in solution, enforcing once more that the disassembly properties of the engineered

complexes primarily depend on the length of the VAMP2 domain only. However, GST itself is sensitive to high temperatures: its T_m is around 70°C, but tends to aggregate even below this threshold⁽¹⁰⁵⁾. Therefore, the release of VS-L above 60°C may be due to the disruption of the bond between GST and the GSH Sepharose beads.

To assess the capture-and-release properties of the Sepharose-GST-HH/VS system over several cycles of heating and cooling at room temperature (20°C), the pull-down was repeated, but the retention of Cy5 fluorescence was measured after up to 4 cycles of heating and cooling (Figure 3.14). The heating temperature was set depending on the length of VS: 80°C was used for VS-L and 50°C for VS-S.

The results show that the latter complex was still functional after four cycles. This outcome highlights that the use of natively unstructured proteins like the SNARE domains allows the engineering of an immobilisation system that is insensitive to denaturation or aggregation of the immobilisation tags and can be therefore regenerated.

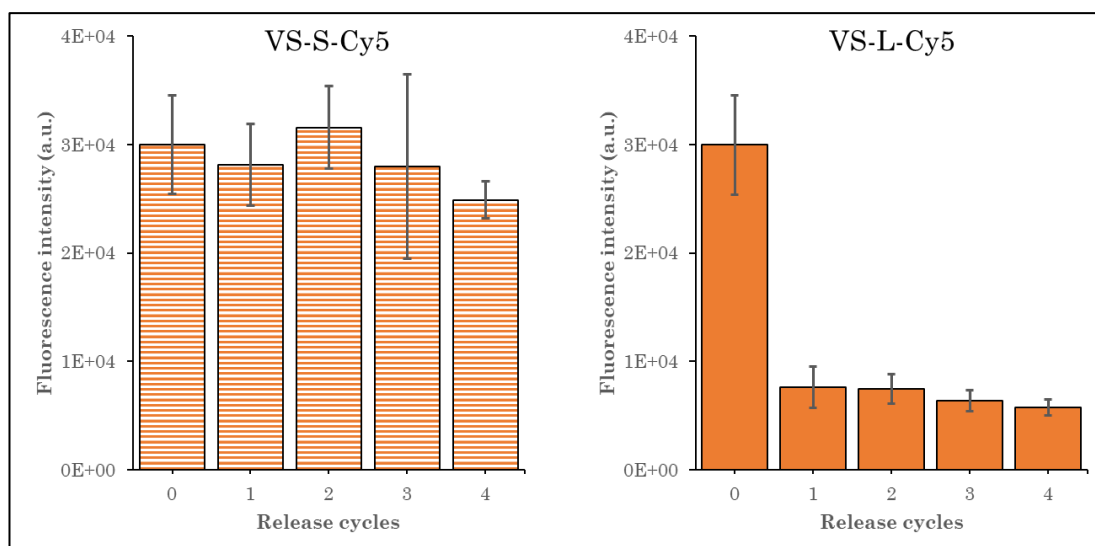


Figure 3.14 VS-L-Cy5 and VS-S-Cy5 residual fluorescence intensity after heating-cooling cycles. Fluorescence intensity of captured VS-S-Cy5 and VS-L-Cy5 after Sepharose-GST-HH was heated and cooled for 0 to 4 cycles. GST-HH was immobilised on GSH Sepharose beads; when incubated with VS-L-Cy5 the release temperature used was 80°C, whereas 50°C was used for VS-S-Cy5. Sepharose-GST-HH ability to capture and release VSS is expressed as residual fluorescence intensity after n cycles of heating and cooling. Average of three measurements, error bars represent the standard deviation.

However, the interface with VS-L that was heated to 80°C lost a considerable amount of fluorescence intensity after just one cycle. In the absence of a control test with GST alone, it was assumed that this behavior was due to the denaturation of GST and loss of binding ability, suggesting that the assay to test regeneration cannot be performed at high temperatures. The future addition of GST only as a control may clarify its role in the capture-and-release of VS-L from GST-HH.

As our focus was on the optimisation of a SNARE complex for thermoresponsive release, rather than on the strategy for the immobilisation on the surface, we concluded that the development of a binary SNARE system was entirely successful. It consisted of an immobilisation protein named HH that could be regenerated, and thermoresponsive tags VS-S and VS-L that could be released in a temperature range between 45 and 80°C.

4. DISCUSSION AND CONCLUSIONS

The design of a thermoresponsive interface began with the investigation of the *Rattus norvegicus* neuronal SNARE complex and its structural features. The complex is a parallel coiled-coil structure, and its formation is possible thanks to the SNARE motif, which assumes an α -helical structure only when combined with the other SNARE motif domains as an arrangement of several hydrophobic layers in the direction of the core complex.

The remarkable strength and peculiarity of the SNARE complex have proven fundamental for the design of a thermoresponsive interface. The recombinant SNAREs intended for this project focused on the preservation of the SNARE motif, eliminating the additional domains from the designed sequences.

Newly designed syntaxin 1 and VAMP2 had matching length, which covers the 54-amino acid long SNARE motif strand. First, recombinant SNAP25, syntaxin 1 and VAMP2 were expressed and purified in *E. coli* and used to characterise the thermal stability of the full-length SNARE complex in solution. A truncated version of VAMP, reducing its SNARE motif from 54 to 25 amino acids, was developed to test the SNARE complex thermal stability since there was evidence to support that shortening one helix still allows the formation of the complex^(60,94). The ionic layer was removed

from the VAMP2-S to rule out disturbances of pH and charge when interpreting the results. For the first time, VAMP was shortened to roughly half of its native size; the ionic layer was excluded to examine the association and disassociation of the complex. SNARE proteins were tested individually and in pairs; Far-UV SRCD spectra confirmed that single proteins are unstructured (Figure 3.1) and that there is partial assembly only in the SNAP25/syntaxin 1 pair, as previously observed (75).

The choice of shortening VAMP2 instead of syntaxin or one of the SNARE motifs of SNAP25 derived from the knowledge that it is the last protein, among the three mentioned, to assemble into the SNARE complex. It would be interesting to study the differences when shortening a different α -helix, and further explore the role of the ionic layer residue if left on the truncated version.

Far-UV SRCD spectra of both complexes containing SNAP25, syntaxin 1 and either VAMP2-L or VAMP-S (Figure 3.2) showed the typical α -helical spectrum shape; however, the SNARE complex formed with VAMP-S revealed a less intense CD signal. The reduction of the α -helical component, compared to the one with VAMP-L, can be explained with the reduced size of the structured domains.

Moreover, using SRCD temperature scans, it was possible to obtain a melting temperature curve. From the 79.6°C disassembly temperature of the long VAMP complex, the SNARE complex with the truncated VAMP

dropped to 42.5°C (melting temperatures extracted from Figure 3.3). It is, therefore, possible to modulate the SNARE complex's melting temperature by shortening of SNARE domains while maintaining the structural features that allow self-assembly.

Since the ultimate goal of the project was the immobilisation of a protein system, the SNARE complex would benefit from being binary rather than ternary. One protein could be immobilised on a surface of interest, while the thermoresponsive tag for controlled release could be fused to a protein of interest ⁽⁸¹⁾. The modular approach developed to repeatedly clone different combinations of SNARE domains, starting from a limited number of SNAREs' inserts, was crucial to transition from a ternary to a binary SNARE complex.

A new version of SNAP25 was built truncating its SNARE motifs (on their respective C-terminal) to match the length of VAMP and syntaxin. The unstructured linker between the two α -helices was preserved to connect them; the complete recombinant protein, consisting of three fragments (helix one, linker and helix two) was named HH to highlight the presence of two helices.

To preserve the thermal stability properties of the SNARE complexes formed with the long and short VAMP, while reducing it to a binary system, VAMP and syntaxin were fused together. A polypeptide separates the N-terminal of VAMP2 and the C-terminal of syntaxin motifs; this linker is the one found between the two helices of SNAP25. The new VAMP2-syntaxin (VS) recombinant proteins were named VS-L and VS-S, differing on the length of VAMP2 domain (54 or 25 amino acids long, respectively).

These fusion proteins were successfully expressed in *E. coli* and purified. Many SNARE fusions were either poorly expressed or difficult to elute due to low solubility; the modular cloning approach developed to link together separate SNARE domains (see Section 2.2.3) was essential to try different combinations of SNAREs in a methodical way. Of the numerous attempts to express the three SNARE proteins into a binary construct, VSs were the successful ones. Previous studies showed that syntaxin 1 fusions have lower expression in bacteria ⁽⁸⁴⁾; consequently, syntaxin 3 replaced syntaxin 1 in the design of the VS fusion proteins. SRCD was performed on syntaxin 1 and 3, individually and along with VAMP2 and SNAP25. Far-UV spectra confirmed that there are no differences between syntaxin 1 and syntaxin 3 in their ability to form a SNARE complex (Figure 3.4).

HH and VS are partners in the formation of the SNARE complex; circular dichroism spectroscopy was used to assess their assembly properties. HH,

coupled with both VS-L and VS-S, was able to form the SNARE complex analogously to their ternary counterpart (Figure 3.5). Moreover, the SNARE fusions are unstructured when alone, acquiring an α -helical conformation only when together.

The melting temperatures of HH/VS-L and HH/VS-S binary complexes were measured using SRCD; the obtained values were very similar to the ones obtained for the ternary complexes. HH/VS-L disassembles at 79.9°C (the ternary counterpart at 79.6°C), and HH/VS-S loses its α -helicity at 43.3°C (against the 42.5°C recorded for the ternary shortened SNARE complex (Figure 3.6).

These results confirmed that, by shortening one helix, it is possible to manipulate the SNARE complex's melting temperature; in particular, the effort of reaching a T_m compatible with the use *in vivo* was successful. Hyperthermia studies conducted in the past showed that the body can withstand local temperatures around 45°C, temperature at which VS-S is able to be released from a surface. The combination of the thermoresponsive properties of VS-S with designed nanocarriers would be useful for the development of hyperthermia-directed protein therapeutics. The thermoresponsive protein interface obtained, VS-S, may contribute to the growing interest towards magneto-responsive local release of therapeutics.

The VS constructs carry the native unstructured linker existing between SNAP25's SNARE motifs; to exclude possible interactions between HH and the linker, an alternative one made of a glycine and serine sequence was inserted between VAMP-L and syntaxin 3, obtaining a new construct called VS-L2. VS-L and VS-L2 were analysed with circular dichroism spectroscopy: both spectra and temperature scans (Figure 3.7 and 3.8, respectively) indicated no differences between the two fusion proteins.

These results prove that the new SNARE constructs preserved similar thermal stability properties compared to their original ternary counterparts. Thanks to the re-arrangement of SNARE domains, including the shortened ones, it is possible to engineer a thermoresponsive binary SNARE complex.

All the SNARE constructs were expressed as a Glutathione S-Transferase (GST) tagged proteins (on its C-terminal); therefore, every recombinant protein had a high affinity for GST-modified resins, making them an appropriate method to purify the resulting recombinant proteins from the bacterial lysate (106). The GST affinity tag could then be removed by thrombin cleavage or retained for other purposes, as to easily immobilise GST-tagged proteins on a surface. Other materials may be more suitable for the immobilisation of the SNARE recombinants in order to release them from a surface, as peptides with high affinity for carbon- and silica-based

materials (^{107,108}); however, the GST-tag was a convenient way to achieve proof-of-concept, while other methods will be investigated in the future.

Considering that the ultimate goal was the immobilisation and temperature-mediated release of the binary SNARE complex from a surface, HH was purified as a GST-tagged protein and immobilised on GSH Sepharose beads. The GST/GSH interaction showed high affinity and remarkable stability; together with the high solubility of the GST tag, this system becomes suitable for strong immobilisation of recombinant proteins on GSH-modified resins or other surfaces, such as plates, biosensors, magnetic beads. Previous studies showed that GST has a high affinity to gold, and can thus be used to decorate gold nanoparticles (^{94,97}).

The ability of GST-HH to capture its VS partner at different temperature was analysed with a pulldown experiment. Sepharose-GST-HH was able to bind both VS-L and VS-S; in addition, the inability of Sepharose-GST to bind the VS constructs confirmed the specific binding existing between HH and VSs, ruling out possible interference by GST or the surface itself (Figure 3.10).

The pulldown results were evaluated with an SDS-PAGE; this method, however, provides only a qualitative or semi-quantitative estimate of the protein amount captured by the functionalised beads. To allow an easier detection of the captured protein, the two VS constructs were then fluorescently labelled with Cy5-maleimide. The Cy5 fluorophore molecule

was connected the VS constructs via chemical cross-linking; the two VAMP-syntaxin fusion proteins carry a cysteine residue on VAMP2's C-terminal (Figure 3.11), explicitly introduced to allow fluorescence-labelling. VS-L-Cy5 and VS-S-Cy5 were then purified and run on SDS-PAGE (Figure 3.12).

A pulldown assay similar to the one above was carried out with fluorescent VSs. Sepharose-GST-HH was incubated with an excess of either VS-L-Cy5 or VS-S-Cy5 at different temperatures to saturate the system. After extensive washing at the same temperature to remove the unbound protein, the residual Cy5 fluorescence was measured to assess the proportion of captured protein, as indicated by the intensity of the fluorescent signal of VS still bound on Sepharose-GST-HH at a given temperature. Above 80°C neither VS was bound the beads; at 50°C, most of VS-L-Cy5 was still bound to the surface, while the fluorescence intensity of VS-S-Cy5 dropped abruptly (Figure 3.13). Some of the residual fluorescence of both VSs was lost below 35°C, possibly due to incorrect alignment or wrong stoichiometry between SNARE domains of VS and HH⁽⁸⁴⁾. Further experiments may be conducted lowering the concentration of GST-HH to avoid the incorrect formation of the SNARE complex with syntaxin and VAMP2 belonging to different VS fusions.

The lack of a control, performed with GST only, makes this method unreliable for measurements over $\sim 60^{\circ}\text{C}$, as this is the near the assumed melting temperature for GST. The release of VS-L from Sepharose-GST-HH is dependent on GST and its ability to bind GSH Sepharose beads. When this bound is lost, it is not possible to assess at what temperature VS-L and GST-HH complex unfolds. Similar experiments could be performed using a resin other than GSH-Sepharose: for example, cyanogen bromide-activated-Sepharose, which provides covalent cross-linking to the protein of interest.

However, all the data discussed above proved that HH could capture and release both VSs when immobilised on a surface (Sepharose GSH beads). To understand if such property could be maintained after numerous cycles of heating and cooling, both Sepharose-GST-HH/VS systems were tested. Since they respond to different temperatures, the molecular interface carrying the VS-S-Cy5 was heated to 50°C , while the one with VS-L-Cy5 reached 80°C ; both systems were heated four times and cooled at 20°C after each cycle (Figure 3.14).

The behaviour of the two interfaces was very different, as Sepharose-GST-HH/VS-S-Cy5 showed no significant changes after four cycles. The moiety carrying VS-L and heated at high temperature showed a loss of fluorescence intensity after one cycle. SNARE mimics are naturally unstructured and unlikely to denature and lose function permanently;

however, as assumed before, this result could be attributed to the partial loss of function of GST at temperatures higher than 56°C. Moreover, this result is consistent with the trend observed before (Figure 1.13), where VS-L-Cy5's release rate increased when the temperature was over 50°C. Future experiments may direct the attention on GST and how to avoid its interference when studying the release of VS-L at high temperatures.

The results obtained confirmed that the engineered HH/VS binary complex is thermoresponsive, and it preserves its thermal stability properties when immobilised on a surface; it can, therefore, be potentially used as an interface to release proteins from a surface when triggered by a local increase of temperature.

Protein-protein interactions often lead to protein aggregation and require substantial optimisations effort (¹⁰⁹); on the contrary, here, no irreversible protein aggregation was observed between the SNARE mimics. Interestingly, the designed SNARE constructs were able to refold when immobilised on a surface; besides, the possibility to regenerate the surface after subsequent cycles of capture and release was here demonstrated. These remarkable properties suggest that the interactions involved in the formation of the SNARE complex are fully reversible and therefore compatible with dynamic and programmable surfaces involving biomolecules (¹¹⁰).

The design of this thermoresponsive interface originated after extensive study of the previous engineering of the coiled-coil structure of the neuronal SNARE complex and other coiled-coil motifs ⁽¹¹¹⁾. The background study allowed the modulation of the disassembly temperature down to reasonable physiological conditions for *in vivo* applications, such as the use of engineered hyperthermia-directed therapeutics ⁽¹¹²⁾.

Hyperthermia was used with thermoresponsive polymers before, as in the case of hybrid peptide-lipid vesicles. These nanoscale thermoresponsive carriers were tested *in vivo*, with the successful release of doxorubicin after hyperthermia treatment ⁽¹¹³⁾. In Europe, the treatment of glioblastoma already utilises magnetic hyperthermia: iron oxide nanoparticles are used to induce a local increase of temperature ⁽¹¹⁴⁾. The latter could be a promising method for local release of therapeutics in response to a magnetic stimulus, towards which the thermoresponsive protein interface described here may contribute.

Nanoparticle-based systems for local drug delivery are found not only among the magnetic responsive materials but also among those who retain the ability to absorb energy in the near-infrared (NIR) spectrum. NIR can be used to trigger a local and controlled increase of temperature *in vivo*; the advantage of these systems is that NIR light is absorbed in minimal part by tissues, as it can penetrate in the micro- and centi-scale, allowing

photo-thermal drug release (27). In the last twenty years, numerous research groups developed gold nanorods with a strong absorbance in the NIR range working both *in vitro* and *in vivo* (115,116): these systems can be triggered to change their conformation in response to NIR irradiation, releasing biomolecules. The thermoresponsive protein release tag properties reported here may be a suitable interface for magnetic responsive and photo-thermal therapy.

To exploit the use of HH/VS-S as an interface for drug delivery, the binary complex would need further characterisation, both *in vitro* and *in vivo*. First, it is essential to find a suitable carrier, and how to best bind HH to it. Secondly, a refined tuning of the ability of such engineered carrier to capture and release its VS counterpart needs to be carried out. As for the *in vivo* studies, extensive work may be carried out to study the interface behaviour in the bloodstream, with particular attention to interactions with plasma proteins and/or opsonisation to avoid HH/VS inactivation and quick degradation.

The surface chemistry of nanomaterials used for drug delivery can be tuned so that adhesion of plasma-protein is minimised and the size of the nanoparticle carrier can be selected big enough to limit renal clearance. Furthermore, modifications such as PEGylation may increase its plasma half-life; if intended to be used for targeted delivery, an additional targeting system (a specific protein sequence, or a small molecule) could be

added to the system. However, the conjugation of further functional protein, as described here, may change the surface properties substantially. Therefore protein-nanoparticle conjugates have to be tested and considered on a case-by-case base, as it is not possible to predict how a specific protein would interact with plasma proteins and renal clearance mechanism.

The results described in this thesis suggest that the release temperature of an engineered SNARE complex can be modulated by changing the length of one SNARE motif. Previous studies showed that, by shortening one α -helix, it was possible to weaken the chemical stability of the SNARE complex. However, this research did not provide any data on the complex's thermal stability; hence the analysis carried out in this work. The truncation of a SNARE motif proves that it would be possible to obtain a wide array of thermoresponsive tags reacting to temperatures in the range of 43-80°C. Alternatively, a similar approach could be used to modulate its pH sensitivity.

To fully develop the potential of these new interface proteins, the immobilisation on surfaces other than GSH Sepharose beads should be explored further. For example, GST could be replaced by available peptides with affinity to specific materials; alternatively, the SNAREs could be

directly linked to a surface using available chemical bioconjugation methods (^{117,118}).

Once fused to thermoresponsive VS, recombinant proteins of interest could be used for immobilisation and release from HH-modified materials, regardless of HH's immobilisation method. On the other hand, HH-activated materials could be used for the immobilisation and release of any VS-tagged recombinant protein, emphasising the modularity and flexibility of the system described here. Thermoresponsive SNARE-derived tags may have a role in the future design of interfaces with programmable, protein-mediated functions.

5. REFERENCES

1. Hudecki A, Kiryczyński G, Łos MJ. Biomaterials, Definition, Overview. *Stem Cells Biomater Regen Med.* 2019;(ii):85-98. doi:10.1016/b978-0-12-812258-7.00007-1
2. Patel N, Gohil P. A review on biomaterials: scope, applications & human anatomy significance. *Int J Emerg Technol Adv Eng.* 2012;2(4):91-101.
3. van Gestel NAP, Geurts J, Hulsen DJW, van Rietbergen B, Hofmann S, Arts JJ. Clinical Applications of S53P4 Bioactive Glass in Bone Healing and Osteomyelitic Treatment: A Literature Review. *Biomed Res Int.* 2015;2015:1-12. doi:10.1155/2015/684826
4. Bures P, Huang Y, Oral E, Peppas NA. Surface modifications and molecular imprinting of polymers in medical and pharmaceutical applications. *J Control Release.* 2001;72(1-3):25-33. doi:10.1016/S0168-3659(01)00259-0
5. Abulatefeh SR, Spain SG, Aylott JW, Chan WC, Garnett MC, Alexander C. Thermoresponsive polymer colloids for drug delivery and cancer therapy. *Macromol Biosci.* 2011;11(12):1722-1734. doi:10.1002/mabi.201100252
6. Galaev I, Mattiasson B. "Smart" polymers and what they could do in biotechnology and medicine. *Trends Biotechnol.* 1999;17(8):335-340. doi:10.1016/S0167-7799(99)01345-1

7. Alarcón C de las H, Pennadam S, Alexander C. Stimuli responsive polymers for biomedical applications. *Chem Soc Rev.* 2005;34(3):276-285. doi:10.1039/B406727D
8. Macleod JJR. Insulin. *Physiol Rev.* 1924;4(1):21-68. doi:10.1152/physrev.1924.4.1.21
9. Winter G, Milstein C. Man-made antibodies. *Nature.* 1991;349(6307):293-299. doi:10.1038/349293a0
10. Serna N, Sánchez-García L, Unzueta U, et al. Protein-Based Therapeutic Killing for Cancer Therapies. *Trends Biotechnol.* 2018;36(3):318-335. doi:10.1016/j.tibtech.2017.11.007
11. Mura S, Nicolas J, Couvreur P. Stimuli-responsive nanocarriers for drug delivery. *Nat Mater.* 2013;12(11):991-1003. doi:10.1038/nmat3776
12. Hoffman AS. Stimuli-responsive polymers: Biomedical applications and challenges for clinical translation. *Adv Drug Deliv Rev.* 2013;65(1):10-16. doi:10.1016/j.addr.2012.11.004
13. Kumar A, Srivastava A, Galaev IY, Mattiasson B. Smart polymers: Physical forms and bioengineering applications. *Prog Polym Sci.* 2007;32(10):1205-1237. doi:10.1016/j.progpolymsci.2007.05.003
14. Bawa P, Pillay V, Choonara YE, du Toit LC. Stimuli-responsive polymers and their applications in drug delivery. *Biomed Mater.* 2009;4(2):022001. doi:10.1088/1748-6041/4/2/022001

15. Lu Y, Sun W, Gu Z. Stimuli-responsive nanomaterials for therapeutic protein delivery. *J Control Release*. 2014;194:1-19. doi:10.1016/j.jconrel.2014.08.015
16. Kost J, Langer R. Responsive polymeric delivery systems. *Adv Drug Deliv Rev*. 2012;64(SUPPL.):327-341. doi:10.1016/j.addr.2012.09.014
17. Wu W, Mitra N, Yan ECY, Zhou S. Multifunctional Hybrid Nanogel for Integration of Optical Glucose Sensing and Self-Regulated Insulin Release at Physiological pH. *ACS Nano*. 2010;4(8):4831-4839. doi:10.1021/nn1008319
18. Matsumoto A, Ishii T, Nishida J, Matsumoto H, Kataoka K, Miyahara Y. A Synthetic Approach Toward a Self-Regulated Insulin Delivery System. *Angew Chemie Int Ed*. 2012;51(9):2124-2128. doi:10.1002/anie.201106252
19. Elshaarani T, Yu H, Wang L, et al. Dextran-crosslinked glucose responsive nanogels with a self-regulated insulin release at physiological conditions. *Eur Polym J*. 2020;125:109505. doi:10.1016/j.eurpolymj.2020.109505
20. Ward MA, Georgiou TK. Thermoresponsive polymers for biomedical applications. *Polymers (Basel)*. 2011;3(3):1215-1242. doi:10.3390/polym3031215
21. Schmidt AM. Thermoresponsive magnetic colloids. *Colloid Polym Sci*. 2007;285(9):953-966. doi:10.1007/s00396-007-1667-z

22. Zardad AZ, Choonara YE, du Toit LC, et al. A review of thermo- and ultrasound-responsive polymeric systems for delivery of chemotherapeutic agents. *Polymers (Basel)*. 2016;8(10):1-22. doi:10.3390/polym8100359
23. Zhang Z, Wang J, Nie X, et al. Near Infrared Laser-Induced Targeted Cancer Therapy Using Thermoresponsive Polymer Encapsulated Gold Nanorods. *J Am Chem Soc*. 2014;136(20):7317-7326. doi:10.1021/ja412735p
24. Yildirim A, Blum NT, Goodwin AP. Colloids, nanoparticles, and materials for imaging, delivery, ablation, and theranostics by focused ultrasound (FUS). *Theranostics*. 2019;9(9):2572-2594. doi:10.7150/thno.32424
25. Vaupel P, Kallinowski F, Okunieff P. Blood Flow, Oxygen and Nutrient Supply, and Metabolic Microenvironment of Human Tumors: A Review. *Cancer Res*. 1989;49(23):6449-6465.
26. Wagner V, Dullaart A, Bock AK, Zweck A. The emerging nanomedicine landscape. *Nat Biotechnol*. 2006;24(10):1211-1217. doi:10.1038/nbt1006-1211
27. Timko BP, Dvir T, Kohane DS. Remotely triggerable drug delivery systems. *Adv Mater*. 2010;22(44):4925-4943. doi:10.1002/adma.201002072
28. Kumar CSSR, Mohammad F. Magnetic nanomaterials for hyperthermia-based therapy and controlled drug delivery. *Adv*

- Drug Deliv Rev.* 2011;63(9):789-808. doi:10.1016/j.addr.2011.03.008
29. Mendes PM. Stimuli-responsive surfaces for bio-applications. *Chem Soc Rev.* 2008;37(11):2512-2529. doi:10.1039/b714635n
30. Klouda L, Mikos AG. Thermoresponsive hydrogels in biomedical applications. *Eur J Pharm Biopharm.* 2008;68(1):34-45. doi:10.1016/j.ejpb.2007.02.025
31. Ashraf S, Park H-K, Park H, Lee S-H. Snapshot of phase transition in thermoresponsive hydrogel PNIPAM: Role in drug delivery and tissue engineering. *Macromol Res.* 2016;24(4):297-304. doi:10.1007/s13233-016-4052-2
32. Boustta M, Colombo P-E, Lenglet S, Poujol S, Vert M. Versatile UCST-based thermoresponsive hydrogels for loco-regional sustained drug delivery. *J Control Release.* 2014;174:1-6. doi:10.1016/j.jconrel.2013.10.040
33. Greenwald RB. PEG drugs: An overview. *J Control Release.* 2001;74(1-3):159-171. doi:10.1016/S0168-3659(01)00331-5
34. Albanese A, Tang PS, Chan WCW. The Effect of Nanoparticle Size, Shape, and Surface Chemistry on Biological Systems. *Annu Rev Biomed Eng.* 2012;14(1):1-16. doi:10.1146/annurev-bioeng-071811-150124
35. Ekladios I, Colson YL, Grinstaff MW. Polymer–drug conjugate therapeutics: advances, insights and prospects. *Nat Rev Drug Discov.* 2019;18(4):273-294. doi:10.1038/s41573-018-0005-0

36. Badi N, Lutz JF. PEG-based thermogels: Applicability in physiological media. *J Control Release*. 2009;140(3):224-229. doi:10.1016/j.jconrel.2009.04.012
37. Nova A, Keten S, Pugno NM, Redaelli A, Buehler MJ. Molecular and Nanostructural Mechanisms of Deformation, Strength and Toughness of Spider Silk Fibrils. *Nano Lett*. 2010;10(7):2626-2634. doi:10.1021/nl101341w
38. Viidik A, Danielsen CC, Oxlund H. On fundamental and phenomenological models, structure and mechanical properties of collagen, elastin and glycosaminoglycan complexes. *Biorheology*. 1982;19(3):437-451. doi:10.3233/BIR-1982-19305
39. Li B, Alonso DO., Daggett V. The molecular basis for the inverse temperature transition of elastin¹¹Edited by A. R. Fersht. *J Mol Biol*. 2001;305(3):581-592. doi:10.1006/jmbi.2000.4306
40. Reguera J, Urry DW, Parker TM, McPherson DT, Rodríguez-Cabello JC. Effect of NaCl on the exothermic and endothermic components of the inverse temperature transition of a model elastin-like polymer. *Biomacromolecules*. 2007;8(2):354-358. doi:10.1021/bm060936l
41. Nettles DL, Chilkoti A, Setton LA. Applications of elastin-like polypeptides in tissue engineering. *Adv Drug Deliv Rev*. 2010;62(15):1479-1485. doi:10.1016/j.addr.2010.04.002

42. Salvagni E, Berguig G, Engel E, et al. A bioactive elastin-like recombinamer reduces unspecific protein adsorption and enhances cell response on titanium surfaces. *Colloids Surfaces B Biointerfaces*. 2014;114:225-233. doi:10.1016/j.colsurfb.2013.10.008
43. Ryu JS, Raucher D. Anti-tumor efficacy of a therapeutic peptide based on thermo-responsive elastin-like polypeptide in combination with gemcitabine. *Cancer Lett*. 2014;348(1-2):177-184. doi:10.1016/j.canlet.2014.03.021
44. Bessa PC, Machado R, Nürnberger S, et al. Thermoresponsive self-assembled elastin-based nanoparticles for delivery of BMPs. *J Control Release*. 2010;142(3):312-318. doi:10.1016/j.jconrel.2009.11.003
45. Massodi I, Moktan S, Rawat A, Bidwell GL, Raucher D. Inhibition of ovarian cancer cell proliferation by a cell cycle inhibitory peptide fused to a thermally responsive polypeptide carrier. *Int J Cancer*. 2010;126(2):533-544. doi:10.1002/ijc.24725
46. Chilkoti A, Dreher MR, Meyer DE. Design of thermally responsive, recombinant polypeptide carriers for targeted drug delivery. *Adv Drug Deliv Rev*. 2002;54(8):1093-1111. doi:10.1016/S0169-409X(02)00060-1
47. Moktan S, Perkins E, Kratz F, Raucher D. Thermal Targeting of an Acid-Sensitive Doxorubicin Conjugate of Elastin-like Polypeptide Enhances the Therapeutic Efficacy Compared with the Parent

- Compound In Vivo. *Mol Cancer Ther.* 2012;11(7):1547-1556.
doi:10.1158/1535-7163.MCT-11-0998
48. Mastria EM, Chen M, McDaniel JR, et al. Doxorubicin-conjugated polypeptide nanoparticles inhibit metastasis in two murine models of carcinoma. *J Control Release.* 2015;208:52-58.
doi:10.1016/j.jconrel.2015.01.033
49. Wong CK, Laos AJ, Soeriyadi AH, et al. Polymersomes Prepared from Thermoresponsive Fluorescent Protein-Polymer Bioconjugates: Capture of and Report on Drug and Protein Payloads. *Angew Chemie Int Ed.* 2015;54(18):5317-5322. doi:10.1002/anie.201412406
50. Ji S, Li N, Shen Y, Li Q, Qiao J, Li Z. Poly(amino acid)-based thermoresponsive molecularly imprinted magnetic nanoparticles for specific recognition and release of lysozyme. *Anal Chim Acta.* 2016;909:60-66. doi:10.1016/j.aca.2016.01.005
51. Costa RR, Custódio CA, Arias FJ, Rodríguez-Cabello JC, Mano JF. Nanostructured and thermoresponsive recombinant biopolymer-based microcapsules for the delivery of active molecules. *Nanomedicine Nanotechnology, Biol Med.* 2013;9(7):895-902.
doi:10.1016/j.nano.2013.01.013
52. Chen YA, Scheller RH. Snare-mediated membrane fusion. *Nat Rev Mol Cell Biol.* 2001;2(2):98-106. doi:10.1038/35052017
53. Jahn R, Lang T, Südhof TC. Membrane fusion. *Cell.* 2003;112(4):519-533. doi:10.1016/S0092-8674(03)00112-0

54. Jahn R. Principles of Exocytosis and Membrane Fusion. *Ann N Y Acad Sci.* 2004;1014(1):170-178. doi:10.1196/annals.1294.018
55. Söllner T, Whiteheart SW, Brunner M, et al. SNAP receptors implicated in vesicle targeting and fusion. *Nature.* 1993;362(6418):318-324. doi:10.1038/362318a0
56. Bennett MK, Scheller RH. The molecular machinery for secretion is conserved from yeast to neurons. *Proc Natl Acad Sci.* 1993;90(7):2559-2563. doi:10.1073/PNAS.90.7.2559
57. Ferro-Novick S, Jahn R. Vesicle fusion from yeast to man. *Nature.* 1994;370(6486):191-193. doi:10.1038/370191a0
58. Rothman JE. Mechanisms of intracellular protein transport. *Nature.* 1994;372(6501):55-63. doi:10.1038/372055a0
59. Sutton RB, Fasshauer D, Jahn R, Brunger AT. Crystal structure of a SNARE complex involved in synaptic exocytosis at 2.4 Å resolution. *Nature.* 1998;395(6700):347-353. doi:10.1038/26412
60. Ernst JA, Brunger AT. High resolution structure, stability, and synaptotagmin binding of a truncated neuronal SNARE complex. *J Biol Chem.* 2003;278(10):8630-8636. doi:10.1074/jbc.M211889200
61. Jahn R, Scheller RH. SNAREs — engines for membrane fusion. *Nat Rev Mol Cell Biol.* 2006;7(9):631-643. doi:10.1038/nrm2002
62. Brunger AT, Weninger K, Bowen M, Chu S. Single-Molecule Studies of the Neuronal SNARE Fusion Machinery. *Annu Rev Biochem.* 2009;78(1):903-928.

doi:10.1146/annurev.biochem.77.070306.103621

63. Harbury PAB. Springs and zippers: Coiled coils in SNARE-mediated membrane fusion. *Structure*. 1998;6(12):1487-1491. doi:10.1016/S0969-2126(98)00147-6
64. Skehel JJ, Wiley DC. Coiled coils in both intracellular vesicle and viral membrane fusion. *Cell*. 1998;95(7):871-874. doi:10.1016/S0092-8674(00)81710-9
65. Misura KMS, Scheller RH, Weis WI. Three-dimensional structure of the neuronal-Sec1-syntaxin 1a complex. *Nature*. 2000;404(6776):355-362. doi:10.1038/35006120
66. Hazzard J, Südhof TC, Rizo J. NMR analysis of the structure of synaptobrevin and of its interaction with syntaxin. *J Biomol NMR*. 1999;14(3):203-207. doi:10.1023/A:1008382027065
67. Fasshauer D, Otto H, Eliason WK, Jahn R, Brünger AT. Structural changes are associated with soluble N-ethylmaleimide-sensitive fusion protein attachment protein receptor complex formation. *J Biol Chem*. 1997;272(44):28036-28041. doi:10.1074/jbc.272.44.28036
68. Fasshauer D, Bruns D, Shen B, Jahn R, Brünger AT. A structural change occurs upon binding of syntaxin to SNAP-25. *J Biol Chem*. 1997;272(7):4582-4590. doi:10.1074/jbc.272.7.4582
69. Fiebig KM, Rice LM, Pollock E, Brunger AT. Folding intermediates of snare complex assembly. *Nat Struct Biol*. 1999;6(2):117-123. doi:10.1038/5803

70. Brunger AT. Structure and function of SNARE and SNARE-interacting proteins. *Q Rev Biophys.* 2005;38(1):1-47.
doi:10.1017/S0033583505004051
71. Sørensen JB, Wiederhold K, Müller EM, et al. Sequential N- To C-terminal SNARE complex assembly drives priming and fusion of secretory vesicles. *EMBO J.* 2006;25(5):955-966.
doi:10.1038/sj.emboj.7601003
72. Fasshauer D, Sutton RB, Brunger AT, Jahn R. Conserved structural features of the synaptic fusion complex: SNARE proteins reclassified as Q- and R-SNAREs. *Proc Natl Acad Sci U S A.* 1998;95(26):15781-15786. doi:10.1073/pnas.95.26.15781
73. Scales SJ, Yoo BY, Scheller RH. The ionic layer is required for efficient dissociation of the SNARE complex by α -SNAP and NSF. *Proc Natl Acad Sci U S A.* 2001;98(25):14262-14267.
doi:10.1073/pnas.251547598
74. Hayashi T, McMahon H, Yamasaki S, et al. Synaptic vesicle membrane fusion complex: action of clostridial neurotoxins on assembly. *EMBO J.* 1994;13(21):5051-5061. doi:10.1002/j.1460-2075.1994.tb06834.x
75. Wiederhold K, Fasshauer D. Is assembly of the SNARE complex enough to fuel membrane fusion? *J Biol Chem.* 2009;284(19):13143-13152. doi:10.1074/jbc.M900703200

76. Fasshauer D, Margittai M. A Transient N-terminal Interaction of SNAP-25 and Syntaxin Nucleates SNARE Assembly. *J Biol Chem.* 2004;279(9):7613-7621. doi:10.1074/jbc.M312064200
77. Meyenberg K, Lygina AS, van den Bogaart G, Jahn R, Diederichsen U. SNARE derived peptide mimic inducing membrane fusion. *Chem Commun.* 2011;47(33):9405. doi:10.1039/c1cc12879e
78. Robson Marsden H, Elbers NA, Bomans PHH, Sommerdijk NAJM, Kros A. A Reduced SNARE Model for Membrane Fusion. *Angew Chemie.* 2009;121(13):2366-2369. doi:10.1002/ange.200804493
79. Kumar P, Guha S, Diederichsen U. SNARE protein analog-mediated membrane fusion. *J Pept Sci.* 2015;21(8):621-629. doi:10.1002/psc.2773
80. Calakos N, Bennett M, Peterson K, Scheller R. Protein-protein interactions contributing to the specificity of intracellular vesicular trafficking. *Science (80-).* 1994;263(5150):1146-1149. doi:10.1126/science.8108733
81. Ferrari E, Darios F, Zhang F, et al. Binary polypeptide system for permanent and oriented protein immobilization. *J Nanobiotechnology.* 2010;8:1-14. doi:10.1186/1477-3155-8-9
82. Matos MF, Mukherjee K, Chen X, Rizo J, Südhof TC. Evidence for SNARE zipper during Ca²⁺-triggered exocytosis in PC12 cells. *Neuropharmacology.* 2003;45(6):777-786. doi:10.1016/S0028-3908(03)00318-6

83. Wang C-C, Shi H, Guo K, et al. VAMP8/Endobrevin as a General Vesicular SNARE for Regulated Exocytosis of the Exocrine System. Malhotra V, ed. *Mol Biol Cell*. 2007;18(3):1056-1063.
doi:10.1091/mbc.e06-10-0974
84. Darios F, Niranjana D, Ferrari E, et al. SNARE tagging allows stepwise assembly of a multimodular medicinal toxin. *Proc Natl Acad Sci*. 2010;107(42):18197-18201. doi:10.1073/pnas.1007125107
85. Hussain R, Jávorfí T, Siligardi G. Circular dichroism beamline B23 at the Diamond Light Source. *Synchrotron Radiat*. 2012;19:132-135.
86. Kelly S, Price N. The Use of Circular Dichroism in the Investigation of Protein Structure and Function. *Curr Protein Pept Sci*. 2000;1(4):349-384. doi:10.2174/1389203003381315
87. Parker JL, Newstead S. The Next Generation in Membrane Protein Structure Determination. *Adv Exp Med Biol*. 2016;922:61-72.
doi:10.1007/978-3-319-35072-1
88. van Mierlo CPM, de Jongh HHJ, Visser AJWG. Circular Dichroism of Proteins in Solution and at Interfaces. *Appl Spectrosc Rev*. 2000;35(4):277-313. doi:10.1081/ASR-100101227
89. Wei Y, Thyparambil AA, Latour RA. Protein helical structure determination using CD spectroscopy for solutions with strong background absorbance from 190 to 230nm. *Biochim Biophys Acta - Proteins Proteomics*. 2014;1844(12):2331-2337.
doi:10.1016/j.bbapap.2014.10.001

90. Margittai M, Fasshauer D, Pabst S, Jahn R, Langen R. Homo- and Heterooligomeric SNARE Complexes Studied by Site-directed Spin Labeling. *J Biol Chem.* 2001;276(16):13169-13177.
doi:10.1074/jbc.M010653200
91. Chen YA, Scales SJ, Duvvuri V, et al. Calcium Regulation of Exocytosis in PC12 Cells. *J Biol Chem.* 2001;276(28):26680-26687.
doi:10.1074/jbc.M103522200
92. Pabst S, Hazzard JW, Antonin W, et al. Selective Interaction of Complexin with the Neuronal SNARE Complex. *J Biol Chem.* 2000;275(26):19808-19818. doi:10.1074/jbc.M002571200
93. Chen X, Tomchick DR, Kovrigin E, et al. Three-dimensional structure of the complexin/SNARE complex. *Neuron.* 2002;33(3):397-409. doi:10.1016/S0896-6273(02)00583-4
94. Ferrari E, Soloviev M, Niranjana D, et al. Assembly of protein building blocks using a short synthetic peptide. *Bioconjug Chem.* 2012;23(3):479-484. doi:10.1021/bc2005208
95. Stein A, Weber G, Wahl M, Jahn R. Helical extension of the neuronal SNARE complex into the membrane. *Nature.* 2009;460:525-528. doi:10.1038/nature08156
96. Foster LJ, Yeung B, Mohtashami M, Ross K, Trimble WS, Klip A. Binary interactions of the SNARE proteins syntaxin-4, SNAP23, and VAMP- 2 and their regulation by phosphorylation. *Biochemistry.* 1998;37(31):11089-11096. doi:10.1021/bi980253t

97. Ma W, Saccardo A, Roccatano D, et al. Modular assembly of proteins on nanoparticles. *Nat Commun.* 2018;9(1).
doi:10.1038/s41467-018-03931-4
98. Stothard P. The Sequence Manipulation Suite: JavaScript Programs for Analyzing and Formatting Protein and DNA Sequences. *Biotechniques.* 2000;28(6):1102-1104.
doi:10.2144/00286ir01
99. Laera S, Ceccone G, Rossi F, et al. Measuring Protein Structure and Stability of Protein–Nanoparticle Systems with Synchrotron Radiation Circular Dichroism. *Nano Lett.* 2011;11(10):4480-4484.
doi:10.1021/nl202909s
100. Hussain R, Benning K, Myatt D, et al. CDApps : integrated software for experimental planning and data processing at beamline B23, Diamond Light Source. Corrigendum. *J Synchrotron Radiat.* 2015;22(3):862-862. doi:10.1107/S1600577515007602
101. Benard V, Bokoch GM. Assay of Cdc42, Rac, and Rho GTPase activation by affinity methods. *Methods Enzymol.* 2002;345:349-359.
102. Schechtman D, Mochly-Rosen D, Ron D. Glutathione S-Transferase Pull-Down Assay. In: *Protein Kinase C Protocols.* Vol 233. New Jersey: Humana Press; 2003:345-350. doi:10.1385/1-59259-397-6:345
103. Hussain R, Siligardi G. Characterisation of Conformational and Ligand Binding Properties of Membrane Proteins Using

- Synchrotron Radiation Circular Dichroism (SRCD). In: *Moraes I. (Eds) The Next Generation in Membrane Protein Structure Determination. Advances in Experimental Medicine and Biology.* Springer, Cham; 2016:43-59. doi:10.1007/978-3-319-35072-1_4
104. Zinna F, Resta C, Górecki M, et al. Circular Dichroism Imaging: Mapping the Local Supramolecular Order in Thin Films of Chiral Functional Polymers. *Macromolecules.* 2017;50(5):2054-2060. doi:10.1021/acs.macromol.6b02590
105. Park SM, Jung HY, Chung KC, Rhim H, Park JH, Kim J. Stress-Induced Aggregation Profiles of GST- α -Synuclein Fusion Proteins: Role of the C-Terminal Acidic Tail of α -Synuclein in Protein Thermosolubility and Stability †. *Biochemistry.* 2002;41(12):4137-4146. doi:10.1021/bi015961k
106. Harper S, Speicher DW. Expression and Purification of GST Fusion Proteins. In: *Current Protocols in Protein Science.* Hoboken, NJ, USA: John Wiley & Sons, Inc.; 2008:6.6.1-6.6.26. doi:10.1002/0471140864.ps0606s52
107. Wang S, Humphreys ES, Chung S-Y, et al. Peptides with selective affinity for carbon nanotubes. *Nat Mater.* 2003;2(3):196-200. doi:10.1038/nmat833
108. Sunna A, Chi F, Bergquist PL. A linker peptide with high affinity towards silica-containing materials. *N Biotechnol.* 2013;30(5):485-492. doi:10.1016/j.nbt.2012.11.022

109. Dudgeon K, Rouet R, Kokmeijer I, et al. General strategy for the generation of human antibody variable domains with increased aggregation resistance. *Proc Natl Acad Sci.* 2012;109(27):10879-10884. doi:10.1073/pnas.1202866109
110. Li L, Li NK, Tu Q, et al. Functional Modification of Silica through Enhanced Adsorption of Elastin-Like Polypeptide Block Copolymers. *Biomacromolecules.* 2018;19(2):298-306. doi:10.1021/acs.biomac.7b01307
111. Pechar M, Pola R. The coiled coil motif in polymer drug delivery systems. *Biotechnol Adv.* 2013;31(1):90-96. doi:10.1016/j.biotechadv.2012.01.003
112. Andrew Mackay J, Chilkoti A. Temperature sensitive peptides: Engineering hyperthermia-directed therapeutics. *Int J Hyperth.* 2008;24(6):483-495. doi:10.1080/02656730802149570
113. Al-Ahmady ZS, Al-Jamal WT, Bossche J V., et al. Lipid–Peptide Vesicle Nanoscale Hybrids for Triggered Drug Release by Mild Hyperthermia in Vitro and in Vivo. *ACS Nano.* 2012;6(10):9335-9346. doi:10.1021/nn302148p
114. Lee N, Yoo D, Ling D, Cho MH, Hyeon T, Cheon J. Iron Oxide Based Nanoparticles for Multimodal Imaging and Magneto-responsive Therapy. *Chem Rev.* 2015;115(19):10637-10689. doi:10.1021/acs.chemrev.5b00112

115. Chen CC, Lin YP, Wang CW, et al. DNA-gold nanorod conjugates for remote control of localized gene expression by near infrared irradiation. *J Am Chem Soc.* 2006;128(11):3709-3715.
doi:10.1021/ja0570180
116. Charan S, Sanjiv K, Singh N, et al. Development of Chitosan Oligosaccharide-Modified Gold Nanorods for in Vivo Targeted Delivery and Noninvasive Imaging by NIR Irradiation. *Bioconjug Chem.* 2012;23(11):2173-2182. doi:10.1021/bc3001276
117. Sapsford KE, Algar WR, Berti L, et al. Functionalizing Nanoparticles with Biological Molecules: Developing Chemistries that Facilitate Nanotechnology. *Chem Rev.* 2013;113(3):1904-2074.
doi:10.1021/cr300143v
118. Sola L, Gori A, Cretich M, Finetti C, Zilio C, Chiari M. Clickable Polymeric Coating for Oriented Peptide Immobilization. In: Cretich M, Chiari M, eds. *Peptide Microarrays*. Springer US; 2016:167-182.
doi:10.1007/978-1-4939-3037-1_13

6. APPENDIX

A. Protein sequences

Protein	Amino acid sequence	MW (kDa)
Syntaxin 1	GSEIIKLENSIRELHDMFMDMAMLVESQGEMIDRIEYNVEHAVDYVERAVSDTKKAGS	6.6
VAMP2-L	GSRLQQTQAQVDEVVDIMRVNVDKVLERDQKLSLDDRADALQAGASQFETSAAKLCGS	6.6
VAMP2-S	GSRLQQTQAQVDEVVDIMRVNVDKVLECGS	3.3
Syntaxin 3	GSDIVRLESSIKELHDMFMDIAMLVENQGEMLDNIELNVMHTVDHVEKARDETKRAGS	6.4
SNAP25	GSMAEDADMRNELEEMQRRADQLADESLESTRRMLQLVEESKDAGIRTLVMLDEQGEQL ERIEEGMDQINKDMKEAEKNLTDLGKFAGLAVAFANKLKSSDAYKKAAGNNQDGVVASQ PARVVDEREQMAISGGFIRRVTNDARENEMDENLEQVSGIIGNLRHMALDMGNEIDTQN RQIDRIMEKADSNKTRIDEANQRATKMLGSG	23.3
HH	GSSTRRMLQLVEESKDAGIRTLVMLDEQGEQLERIEEGMDQINKDMKEAEKNLTDLGSG KFAGLAVAFANKLKSSDAYKKAAGNNQDGVVASQPARVVDEREQMAISGGFIRRVTND ARENEMDEGSNLEQVSGIIGNLRHMALDMGNEIDTQNRQIDRIMEKADSNKTRIDEANQR ATKMG	20.3
VS-L	GSRLQQTQAQVDEVVDIMRVNVDKVLERDQKLSLDDRADALQAGASQFETSAAKLCGS GKFAGLAVAFANKLKSSDAYKKAAGNNQDGVVASQPARVVDEREQMAISGGFIRRVTND ARENEMDEGSDIVRLESSIKELHDMFMDIAMLVENQGEMLDNIELNVMHTVDHVEKAR ETKRAGS	21.3
VS-S	GSRLQQTQAQVDEVVDIMRVNVDKVLECGSGKFAGLAVAFANKLKSSDAYKKAAGNNQD GVVASQPARVVDEREQMAISGGFIRRVTNDARENEMDEGSDIVRLESSIKELHDMFMDI AMLVENQGEMLDNIELNVMHTVDHVEKARDETKRAGS	17.2
VS-L2	GSRLQQTQAQVDEVVDIMRVNVDKVLERDQKLSLDDRADALQAGASQFETSAAKLCGS GGGGSGGGSGGGSGGAGSGGGAGSGGGAGSGGGSGGAGSGGGSGGGSDIVRLESSI KELHDMFMDIAMLVENQGEMLDNIELNVMHTVDHVEKARDETKRAGS	16.1
GST	MSPILGYWKIKGLVQPTRLLLEYLEEKYEELHYERDEGDKWRNKKFELGLEFPNLPYYI DGDVKTQSMATIRYIADKHNMLGGCPKERAESMLEGAVLDIRYGVSR IAYS KDFETL KVDFLSKLPEMLKMFEDRLCHKTYLNGDHVTHPDFMLYDALDVVLYMDPMCCLDAFPKLV CFKKRIEAI PQIDKYLKSSKY IAWPLQGWQATFGGGDHPPKSDLVPRGSPGISGGGGGI LDSMGRLELKLNS	28.6
GST-HH	MSPILGYWKIKGLVQPTRLLLEYLEEKYEELHYERDEGDKWRNKKFELGLEFPNLPYYI DGDVKTQSMATIRYIADKHNMLGGCPKERAESMLEGAVLDIRYGVSR IAYS KDFETL KVDFLSKLPEMLKMFEDRLCHKTYLNGDHVTHPDFMLYDALDVVLYMDPMCCLDAFPKLV CFKKRIEAI PQIDKYLKSSKY IAWPLQGWQATFGGGDHPPKSDLVPRGSSSTRRMLQLVE ESKDAGIRTLVMLDEQGEQLERIEEGMDQINKDMKEAEKNLTDLGSGKFAGLAVAFANK LKSSDAYKKAAGNNQDGVVASQPARVVDEREQMAISGGFIRRVTNDARENEMDEGSNLE QVSGIIGNLRHMALDMGNEIDTQNRQIDRIMEKADSNKTRIDEANQRATKMG	45.3

Table A.1 SNARE protein sequences. Amino acid sequences of recombinant proteins and their molecular weight. The amino acid sequences are represented in different colour: red = syntaxin SNARE domains, blue = VAMP2 SNARE domains, dark green = N-terminal SNARE domain (H1) of SNAP25, light green = C-terminal H2 domain of SNAP25, purple = linker 1 (natural linker occurring between SNARE domains of SNAP25), yellow = artificial linker k, light blue = GST, black = glycine and serine (GS) residues originated from the cloning strategy. The cysteine-to-alanine substitutions and the extra cysteine residues introduced for chemical cross-linking are highlighted in yellow and blue, respectively.

B. DNA sequencing data

DNA sequencing was used to determine the sequence of plasmids obtained from plasmid cloning (See Section 2.2.7). 0.5 µg of each sample (100ng/µl, 5µl) were sent to Source Bioscience for sequencing, using suitable primers for pGEX-KG, both forward and reverse.

All the constructs were successfully cloned, as seen in Figures B.1-8.

SCORE	EXPECT	IDENTITIES	GAPS	STRAND
337 bits (182)	6e-97	182/182 (100%)	0/182 (0%)	Plus/Plus
SYNT1_T	1	GATCAGAAATTATTAACACTGAAAAACAGCATTTCGCGAACTGCATGATATGTTTATGGATA	60	
SYNT1_E	35	GATCAGAAATTATTAACACTGAAAAACAGCATTTCGCGAACTGCATGATATGTTTATGGATA	94	
SYNT1_T	61	TGGCGATGCTGGTGGAAAGCCAGGGCGAAATGATTGATCGCATTGAATATAACGTGGAAC	120	
SYNT1_E	95	TGGCGATGCTGGTGGAAAGCCAGGGCGAAATGATTGATCGCATTGAATATAACGTGGAAC	154	
SYNT1_T	121	ATGCGGTGGATTATGTGGAACGCGCGGTGAGCGATAACAAAAAGCGGGATCCTAGGAGC	180	
SYNT1_E	155	ATGCGGTGGATTATGTGGAACGCGCGGTGAGCGATAACAAAAAGCGGGATCCTAGGAGC	214	
SYNT1_T	181	TC	182	
SYNT1_E	215	TC	216	

Figure B.1 Alignment of the theoretical and experimental sequence of syntaxin 1. SYNT1_T was obtained *in silico* (Theoretical, T) from reverse translation of syntaxin 1 sequence. SYNT1_E is the result of the sequencing (Source Bioscience) of the plasmid obtained *in vitro* (Experimental, E). They were aligned with Blastn (NCBI) to verify their validity: there are 100% identity and 0% gaps between the two sequences.

SCORE	EXPECT	IDENTITIES	GAPS	STRAND
337 bits (182)	7e-97	182/182 (100%)	0/182 (0%)	Plus/Plus
SYNT3_T	1	GATCAGATATTGTGCGCCTGAAAGCAGCATTAAAGAAGTGCATGATATGTTTATGGATA	60	
SYNT3_E	32	GATCAGATATTGTGCGCCTGAAAGCAGCATTAAAGAAGTGCATGATATGTTTATGGATA	91	
SYNT3_T	61	TTGCGATGCTGGTGGAAAACCGGGCGAAATGCTGGATAACATTGAACTGAACGTGATGC	120	
SYNT3_E	92	TTGCGATGCTGGTGGAAAACCGGGCGAAATGCTGGATAACATTGAACTGAACGTGATGC	151	
SYNT3_T	121	ATACCGTGGATCATGTGGA AAAAGCGCGCATGAAACCAAACGCGGGATCCTAGGAGC	180	
SYNT3_E	152	ATACCGTGGATCATGTGGA AAAAGCGCGCATGAAACCAAACGCGGGATCCTAGGAGC	211	
SYNT3_T	181	TC	182	
SYNT3_E	212	TC	213	

Figure B.2 Alignment of the theoretical and experimental sequence of syntaxin 3. SYNT3_T was obtained *in silico* (Theoretical, T) from reverse translation of syntaxin 3 sequence. SYNT3_E is the result of the sequencing (Source Bioscience) of the plasmid obtained *in vitro* (Experimental, E). They were aligned with Blastn (NCBI) to verify their validity: there are 100% identity and 0% gaps between the two sequences.

SCORE	EXPECT	IDENTITIES	GAPS	STRAND
342 bits(185)	7e-99	185/185(100%)	0/185(0%)	Plus/Plus
VAMP2L_T	1	GATCACGCCTGCAGCAGACCCAGGCGCAGGTGGATGAAGTGGTGGATATTATGCGCGTGA	60	
VAMP2L_E	36	GATCACGCCTGCAGCAGACCCAGGCGCAGGTGGATGAAGTGGTGGATATTATGCGCGTGA	95	
VAMP2L_T	61	ACGTGGATAAAGTGCTGGAACGCGATCAGAACTGAGCGAACTGGATGATCGCGCGGATG	120	
VAMP2L_E	96	ACGTGGATAAAGTGCTGGAACGCGATCAGAACTGAGCGAACTGGATGATCGCGCGGATG	155	
VAMP2L_T	121	CGCTGCAGCGGGCGCGAGCCAGTTTGAACCAGCGCGGCGAACTGTGCGGATCCTAGG	180	
VAMP2L_E	156	CGCTGCAGCGGGCGCGAGCCAGTTTGAACCAGCGCGGCGAACTGTGCGGATCCTAGG	215	
VAMP2L_T	181	AGCTC	185	
VAMP2L_E	216	AGCTC	220	

Figure B.3 Alignment of the theoretical and experimental sequence of VAMP2-L. VAMP2-L_T was obtained *in silico* (Theoretical, T) from reverse translation of VAMP2-L sequence. VAMP2-L_E is the result of the sequencing (Source Bioscience) of the plasmid obtained *in vitro* (Experimental, E). They were aligned with Blastn (NCBI) to verify their validity: there are 100% identity and 0% gaps between the two sequences.

SCORE	EXPECT	IDENTITIES	GAPS	STRAND
182 bits(98)	2e-50	98/98(100%)	0/98(0%)	Plus/Minus
VAMP2S_T	1	GATCACGCCTGCAGCAGACCCAGGCGCAGGTGGATGAAGTGGTGGATATTATGCGCGTGA	60	
VAMP2S_E	155	GATCACGCCTGCAGCAGACCCAGGCGCAGGTGGATGAAGTGGTGGATATTATGCGCGTGA	96	
VAMP2S_T	61	ACGTGGATAAAGTGCTGGAATGCGGATCCTAGGAGCTC	98	
VAMP2S_E	95	ACGTGGATAAAGTGCTGGAATGCGGATCCTAGGAGCTC	58	

Figure B.4 Alignment of the theoretical and experimental sequence of VAMP2-S. VAMP2-S_T was obtained *in silico* (Theoretical, T) from reverse translation of VAMP2-S sequence. VAMP2-S_E is the result of the sequencing (Source Bioscience) of the plasmid obtained *in vitro* (Experimental, E). They were aligned with Blastn (NCBI) to verify their validity: there are 100% identity and 0% gaps between the two sequences.

SCORE	EXPECT	IDENTITIES	GAPS	STRAND
1011 bits (547)	0.0	547/547 (100%)	0/547 (0%)	Plus/Plus
HH_T	1	GATCAAGCACCCGCCGCATGCTGCAGCTGGTGGAAAGAAAGCAAAGATGCGGGCATTTCGCA	60	
HH_E	36	GATCAAGCACCCGCCGCATGCTGCAGCTGGTGGAAAGAAAGCAAAGATGCGGGCATTTCGCA	95	
HH_T	61	CCCTGGTGATGCTGGATGAACAGGGCGAACAGCTGGAACGCATTGAAGAAGGCATGGATC	120	
HH_E	96	CCCTGGTGATGCTGGATGAACAGGGCGAACAGCTGGAACGCATTGAAGAAGGCATGGATC	155	
HH_T	121	AGATTAACAAAGATATGAAAGAAGCGGaaaaaaaaCCTGACCGATCTGGGATCAGGCAAAT	180	
HH_E	156	AGATTAACAAAGATATGAAAGAAGCGGAAAAAAAAACCTGACCGATCTGGGATCAGGCAAAT	215	
HH_T	181	TTGCGGGCCTGGCGGTGGCGCCGCGGAACAAACTGAAAAGCAGCGATGCGTATAAAAAAG	240	
HH_E	216	TTGCGGGCCTGGCGGTGGCGCCGCGGAACAAACTGAAAAGCAGCGATGCGTATAAAAAAG	275	
HH_T	241	CGTGGGGCAACAACCAGGATGGCGTGGTGGCGAGCCAGCCGGCGCGCTGGTGGATGAAC	300	
HH_E	276	CGTGGGGCAACAACCAGGATGGCGTGGTGGCGAGCCAGCCGGCGCGCTGGTGGATGAAC	335	
HH_T	301	GCGAACAGATGGCGATTAGCGCGGCTTTATTCGCCGCGTGACCAACGATGCGCGCGAAA	360	
HH_E	336	GCGAACAGATGGCGATTAGCGCGGCTTTATTCGCCGCGTGACCAACGATGCGCGCGAAA	395	
HH_T	361	ACGAAATGGATGAAGGATCAAACCTGGAACAGGTGAGCGGCATTATTGGCAACCTGCGCC	420	
HH_E	396	ACGAAATGGATGAAGGATCAAACCTGGAACAGGTGAGCGGCATTATTGGCAACCTGCGCC	455	
HH_T	421	ATATGGCGCTGGATATGGGCAACGAAATTGATACCCAGAACC GCCAGATTGATCGCATT	480	
HH_E	456	ATATGGCGCTGGATATGGGCAACGAAATTGATACCCAGAACC GCCAGATTGATCGCATT	515	
HH_T	481	TGGAAAAAGCGGATAGCAACAAAACCCGCATTGATGAAGCGAACCGCGCGACCAAAA	540	
HH_E	516	TGGAAAAAGCGGATAGCAACAAAACCCGCATTGATGAAGCGAACCGCGCGACCAAAA	575	
HH_T	541	TGGGATC	547	
HH_E	576	TGGGATC	582	

Figure B.5 Alignment of the theoretical and experimental sequence of HH. HH_T was obtained *in silico* (Theoretical, T) from reverse translation of H1, linker 1 and H2 from SNAP25 sequence. HH_E is the result of the sequencing (Source Bioscience) of the plasmid obtained *in vitro* (Experimental, E). They were aligned with Blastn (NCBI) to verify their validity: there are 100% identity and 0% gaps between the two sequences.

SCORE	EXPECT	IDENTITIES	GAPS	STRAND
1035 bits (560)	0.0	560/560 (100%)	0/560 (0%)	Plus/Minus
VS-L_T	1	GATCAGCCTGCAGCAGACCCAGGCGCAGGTGGATGAAGTGGTGGATATTATGCGCGTGA	60	
VS-L_E	614	GATCAGCCTGCAGCAGACCCAGGCGCAGGTGGATGAAGTGGTGGATATTATGCGCGTGA	555	
VS-L_T	61	ACGTGGATAAAGTGTGGAACGCGATCAGAACTGAGCGAACTGGATGATCGCGCGGATG	120	
VS-L_E	554	ACGTGGATAAAGTGTGGAACGCGATCAGAACTGAGCGAACTGGATGATCGCGCGGATG	495	
VS-L_T	121	CGCTGCAGGCGGGCGCGAGCCAGTTTGAAACCGCGCGGCGAACTGTGCGGATCAGGCA	180	
VS-L_E	494	CGCTGCAGGCGGGCGCGAGCCAGTTTGAAACCGCGCGGCGAACTGTGCGGATCAGGCA	435	
VS-L_T	181	AATTTGCGGGCCTGGCGGTGGCGCGGCGGAACAACTGAAAAGCAGCGATGCGTATAAAA	240	
VS-L_E	434	AATTTGCGGGCCTGGCGGTGGCGCGGCGGAACAACTGAAAAGCAGCGATGCGTATAAAA	375	
VS-L_T	241	AAGCGTGGGGCAACAAC CAGGATGGCGTGGTGGCGAGCCAGCCGCGCGCGTGGTGGATG	300	
VS-L_E	374	AAGCGTGGGGCAACAAC CAGGATGGCGTGGTGGCGAGCCAGCCGCGCGCGTGGTGGATG	315	
VS-L_T	301	AACGCGAACAGATGGCGATTAGCGGCGGCTTTATTCGCCGCGTGACCAACGATGCGCGCG	360	
VS-L_E	314	AACGCGAACAGATGGCGATTAGCGGCGGCTTTATTCGCCGCGTGACCAACGATGCGCGCG	255	
VS-L_T	361	AAAACGAAATGGATGAAGGATCAGATATTGTGCGCCTGAAAAGCAGCATTAAAGAAGTGC	420	
VS-L_E	254	AAAACGAAATGGATGAAGGATCAGATATTGTGCGCCTGAAAAGCAGCATTAAAGAAGTGC	195	
VS-L_T	421	ATGATATGTTTATGGATATTGCGATGCTGGTGGAAAAC CAGGGCGAAATGCTGGATAACA	480	
VS-L_E	194	ATGATATGTTTATGGATATTGCGATGCTGGTGGAAAAC CAGGGCGAAATGCTGGATAACA	135	
VS-L_T	481	TGAACTGAACGTGATGCATACCGTGGATCATGTGGA AAAAGCGCGGATGAAACCAAAC	540	
VS-L_E	134	TGAACTGAACGTGATGCATACCGTGGATCATGTGGA AAAAGCGCGGATGAAACCAAAC	75	
VS-L_T	541	GCGCGGGATCCTAGGAGCTC	560	
VS-L_E	74	GCGCGGGATCCTAGGAGCTC	55	

Figure B.6 Alignment of the theoretical and experimental sequence of VS-L. VS-L_T was obtained *in silico* (Theoretical, T) from reverse translation of VAMP2-L, linker 1 and syntaxin 3 as a fusion complex. VS-L_E is the result of the sequencing (Source Bioscience) of the plasmid obtained *in vitro* (Experimental, E). They were aligned with Blastn (NCBI) to verify their validity: there are 100% identity and 0% gaps between the two sequences.

SCORE	EXPECT	IDENTITIES	GAPS	STRAND
874 bits(473)	0.0	473/473(100%)	0/473(0%)	Plus/Plus
VS-S_T	1	GATCACGCCTGCAGCAGACCCAGGCGCAGGTGGATGAAGTGGTGGATATTATGCGCGTGA	60	
VS-S_E	418	GATCACGCCTGCAGCAGACCCAGGCGCAGGTGGATGAAGTGGTGGATATTATGCGCGTGA	477	
VS-S_T	61	ACGTGGATAAAGTGTGGAATGCGGATCAGGCAAATTTGCGGGCCTGGCGGTGGCGCCGG	120	
VS-S_E	478	ACGTGGATAAAGTGTGGAATGCGGATCAGGCAAATTTGCGGGCCTGGCGGTGGCGCCGG	537	
VS-S_T	121	CGAACAAACTGAAAAGCAGCGATGCGTATAAAAAAGCGTGGGGCAACAACCAGGATGGCG	180	
VS-S_E	538	CGAACAAACTGAAAAGCAGCGATGCGTATAAAAAAGCGTGGGGCAACAACCAGGATGGCG	597	
VS-S_T	181	TGGTGGCGAGCCAGCCGGCGCGCGTGGTGGATGAACGCGAACAGATGGCGATTAGCGGCG	240	
VS-S_E	598	TGGTGGCGAGCCAGCCGGCGCGCGTGGTGGATGAACGCGAACAGATGGCGATTAGCGGCG	657	
VS-S_T	241	GCTTTATTCGCCCGGTGACCAACGATGCGCGCGAAAACGAAATGGATGAAGGATCAGATA	300	
VS-S_E	658	GCTTTATTCGCCCGGTGACCAACGATGCGCGCGAAAACGAAATGGATGAAGGATCAGATA	717	
VS-S_T	301	TTGTGCGCCTGGAAAGCAGCATTAAAGAACTGCATGATATGTTTATGGATATTGCGATGC	360	
VS-S_E	718	TTGTGCGCCTGGAAAGCAGCATTAAAGAACTGCATGATATGTTTATGGATATTGCGATGC	777	
VS-S_T	361	TGGTGGAAAACAGGGCGAAATGCTGGATAACATTGAACTGAACGTGATGCATACCGTGG	420	
VS-S_E	778	TGGTGGAAAACAGGGCGAAATGCTGGATAACATTGAACTGAACGTGATGCATACCGTGG	837	
VS-S_T	421	ATCATGTGAAAAAGCGCGGATGAAACCAAACGCGGGATCCTAGGAGCTC	473	
VS-S_E	838	ATCATGTGAAAAAGCGCGGATGAAACCAAACGCGGGATCCTAGGAGCTC	890	

Figure B.7 Alignment of the theoretical and experimental sequence of VS-S. VS-S_T was obtained *in silico* (Theoretical, T) from reverse translation of VAMP2-S, linker 1 and syntaxin 3 as a fusion complex. VS-S_E is the result of the sequencing (Source Bioscience) of the plasmid obtained *in vitro* (Experimental, E). They were aligned with Blastn (NCBI) to verify their validity: there are 100% identity and 0% gaps between the two sequences.

SCORE	EXPECT	IDENTITIES	GAPS	STRAND
929 bits(503)	0.0	503/503(100%)	0/503(0%)	Plus/Minus
VS-L2_T	1	GATCACGCCTGCAGCAGACCCAGGCCGAGGTGGATGAAGTGGTGGATATTATGCGCGTGA	60	
VS-L2_E	603	GATCACGCCTGCAGCAGACCCAGGCCGAGGTGGATGAAGTGGTGGATATTATGCGCGTGA	544	
VS-L2_T	61	ACGTGGATAAAGTGTGGAACGCGATCAGAACTGAGCGAACTGGATGATCGCGCGGATG	120	
VS-L2_E	543	ACGTGGATAAAGTGTGGAACGCGATCAGAACTGAGCGAACTGGATGATCGCGCGGATG	484	
VS-L2_T	121	CGCTGCAGGCGGGCGAGCCAGTTTAAAACAgcgcgcgcaactgtgcgatcaggcg	180	
VS-L2_E	483	CGCTGCAGGCGGGCGAGCCAGTTTAAAACAgcgcgcgcaactgtgcgatcaggcg	424	
VS-L2_T	181	gtggcggtggcagcggtggcggttctggcggtggcggttagcgcggtgctgctgctg	240	
VS-L2_E	423	GTGGCGGTGGCAGCGGTGGCGGTCTTGGCGGTGGCGGTAGCGCGGTGCGGGTTCTGGCG	364	
VS-L2_T	241	gtggcgccggtggcagtggtggcggttccgcagcggtggcggttccgcggtgctgctg	300	
VS-L2_E	363	GTGGCGCCGTTGGCAGTGGTGGCGGTTCGCGAGCGGTGGCGGTTCGCGCGGTGCTGGCT	304	
VS-L2_T	301	CAGGCGGTGGCTCGGGTGGCGGATCAGATATTGTGCGCCTGAAAAGCAGCATTAAAGAAC	360	
VS-L2_E	303	CAGGCGGTGGCTCGGGTGGCGGATCAGATATTGTGCGCCTGAAAAGCAGCATTAAAGAAC	244	
VS-L2_T	361	TGCATGATATGTTTATGGATATTGCGATGCTGGTGGAAAACAGGGCGAAATGCTGGATA	420	
VS-L2_E	243	TGCATGATATGTTTATGGATATTGCGATGCTGGTGGAAAACAGGGCGAAATGCTGGATA	184	
VS-L2_T	421	ACATTGAACTGAACGTGATGCATACCGTGGATCATGTGGAAAAGCGCGGATGAAACCA	480	
VS-L2_E	183	ACATTGAACTGAACGTGATGCATACCGTGGATCATGTGGAAAAGCGCGGATGAAACCA	124	
VS-L2_T	481	AACGCGCGGGATCCTAGGAGCTC	503	
VS-L2_E	123	AACGCGCGGGATCCTAGGAGCTC	101	

Figure B.8 Alignment of the theoretical and experimental sequence of VS-L2. VS-L2_T was obtained *in silico* (Theoretical, T) from reverse translation of VAMP2-L, linker k and syntaxin 3 as a fusion complex. VS-L2_E is the result of the sequencing (Source Bioscience) of the plasmid obtained *in vitro* (Experimental, E). They were aligned with Blastn (NCBI) to verify their validity: there are 100% identity and 0% gaps between the two sequences.

C. Protein purification

After low-temperature expression in BL21-gold (DE3) pLysS cells (See Section 2.3), all the proteins were purified through affinity purification on GSH Sepharose beads, followed by size exclusion chromatography.

- Syntaxin 1

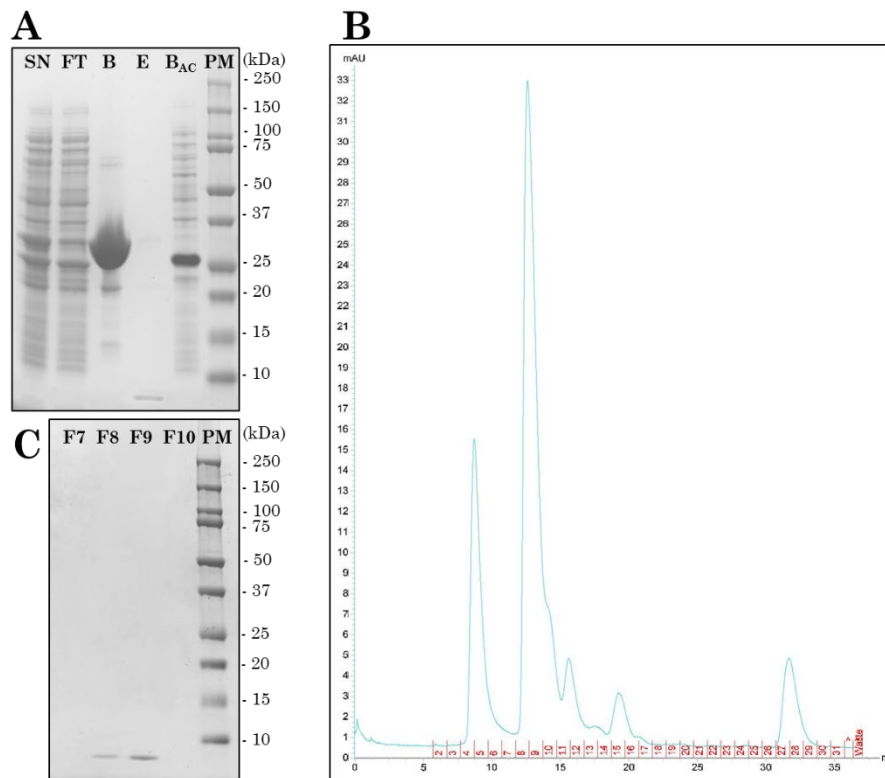


Figure C.1 Purification of syntaxin 1. A) SDS-PAGE of the affinity purification on GSH beads and thrombin cleavage of Syntaxin 1. The bacterial lysate was incubated with GSH Sepharose beads, leading to the immobilisation of GST-syntaxin 1 onto them; the elution of syntaxin 1, obtained by thrombin cleavage, was not well visible on the SDS-PAGE due to small protein size (lane E, band below 10kDa). Abbreviations: SN = supernatant, FT = flow through, B = beads, E = eluate, B_{AC} = beads after cleavage. B) Size exclusion chromatography chromatogram; red numbers on the bottom indicate the fractions collected by the ÄKTA Pure chromatography system (GE Healthcare). On the X-

axis, the elution volume (in ml); on the Y-axis, the UV-light absorption at 280nm, expressed in mAU (milli Absorbance Units). C) SDS-PAGE of the fractions collected by the FPLC. This gel confirms that syntaxin 1 is in F8 and F9.

- **VAMP2-L**

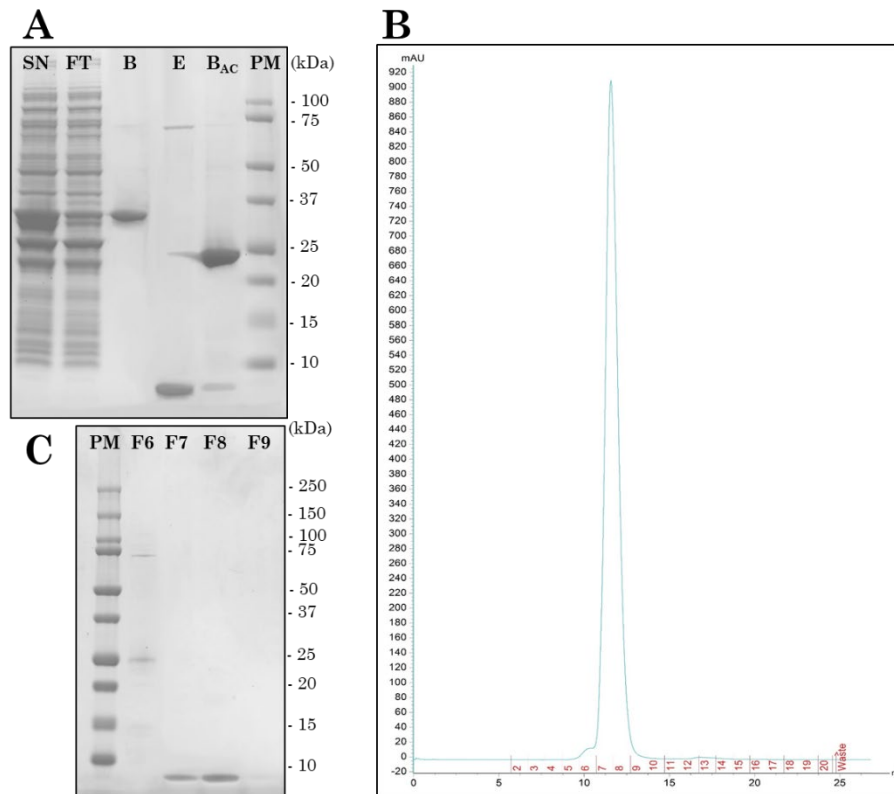


Figure C.2 Purification of VAMP2-L. A) SDS-PAGE of the affinity purification on GSH beads and thrombin cleavage of VAMP2-L. The bacterial lysate was incubated with GSH Sepharose beads, leading to the immobilisation of GST-VAMP2-L onto them; the elution of VAMP2-L was obtained by thrombin cleavage. In the eluate E, other than the band corresponding to VAMP2-L (~6.6kDa), there are two more bands at 25 and ~75kDa. Abbreviations: SN = supernatant, FT = flow through, B = beads, E = eluate, B_{AC} = beads after cleavage. B) Size exclusion chromatography chromatogram; red numbers on the bottom indicate the fractions collected by the ÄKTA Pure chromatography system (GE Healthcare). On the X-axis, the elution volume (in ml); on the Y-axis, the UV-light absorption at 280nm, expressed in mAU (milli Absorbance Units). C) SDS-PAGE of the fractions collected by the FPLC incubated with 5µM TCEP to avoid the formation of dimers. In lane F6, the two bands found in the eluate E, separated from the protein of interest: this gel confirms that VAMP2-L is mostly in F7 and F8.

- VAMP2-S

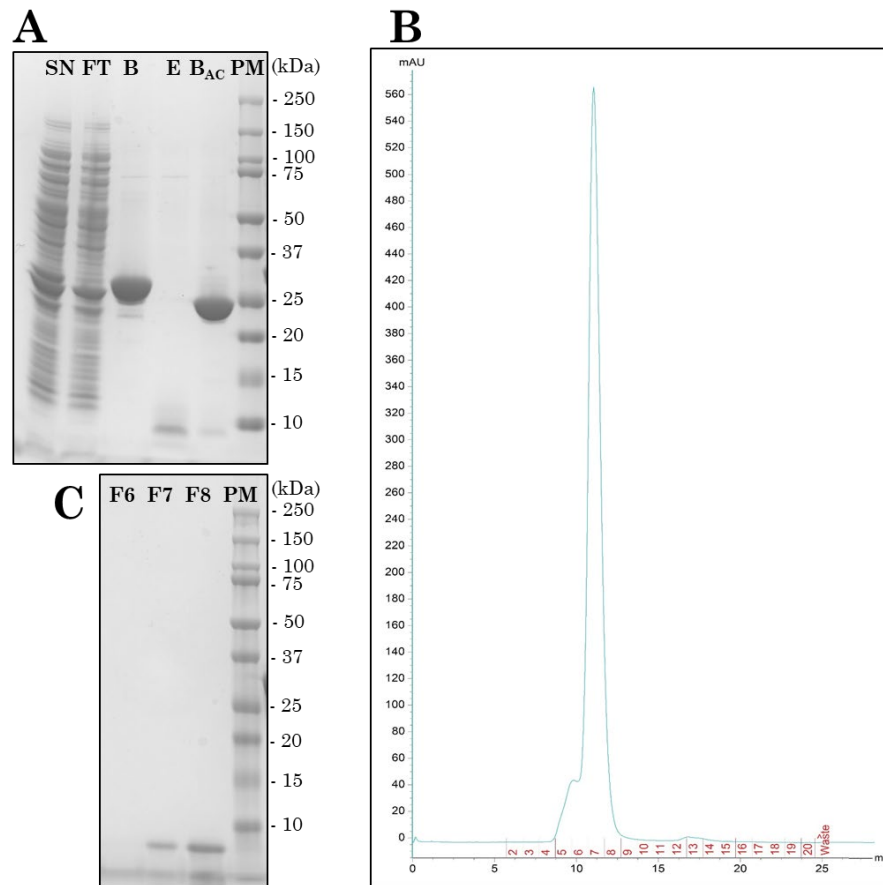


Figure C.3 Purification of VAMP2-S. A) SDS-PAGE of the affinity purification on GSH beads and thrombin cleavage of VAMP2-S. The bacterial lysate was incubated with GSH Sepharose beads, leading to the immobilisation of GST-VAMP2-S onto them; the elution of VAMP2-S was obtained by thrombin cleavage. VAMP2-S's molecular weight is 3.3kDa, but it migrated mostly as a dimer in the eluate (E) lane. Abbreviations: SN = supernatant, FT = flow through, B = beads, E = eluate, B_{AC} = beads after cleavage. B) Size exclusion chromatography chromatogram; red numbers on the bottom indicate the fractions collected by the ÄKTA Pure chromatography system (GE Healthcare). On the X-axis, the elution volume (in ml); on the Y-axis, the UV-light absorption at 280nm, expressed in mAU (milli Absorbance Units). C) SDS-PAGE of the fractions collected by the FPLC and incubated with 5µM TCEP to avoid the formation of dimers. This gel confirms that VAMP2-S is in F7 and F8.

- **Syntaxin 3**

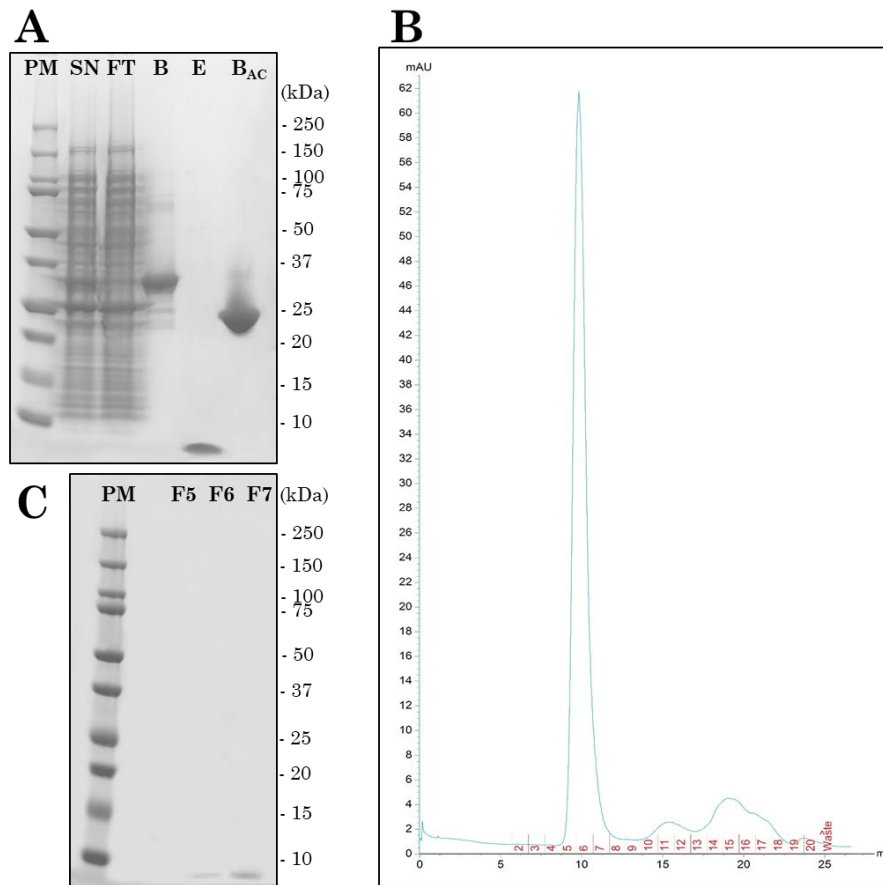


Figure C.4 Purification of syntaxin 3. A) SDS-PAGE of the affinity purification on GSH beads and thrombin cleavage of syntaxin 3. The bacterial lysate was incubated with GSH Sepharose beads, leading to the immobilisation of GST-syntaxin 3 onto them; the elution of syntaxin 3 was obtained by thrombin cleavage (6.4kDa, lane E). The expression and elution of syntaxin 3 are better than the one from syntaxin 1 (Figure C.1). Abbreviations: SN = supernatant, FT = flow through, B = beads, E = eluate, B_{AC} = beads after cleavage. B) Size exclusion chromatography chromatogram; red numbers on the bottom are the fractions collected by the ÄKTA Pure chromatography system (GE Healthcare). On the X-axis, the elution volume (in ml); on the Y-axis, the UV-light absorption at 280nm, expressed in mAU (milli Absorbance Units). C) SDS-PAGE of the fractions collected by the FPLC. This gel confirms that syntaxin 3 is in F6 and F7.

- SNAP25

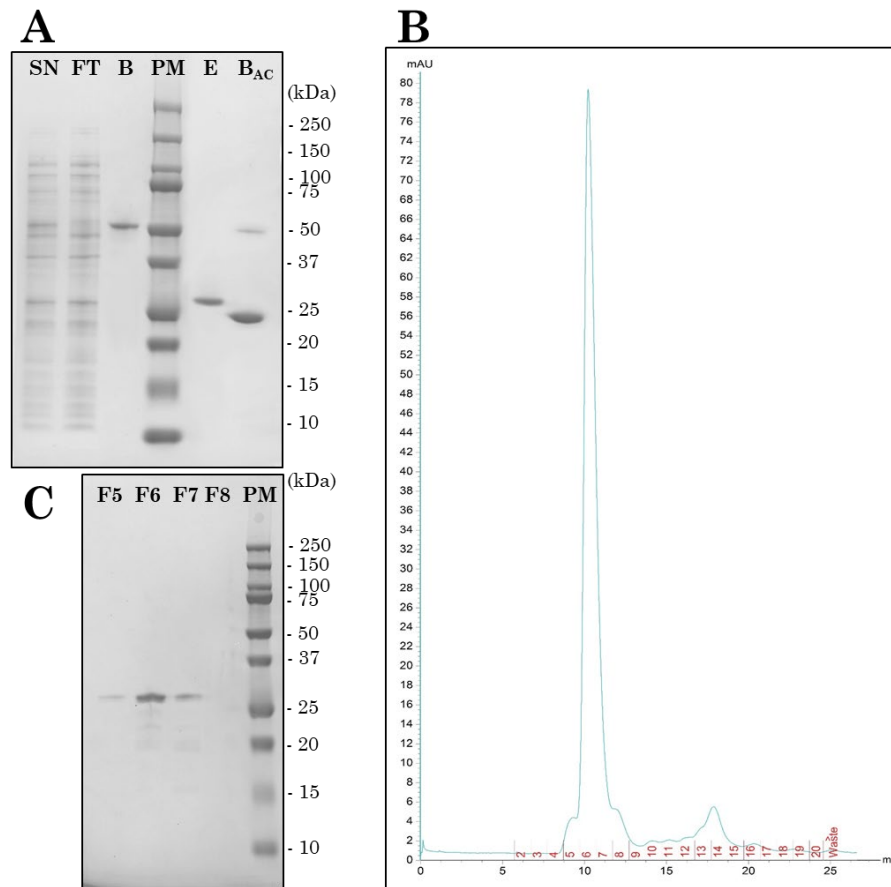


Figure C.5 Purification of SNAP25. A) SDS-PAGE of the affinity purification on GSH beads and thrombin cleavage of SNAP25. The bacterial lysate was incubated with GSH Sepharose beads, leading to the immobilisation of GST-SNAP25 onto them; the elution of SNAP25 was obtained by thrombin cleavage. The elution was not 100% efficient, as there is still some SNAP25 on the final beads (B_{AC}). In spite of its molecular weight being 23.3kDa, SNAP25 migrates as a heavier protein, approximately 28kDa. Abbreviations: SN = supernatant, FT = flow through, B = beads, E = eluate, B_{AC} = beads after cleavage. B) Size exclusion chromatography chromatogram; red numbers on the bottom are the fractions collected by the ÄKTA Pure chromatography system (GE Healthcare). On the X-axis, the elution volume (in ml); on the Y-axis, the UV-light absorption at 280nm, expressed in mAU (milli Absorbance Units). C) SDS-PAGE of the fractions collected by the FPLC. This gel confirms that SNAP25 is mostly in F6.

- HH

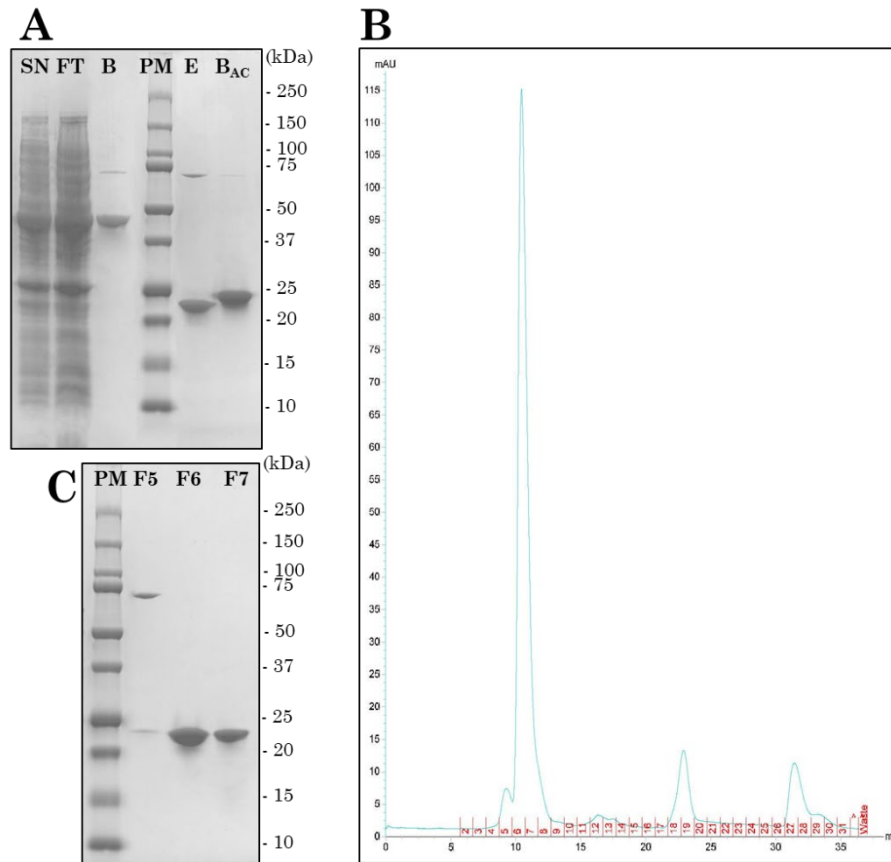


Figure C.6 Purification of HH. A) SDS-PAGE of the affinity purification on GSH beads and thrombin cleavage of HH. The bacterial lysate was incubated with GSH Sepharose beads, leading to the immobilisation of GST-HH onto them; the elution of HH was obtained by thrombin cleavage. As its equivalent SNAP25, it migrates as a slightly higher molecular weight protein (HH weighs 20.3kDa). Abbreviations: SN = supernatant, FT = flow through, B = beads, E = eluate, B_{AC} = beads after cleavage. B) Size exclusion chromatography chromatogram; red numbers on the bottom are the fractions collected by the ÄKTA Pure chromatography system (GE Healthcare). On the X-axis, the elution volume (in ml); on the Y-axis, the UV-light absorption at 280nm, expressed in mAU (milli Absorbance Units). C) SDS-PAGE of the fractions collected by the FPLC. This gel confirms that HH is mostly in F6 and F7; the high molecular weight band present in the eluate (E, gel A) is in lane F5.

- VS-L

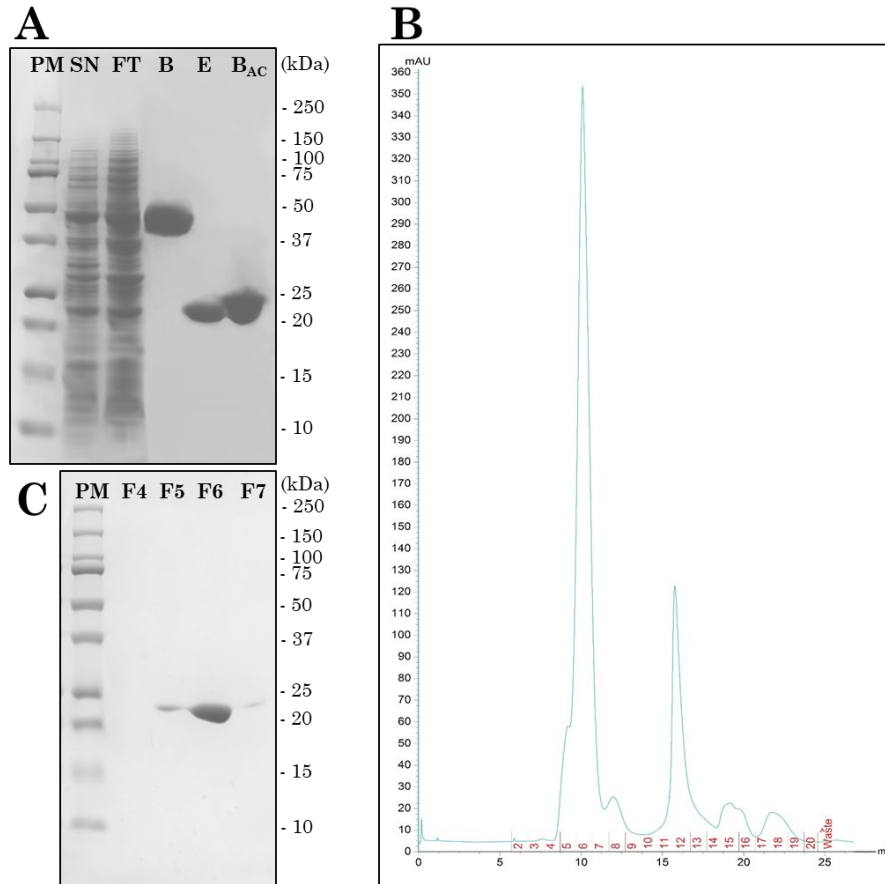


Figure C.7 Purification of VS-L. A) SDS-PAGE of the affinity purification on GSH beads and thrombin cleavage of VS-L. The bacterial lysate was incubated with GSH Sepharose beads, leading to the immobilisation of GST-VS-L onto them; the elution of VS-L (21.3kDa) was obtained by thrombin cleavage. Abbreviations: SN = supernatant, FT = flow through, B = beads, E = eluate, B_{Ac} = beads after cleavage. B) Size exclusion chromatography chromatogram; red numbers on the bottom are the fractions collected by the ÄKTA Pure chromatography system (GE Healthcare). On the X-axis, the elution volume (in ml); on the Y-axis, the UV-light absorption at 280nm, expressed in mAU (milli Absorbance Units). C) SDS-PAGE of the fractions collected by the FPLC incubated with 5 μ M TCEP to avoid the formation of dimers. This gel confirms that VS-L is mostly in F5 and F6.

- VS-S

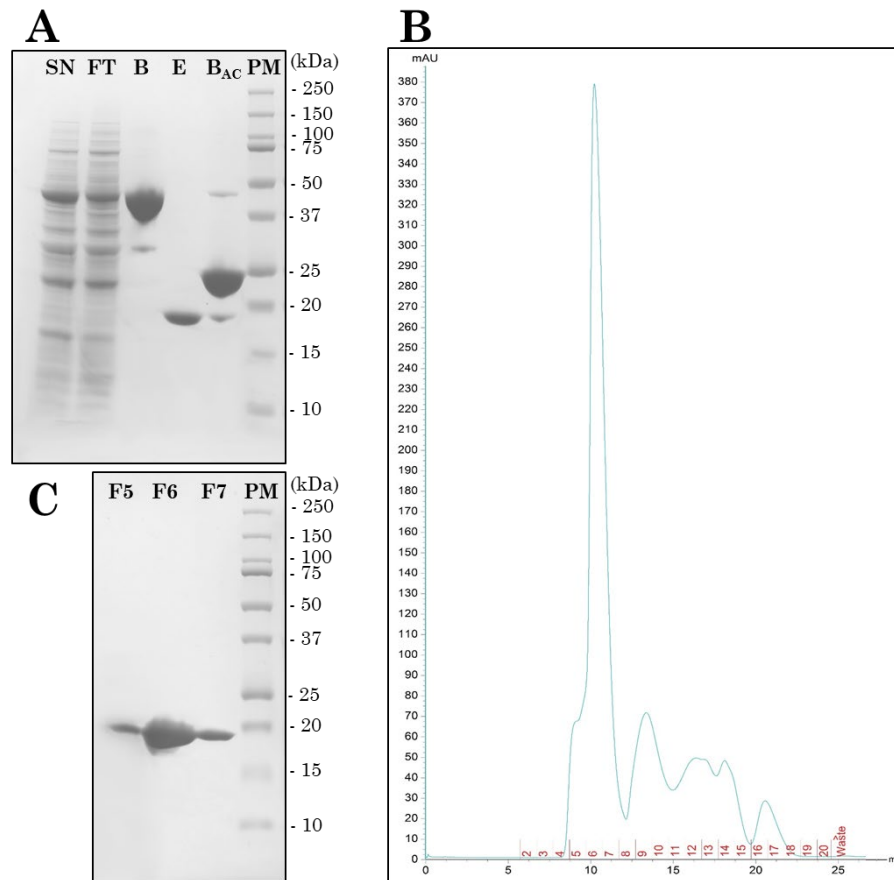


Figure C.8 Purification of VS-S. A) SDS-PAGE of the affinity purification on GSH beads and thrombin cleavage of VS-S. The bacterial lysate was incubated with GSH Sepharose beads, leading to the immobilisation of GST-VS-S onto them; the elution of VS-S (17.2kDa) was obtained by thrombin cleavage. The elution was not 100% efficient, as some VS-S was still immobilised on the final beads (B_{AC}). Abbreviations: SN = supernatant, FT = flow through, B = beads, E = eluate, B_{AC} = beads after cleavage. B) Size exclusion chromatography chromatogram; red numbers on the bottom are the fractions collected by the ÄKTA Pure chromatography system (GE Healthcare). On the X-axis, the elution volume (in ml); on the Y-axis, the UV-light absorption at 280nm, expressed in mAU (milli Absorbance Units). C) SDS-PAGE of the fractions collected by the FPLC incubated with 5 μ M TCEP to avoid the formation of dimers. This gel confirms that VS-S is mostly in F6.

- VS-L2

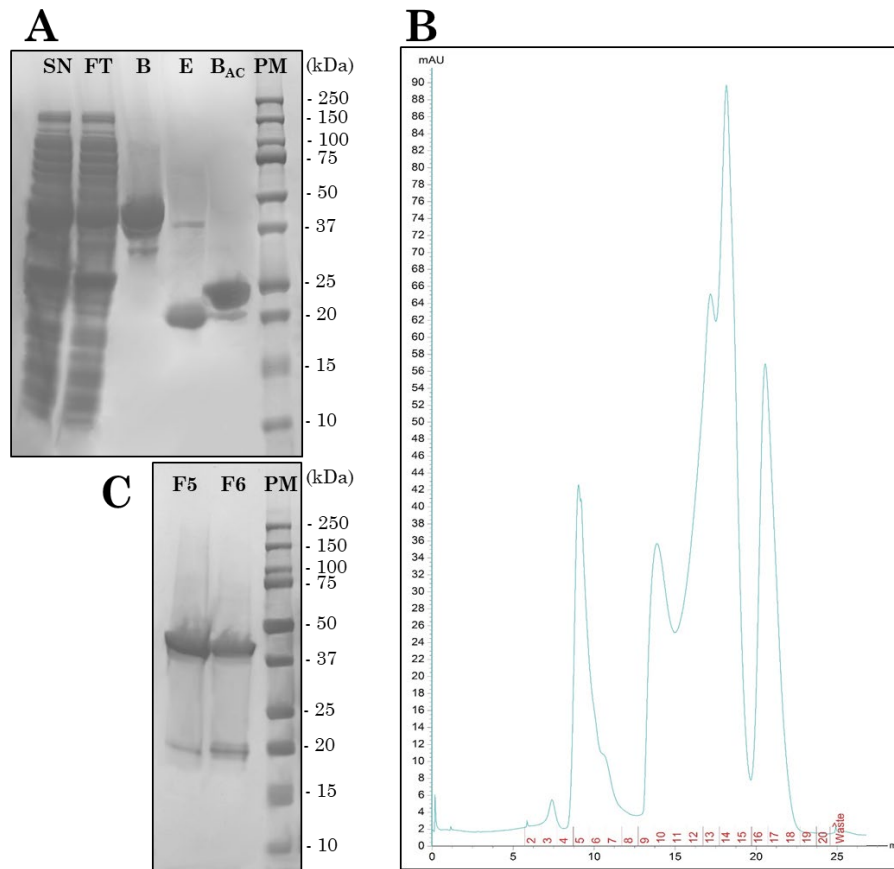


Figure C.9 Purification of VS-L2. A) SDS-PAGE of the affinity purification on GSH beads and thrombin cleavage of VS-L2. The bacterial lysate was incubated with GSH Sepharose beads, leading to the immobilisation of GST-VS-L2 onto them; the elution of VS-L2 was obtained by thrombin cleavage. VS-L2 migrates as a ~20kDa protein, even if its molecular weight is 16.1kDa. Abbreviations: SN = supernatant, FT = flow through, B = beads, E = eluate, BAC = beads after cleavage. B) Size exclusion chromatography chromatogram; red numbers on the bottom are the fractions collected by the ÄKTA Pure chromatography system (GE Healthcare). On the X-axis, the elution volume (in ml); on the Y-axis, the UV-light absorption at 280nm, expressed in mAU (milli Absorbance Units). C) SDS-PAGE of the fractions collected by the FPLC. They were not incubated with a reducing agent, and therefore in both lanes, there is a high concentration of dimer. This gel confirms that VS-L2 is mostly in F5 and F6.

- GST

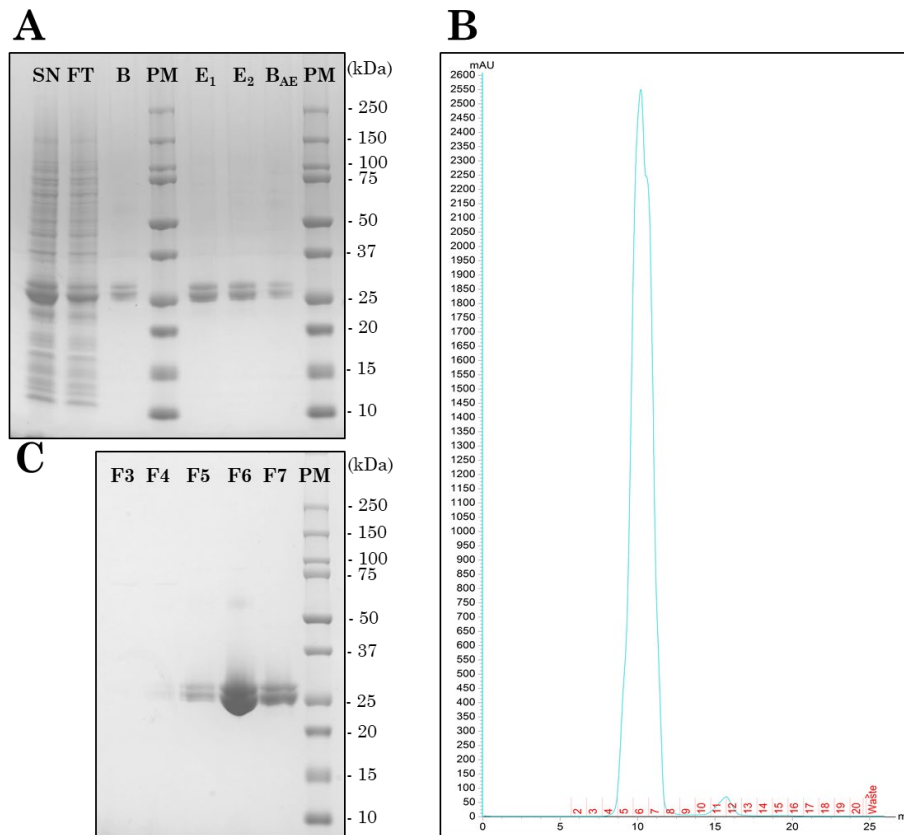


Figure C.10 Purification of GST. A) SDS-PAGE of the affinity purification on GSH beads and GSH elution of GST. The bacterial lysate was incubated with GSH Sepharose beads, leading to the immobilisation of GST onto them; the elution of GST (28.6kDa) was obtained with an excess of GSH solution. Abbreviations: SN = supernatant, FT = flow through, B = beads, E₁,E₂ = eluates, B_{AE} = beads after elution. B) Size exclusion chromatography chromatogram; red numbers on the bottom are the fractions collected by the ÄKTA Pure chromatography system (GE Healthcare). On the X-axis, the elution volume (in ml); on the Y-axis, the UV-light absorption at 280nm, expressed in mAU (milli Absorbance Units). C) SDS-PAGE of the fractions collected by the FPLC. This gel confirms that GST is mostly in F5, F6 and F7. GST migrates as a double band in all fractions, most likely due to partial proteolytic degradation of the thrombin cleavage site near the C-terminal of the protein.

- GST-HH

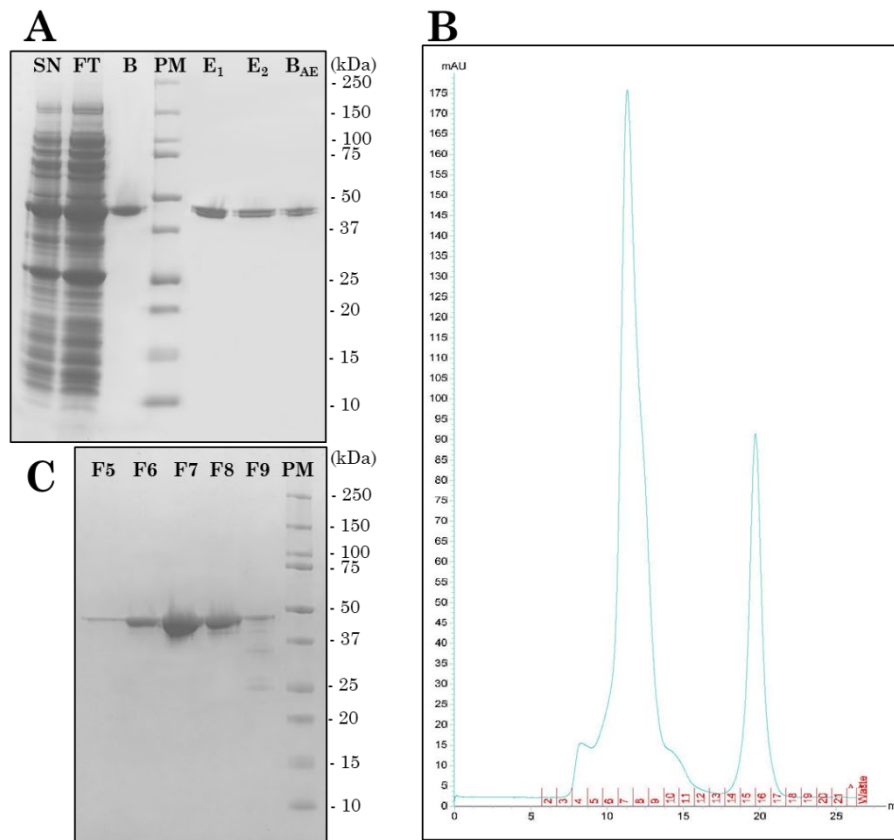


Figure C.11 Purification of GST-HH. A) SDS-PAGE of the affinity purification on GSH beads and elution of GST-HH. The bacterial lysate was incubated with GSH Sepharose beads, leading to the immobilisation of GST-HH onto them; the elution of GST-HH (45.3kDa) was obtained with an excess of GSH solution. Abbreviations: SN = supernatant, FT = flow through, B = beads, E₁, E₂ = eluates, B_{AE} = beads after elution. B) Size exclusion chromatography chromatogram; red numbers on the bottom are the fractions collected by the ÄKTA Pure chromatography system (GE Healthcare). On the X-axis, the elution volume (in ml); on the Y-axis, the UV-light absorption at 280nm, expressed in mAU (milli Absorbance Units). C) SDS-PAGE of the fractions collected by the FPLC. This gel confirms that GST-HH is mostly between F6 and F8; in F9, some breakdowns are visible that were not spotted in any of the eluates (E, gel A).

D. Protein fusion attempts












SNARE fusion attempts	Outcome
Synt1-l-H1-l-H2 	ineffective thrombin cleavage difficult elution
H1-l-H2-l-Synt1 	poor expression; difficult elution
H1-l-H2-k-Synt1 	poor expression; difficult elution
H1-l-H2-k-Synt3 	poor expression; difficult elution
H1-l-H2-l-VAMP2-L 	poor expression; difficult elution
H1-l-H2-k-VAMP2-L 	poor expression; difficult elution
Synt1-l-VAMP2-L 	ineffective thrombin cleavage difficult elution
Synt1-l-VAMP2-S 	ineffective thrombin cleavage difficult elution
VAMP2-L-l-Synt3 	✓
VAMP2-S-l-Synt3 	✓
VAMP2-L-k-Synt3 	✓

Figure D.1 Protein fusion attempts. Eleven SNARE fusions were expressed and purified over this project, of which only three were eventually characterised and used in further experiments. The SNARE fusion attempts that were not carried over are highlighted in yellow, and their outcome indicated, with the reasons for their rejection. The SNARE domains are represented with cylinders of different colours, while the linkers are shown as lines. VAMP2-S is represented here by a cylinder with the same length of the others for illustration purposes only.

E. Published outputs from the project (printed copies only)

Most of the work described in this thesis is part of a manuscript published in *Biomaterials Science*:

Saccardo A, Soloviev M & Ferrari E. “A thermo-responsive, self-assembling biointerface for on demand release of surface-immobilised proteins”, *Biomaterials Science*, 2020.

Part of the work done during the PhD, with regards to modular cloning and engineering of protein-protein interactions for immobilisation on a solid surface, contributed to a published work in *Nature Communications*:

Ma W, Saccardo A, Roccatano D, Aboagye-Mensah D, Alkaseem M, Jewkes M, Di Nezza F, Baron M, Soloviev M & Ferrari E. Modular assembly of proteins on nanoparticles. *Nature Communications* 9, 1489 (2018). <https://doi.org/10.1038/s41467-018-03931-4>

Part of the work done within this PhD project is published within the following book chapter:

Saccardo A, Ma W, Soloviev M & Ferrari E. “Directed and oriented protein immobilization on gold and silver nanoparticles” in *Nanoparticles in Biology and Medicine, Methods and Protocols*, second edition, Springer (April 2020).

The outputs mentioned above are included for consultation as part of the first submission of the printed thesis only. The electronic copy and the next submission will have these omitted to avoid breaching publishers’ copyright.